Université de Neuchâtel

Institut de Microtechnique

Conception and design of illumination light pipes

Thèse

présentée à la Faculté des sciences
pour obtenir le grade de docteur ès sciences

par

Juan Manuel Teijido

Neuchâtel, février 2000

IMPRIMATUR POUR LA THÈSE

Conception and design of illumination light pipes

de M. Juan Manuel Teijido

UNIVERSITÉ DE NEUCHÂTEL

FACULTÉ DES SCIENCES

La Faculté des sciences de l'Université de Neuchâtel sur le rapport des membres du jury,

MM. R. Dändliker (directeur de thèse), H.P. Herzig, P.-J. Erard et J. Braat (Delft NL)

autorise l'impression de la présente thèse.

Neuchâtel, le 29 février 2000

Le doyen:

J.-P. Derendinger

Summary

A critical review of different methods for the design of illumination devices is presented. The strengths and limits of non-sequential ray-tracing are discussed in detail. The use of global illumination algorithms for the design of illumination devices is also evaluated. A design strategy based on the original optical transfer block (OTB) method is proposed to make easier the optimization of illumination light pipes. The main limitation of traditional illumination design tools is thus overcome.

The possible working principles of illumination light pipes are explained. Different light pipe configurations are evaluated based on their optical performances and their manufacturing constraints. Reflective micro-prism light pipes prove to be particularly well adapted for the realization of efficient lighting devices. Finally, the realization of a watch frontal-lighting device based on a micro-prism light pipe is described.

Contents

Chapter 1

Introduction

This thesis is the result of the work done in the scope of an industrial project for the watch industry. The goal of the project was to develop an efficient illumination device for the frontal-lighting of watches. The need for a new generation of light sources in order to satisfy the demanding optical, electrical and mechanical requirements has been early identified. The use of illumination light pipes has proven to be the natural solution for the watch lighting device. This dissertation shows the challenge related to the conception of illumination light pipes. In particular, we describe the strategy used to overcome the limitations of the commercially available design tools.

The context

There are many applications which take profit of the improvements made in the field of optical light sources [1-1]. Technological advances allow to improve the lighting efficiency, to lower the operating costs, and to increase the lifetime of the sources. Nevertheless, for most applications, optical light sources need to be assisted by complementary optics in order to deliver the desired lighting distribution. Traditional designs, which include lenses and mirrors, are not well adapted for the realization of compact and cheap lighting devices. Moreover, some lighting distributions are difficult to achieved with standard optics.

Illumination light pipes are innovative devices that provide an unmatched degree of flexibility and allow to overcome many of the limitations of standard designs. Light pipes have traditionally been used for the lighting of compact displays, but new fields

of application are emerging for the automotive industry, the watch industry, the medical instrumentation, the lighting of buildings, etc.

The challenges

The relatively simple working principle of light pipes allows the quick realization of operational prototypes. However, the use of illumination light pipes for demanding applications requires fine tuning of the design by numerical means. The optimization of illumination devices is a task, which is not yet offered by the commercially available simulation programs.

The problems related to the design optimization of illumination light pipes are summarized hereafter :

- the definition of a good initial design is critical,
- there are too many design parameters,
- the influence of a given parameter on the overall performance of the device is difficult to identify,
- the computation time needed for the analysis of the optical system is too long.

The automatic optimization of the design is difficult due to the number and the various nature of the parameters to be considered during the design process. In fact, the optical function of any illumination device is influenced by its 3-dimensional geometry, the optical properties of the materials, and the roughness of the surfaces. Moreover, the constraints imposed by the manufacturing process have to be taken into account during the design.

The optimization principle consists of varying a few design parameters between two evaluations of the design, hoping that this change will result in an improvement of the optical performance of the illumination device. The process is repeated until a design is found that fulfils the requirements. Optimizations based on purely numerical algorithms, like simulated annealing, result generally in a large number of iterations before obtaining a good design. Since the time necessary for the computation of one single analysis run takes generally several hours, the design of illumination devices becomes

a lengthy process. Alternatively, the choice of the parameters to vary can be done "manually" by the designer. Nevertheless, the influence of a given parameter on the overall performance of the system may be very difficult to predict. Therefore the convergence of the optimization process cannot be guaranteed.

Obviously, a method is needed which allows the rapid convergence of the optimization process. This goal cannot be achieved without a good initial design. This means that the main design options have to be chosen correctly taking into account the optical, electrical, and mechanical requirements, but also the manufacturing constraints. A critical overview of the different design options is needed in order to select the best light pipe configuration for each application.

Our contribution

The purpose of this thesis was to suggest a strategy for the realization of illumination light pipes. This task requires the understanding of very different concepts, like the simulation algorithms, the light pipe working principles, and the manufacturing technologies. This thesis gives a critical review of these different aspects, and proposes some original solutions to overcome some of the limitations of the current design tools.

The next points summarize the topics which are introduced in this thesis :

- presentation of a critical review of the different analysis algorithms,
- proposition of a light pipe design strategy based on an original model called the optical transfer block (OTB) method,
- study of the light pipe working principles and of the possible design options,
- proposition of two encoding schemes for the control of the lighting distribution,
- discussion of manufacturing technologies.

The exact modeling of illumination devices in their surrounding environment is numerically very demanding. Therefore, different analysis algorithms have been proposed which introduce different levels of simplification in view to reduce the computing time to reasonable levels. These algorithms are either based on *ray-tracing*, or on the *radiance equation*. We discuss the working principles and limitations of these models. A

good understanding of the underlying algorithms of each analysis method is necessary to insure the correctness of the simulations.

In order to overcome the lack of optimization modules in the current illumination programs, we propose a hierarchical approach of the design process. The goal is to reduce the number of design parameters. Thus, the influence of each design parameter on the optical performances of the system becomes easier to identify, the selection of the variable design parameters is simplified, and the convergence of the optimization process is guaranteed. The proposed method, called the *optical transfer block* (OTB) method, consists of representing the light pipe by a sequence of adjacent blocks. Each block is characterized by its optical transmission function, which determines the balance of radiant energy passing through the faces of the block. The first step of the design is to find the combination of blocks which gives the required optical function of the light pipe. The fine tuning of the design is finally done with the help of existing analysis programs.

To be successful, any optimization process has to start with a good initial design. The configuration of the illumination light pipe is chosen in function of the requirements of the application. In view to facilitate this choice, we present the working principles of the light pipe. In particular we make a critical review of the different type of light pipe outcouplers. The choice of the outcoupler determines mainly the optical function of the light pipe, as well as the manufacturing technologies.

Light pipes are particularly interesting for the control of the lighting distribution. In particular, they allow the uniform illumination of extended surfaces with very compact devices. The distribution of the illumination is mainly controlled by the density of the outcouplers along the surface of the pipe. The encoding schemes used for the calculation of the outcoupler distribution are described.

Light pipes using reflective micro-prisms as outcouplers have particularly interesting optical properties. Actually, reflective micro-prisms allow a good control of the direction of illumination with minimal optical losses. Moreover, the technologies for the manufacturing of micro-prisms are being constantly improved. We discuss in detail the

properties of micro-prism light pipes (in particular the shadowing effect) and illustrate their potential by describing the realization of a frontal-lighting device for watches.

Organization of the dissertation

Chapter 2 presents the strengths and limits of the different analysis methods. The principle of the optical transfer block (OTB) method is explained and its application for the optimization of illumination light pipes is introduced.

Chapter 3 introduces the light pipe concept. The characteristics of the different types of light pipe outcouplers are evaluated. The calculation of the outcoupler density by the OTB method is described. Finally, the possible manufacturing technologies are presented, and their consequences on the design are discussed.

Chapter 4 illustrates the potential of illumination light pipes for a very demanding application, namely the frontal-lighting of watches. The selected light pipe approach is based on total internal reflection micro-prisms. We describe the benefits of this approach and present the first experimental realizations.

Chapter 5 discusses the achievements of the present thesis and identifies some possible paths for future developments.

Finally, several appendices have been included, which resume some definitions, detail some derivations, or present properties which can be useful for the design of illumination devices.

1.1 References

[1-1] National Research Council, *Harnessing Light, Optical Science and Engineering for the 21st Century*, National Academic Press, Washington, D.C. 1998

Chapter 2

Methodology for the design of illumination devices

Illumination devices are used in many applications such as automotive headlights, automotive stop lamps, back-lighting of flat panel displays, and solar cell concentrators. These devices perform very different optical functions. Automotive headlights are designed in view to generate a well controlled lighting distribution: the street has to be illuminated as brightly as possible, while avoiding to blind the other drivers. Stop lamps need to attract the attention of the other drivers. In this case, the generated illumination has to be very directive. The back-lighting devices need to deliver a bright and uniform illumination over the full screen surface. Finally, the solar cell concentrators have to collect as much light as possible. Furthermore, all these devices have very different electrical, mechanical, thermal, and manufacturing requirements, which directly impact on their respective design. These examples illustrate the variety of requirements, which have to be taken into account during the conception of illumination devices.

Many illumination devices have very simple designs which can be realized intuitively without any simulation tool. However, the design of performing devices, whose goal is to perfectly control the lighting distribution, require the assistance of illumination design programs. For instance, the realization of the freeform reflectors used by the automotive headlamps may require several months of engineering and days of computer simulations.

In this chapter, we review the state of the art in the design of illumination devices. We identify the shortcomings of the process and introduce an original approach to overcome some of the current limitations of the optimization procedure. The goal is to propose an unified design strategy applicable for most of lighting applications.

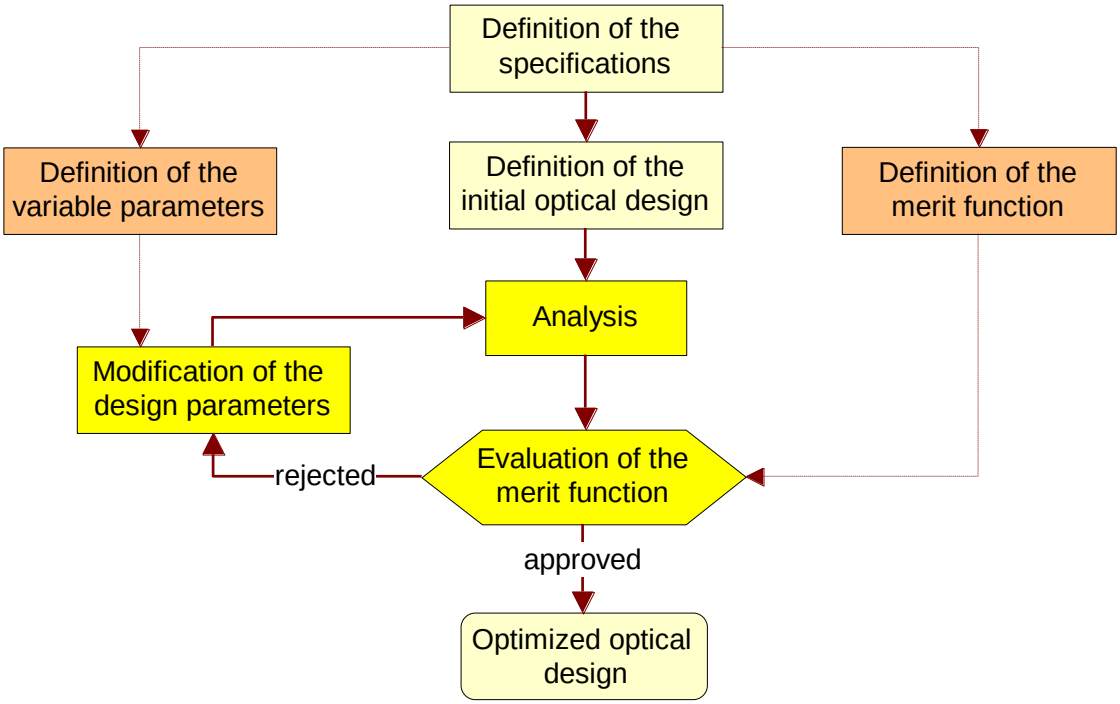

Fig. 2-1 Flowchart of the design process.

The concepts governing the illumination systems are often very simple. An initial design is generally easily defined by simple intuition and experience. The start of the design process often consists in an existing device, whose performances need to be optimized. As shown in Fig. 2-1, the design of an optimized illumination device respects the traditional analysis-and-optimization loop. Nevertheless, the computer intensive nature of the analysis process and the number of the possible variable parameters make the traditional optimization algorithms unsuitable.

Section 2.1 explores the different analysis approaches. Ray-tracing is the analysis tool of choice in optical engineering. We present the particularities of non-sequential ray-tracing and its strengths and weaknesses for the design of illumination devices. The rendering techniques traditionally used in the computer graphic industry represent an

alternative to ray-tracing which is generally ignored by optical engineers. The principle of the algorithms based on the radiance equation and the radiosity are explained and discussed. Some hybrid methods combining ray-tracing and radiosity are discussed as well.

The optimization of illumination devices has traditionally be limited to simple problems like finding the best shape of reflectors [2-1], or concentrators [2-2]. The advent of a new generation of light sources has multiplied the possible applications and therefore the possible lighting device configurations. The related requirements fixes a new challenge for the optimization process. The problems related with the definition of the merit function, the choice of the variable design parameters, and the design evaluation are discussed in section 2.2.

A solution to facilitate the design process would be to consider a simplified version of the optical system. In section 2.3, we propose an approach for which the system is subdivided into functional blocks, called optical transfer blocks (OTB). We get a higher level of abstraction, which minimizes the number of design parameters, and consequently makes easier the optimization process. Finally, a review design strategy is proposed in section 2.4.

2.1 Critical review of analysis methods

The analysis is at the center of the design process. The potential optical performances of the illumination device need to be evaluated before any costly hardware realization. The rule of the analysis tools consists in simulating the optical behavior of the device taking into account the laws of physics.

The next subsections describe different analysis methods, mainly based on ray-tracing and on the radiance equation. Each algorithm is evaluated for its ability to be integrated in the design process of illumination devices. The precision (correctness) and the computer efficiency of the analysis method are the two main evaluation criteria, which are briefly discussed hereafter.

The correctness criteria

The simulation of illumination devices consists of calculating the propagation of light through the optical system. The two main values which need to be taken into account by the simulation are: the direction of propagation of the light and the spatial repartition of the power (flux).

The light sources used for lighting applications are generally incoherent and have an extended surface of emission. In this context, wavefront propagation effects like diffraction and interference (speckles) can be neglected. The propagation and deviation of light is well described by the laws of geometrical optics like reflection, refraction, and the grating equation. However, the calculation of the power repartition requires a deeper knowledge of the interaction between light and matter. In this case, the state of polarization of light, the complex index of refraction of the materials, the microstructuration of the surface profile, and the surface roughness have to be considered.

The knowledge of the state of polarization of light is required for the calculation of Fresnel refraction and reflection, the calculation of single- or multi-layer coatings, the calculation of grating diffraction efficiency, and the calculation of surface and volume scattering. For unpolarized sources, the polarization modes s and p have the same magnitude. On an other hand, polarization may be used for itself in illumination systems (e.g. the use of polarizers in automotive rear-view mirrors).

The simulation of the losses by absorption inside the materials or at the surface requires the precise knowledge of the (complex) refractive indexes. Moreover, some technological processes, like injection molding, may introduce volume scattering, which is often associated with absorption. The in-house characterization of the materials may be required before any serious simulations. For instance, measurements have shown that, depending on the preparation, the absorption of molted PMMA (polymethylmethacrylate) in the visible may vary from $0.4\,dB/m$ to $2\,dB/m$.

Scattering effects are often used by illumination devices in order to influence the lighting distribution. Scattering may also be a disturbing effect that needs to be taken into account in the design of the lighting device (e.g. automotive fog lamps). Scattering re-

sults from the interaction of the light with obstacles having a size close to the wavelength. The distribution of the scattering obstacles can either be stochastic (surface or bulk scattering), or well structured (grating diffraction). The exact simulation of scattering is based on the electromagnetic (EM) diffraction theory. For further details, we refer to Ref. [2-3] for the EM calculation of diffraction gratings, to Ref. [2-4] for the calculation of scattering by particles, and to Ref. [2-5] for the calculation of scattering by rough surfaces. The exact calculation of scattering is too complex to be executed within the illumination analysis programs.

The scattering properties of surfaces, namely the *bidirectional scattering distribution function* (BSDF), are often measured experimentally with some type of goniometric instrument [2-6, 2-7]. The BSDF is defined as the ratio of the scattered surface radiance to the incident surface irradiance (see Appendix B). The measured data is stored in tables which can later be addressed offline by the illumination analysis programs. As shown in Appendix B, the BSDF may also be approximated by an analytical function; in this case, it is directly computed by the illumination analysis program. Whatever technique is used, one condition for a correct analysis consists in knowing exactly the optical characteristics of the constitutive materials and the surface physics.

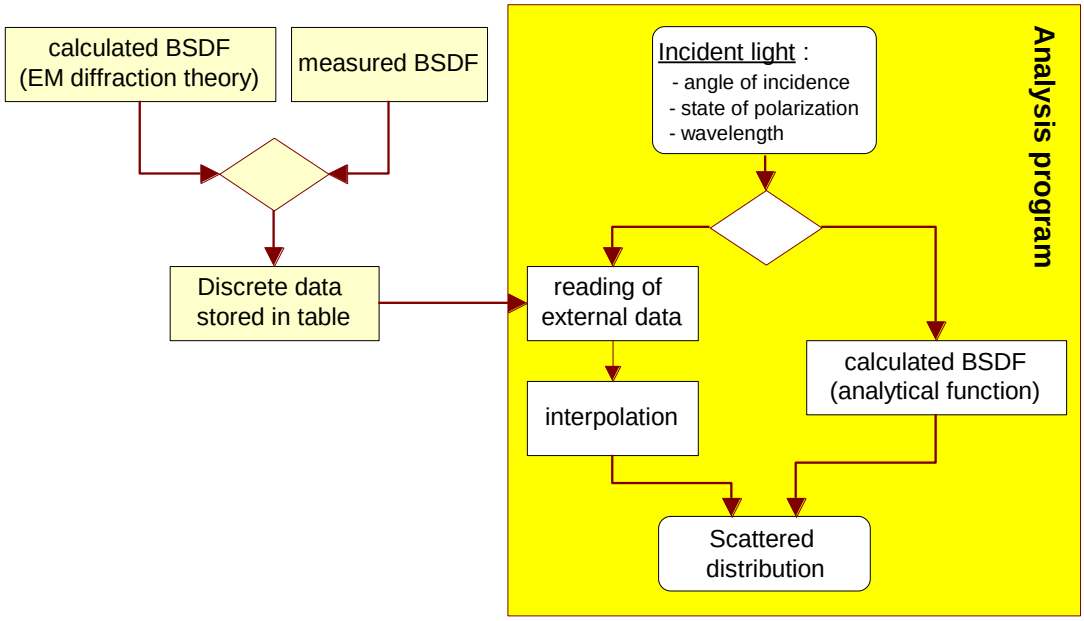

Fig. 2-2 Determination of the scattered light during the analysis process.

Most of the illumination systems are insensitive to chromatic effects. The analysis is then done at one (central) wavelength. However, the fine tuning of some devices may require a polychromatic analysis. For instance, the unwanted bluish effects generated by the automotive xenon headlights could be reduced by the use of wavelength sensitive micro-optical elements. Other devices may have their basic working principle based on wavelength shifts. This is for example the case of fluorescent light sources. In most cases, the polychromatic analysis results from several sequential analysis done at different wavelengths.

The computer efficiency criteria

As shown in Fig. 2-1, the analysis process is in the center of the optimization loop. We show in the next sections that the analysis of illumination devices is time consuming by nature. It is not unusual that a single analysis run takes several days of computation on a Pentium® class computer. In this case, the optimization process may be limited to a few (≤ 10) iterations (in comparison, the optimization of imaging devices may take several thousands of iterations).

Generally, the analysis computation times are function of the required degree of precision. Therefore an adaptive analysis algorithm, for which the degree of precision is increased from run to run, can reduce the overall optimization time by one order of magnitude. The optical transfer block (OTB) approach (introduced in section 2.3), where the optical system is roughly described by functional blocks, can be considered as a first model of analysis.

Thanks to the increasing power of CPUs, which doubles each 18 months following Moore's law, the limits related to the computing times are constantly pushed back. Moreover, the algorithms simulating the propagation of light are perfectly well suited for parallel multiprocessing. At the time of this writing, cheap 4-way workstations are becoming common. As the analysis tools are being adapted to these new computer architectures, the palette of problems, which can reasonably be analyzed (and optimized), grows from year to year.

2.1.1 Ray-tracing

Light has been modeled by rays since the ancient past. However, it took time to understand the fundamental principles of geometric optics. Alhazen (around 1000) was the first to correctly formulate the law of reflection. It was not before 1621 that W. Snell formulated the law of refraction, which was finally described in terms of sines by R. Descartes in 1637. The calculation of the optical aberrations in optical instruments was greatly facilitated by the simplifications introduced by Seidel in the 19th century. The Seidel approximation consists in expanding the trigonometric formulae into Fourier series up to the third order (see Eq. (2-1)). Seidel approximation (also called third order approximation) has been used for the design of optical instruments during nearly one century. In the sixties, with the advent of the first commercially available computers, ray-tracing programs became available. The performances of the optical design process have increased considerably due to the exact calculation of the trigonometric functions and to the automation of the optimization procedure.

$$\begin{aligned} \sin x &= x - \frac{x^3}{3!} + \frac{x^5}{5!} - \frac{x^7}{7!} + \ldots \\ \underbrace{\tan x = x + \frac{1}{3}x^3}_{Seidel's\,approximation} &+ \frac{2}{15}x^5 + \frac{17}{315}x^7 + \ldots \end{aligned} \qquad (2\text{-}1)$$

2.1.1.1 Sequential ray-tracing

Traditionally, ray-tracing has been used for the design of imaging systems (microscope, telescope, camera, …). The goal is to minimize the optical aberrations [2-8]. As illustrated in Fig. 2-3, the rays propagate through the system from the object plane to the image plane (by convention from left to right). In imaging systems, the sequence in which the rays intersect the optical surfaces is predefined. All rays starting from the object plane reach surface #1 first, then surface #2, and so on until they meet the image plane. The programs based on this predefined intersection sequence are called *sequential ray-tracing* programs.

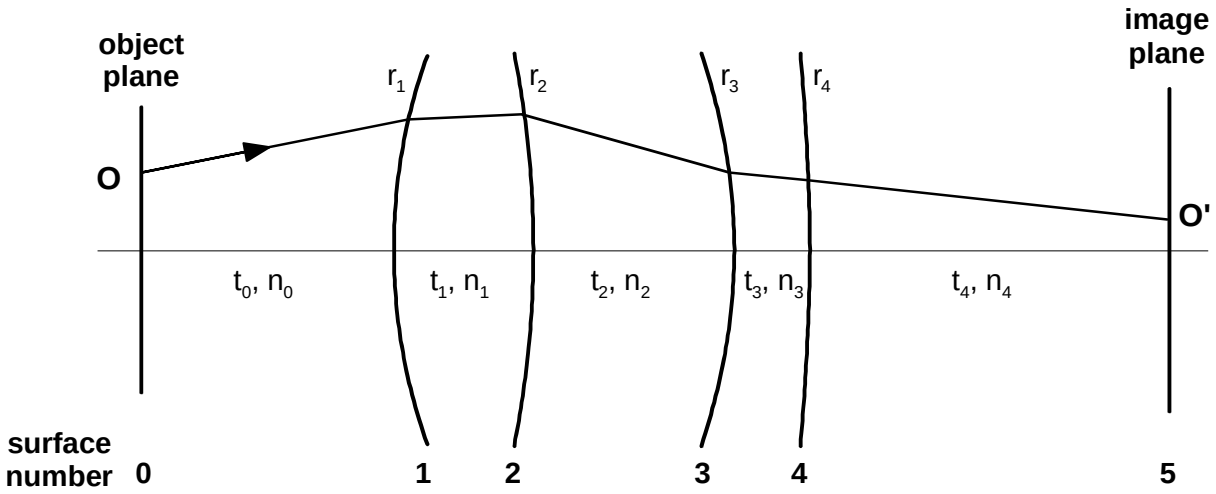

Fig. 2-3 Illustration of sequential ray-tracing.

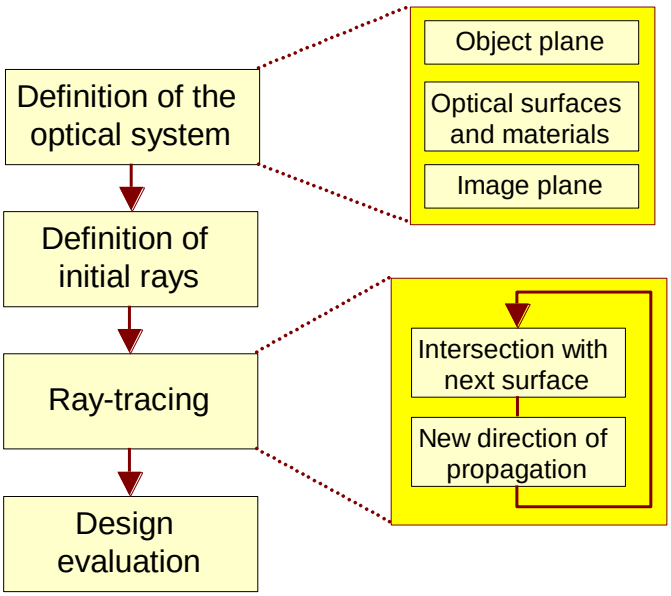

Fig. 2-4 Flowchart of the analysis by sequential ray-tracing.

The flowchart in Fig. 2-4 summarizes the sequential ray-tracing analysis process (we have not included the optimization loop). The first step consists of defining the optical system. Generally the surfaces are defined by the coefficients of analytical functions (i.e. plane, sphere, conic asphere, polynomial asphere, …). The materials are defined by their wavelength dependent index of refraction. The rays are generated in the object plane by launching a grid of rays through the pupil. The analysis of the optical aberrations of the system requires the tracing of a relatively low number of rays (a few thou-

sands as a maximum). The propagation of each ray is simulated by calculating the successive coordinates of intersection and the direction of propagation. The deviation of the rays at the ray-surface intersection is determined by the laws of refraction and reflection (see Appendix A). Finally, the position and the direction of the rays reaching the image plane are stored for the evaluation of the design performances.

2.1.1.2 Non-sequential ray-tracing

The simple sequential ray-tracing approach has some limitations, even for the design of imaging systems. Some imaging instruments, such as microscopes or retro-projectors, incorporate a light source, whose function has to be optimized during the design process. Moreover, the stray-light produced by inter-reflections and the diffusion generated by the surface roughness influences the performances of the device. In view to analyze these effects, a new generation of ray-tracing programs has been developed. These programs take into account the flux per ray and they are able to simulated the non-sequential propagation of the light through the system. Therefore the programs are called *non-sequential ray-tracing* programs [1].

The main goal of non-sequential ray-tracing programs is to calculate the spatial or directional repartition of the power. The radiometric values of interest are : the flux ϕ, the irradiance E, and the radiance L (see Appendix D for the definition of the radiometric and photometric values). The analysis consists of simulating the incident power on one (or several) detector surface(s), which, may represent the eye, the film plane of a camera, a solar cell panel, a flat panel display, etc. Beside the power values, the polarization of the light may be important for some illumination devices. For example, the efficiency of LCD back-lighting devices depends directly on the state of polarization of the light.

---

1 At the time of this writing, the last generation of traditional sequential ray-tracing programs incorporate non-sequential capabilities. However, most of them are still unable to manipulate flux. Their utility for the design of illumination devices remains therefore marginal.

As shown in Figs. 2-4 and 2-5, the four main steps of analysis sessions are similar for sequential and non-sequential ray-tracing. However, the detailed implementation is more complex in the case of non-sequential ray tracing. A basic understanding of the underlying algorithms is necessary for the judicious definition of the analysis parameters and for a correct interpretation of the results.

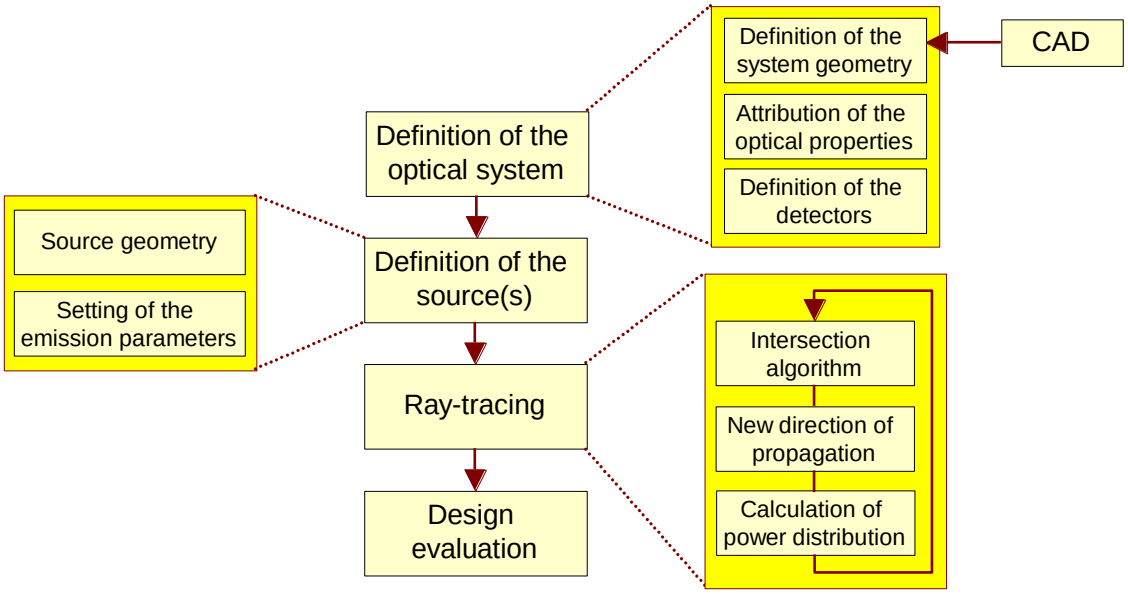

Fig. 2-5 Flowchart of the analysis by non-sequential ray-tracing.

Definition of the optical system

For non-sequential problems, the definition of the optical system geometry takes a significant part of the resources allocated to the design. This task requires the same tools and competences as classical 3D mechanical modeling. Thus most of the analysis tools include the possibility to import data from external CAD tools. In contrary to sequential ray-tracing where the function of the device is exclusively defined by optical elements (lenses, prisms, mirrors, …), all the constitutive elements of the scene (e.g. the mounting) may contribute to the optical performances of the device and need therefore be defined carefully.

The next step consists of attributing the optical properties to the different elements of the scene. The volume properties of each object are defined by the refractive index

(complex for metals) and/or an absorption coefficient. Moreover, each surface has its own optical properties, defined either by the surface roughness, a multi-layer coating, or a diffractive micro-structure. As shown in Appendix B, the optical properties of the surface may generally be defined by the bidirectional distribution function (BSDF). In any case, it is crucial to know the exact optical properties of each element before any ray-tracing. Some preliminary characterization of the materials and surfaces may be required.

The last step before the ray-tracing process consists of defining the observation planes. These observation planes may correspond to physical detectors (eye, CCD, …). They can be dummy planes, which serve for the analysis of the propagation of light at a specific location in space. The choice of the detector resolution (pixel size) depends on the optical function to analyze. The detector resolution determines the minimal number of rays to be traced (finer resolutions need more rays).

Definition of the source

A good simulation of a lighting device requires the accurate modeling of the light source. As illustrated in Fig. 2-6, the geometry of the source can be described respecting all the details of the physical model. The radiance of the filament can be defined precisely taking into account the local variations of the temperature (the emission efficiency depends on the temperature). The filament stands are included as they can cause shadowing or ray reflection, affecting the performances of the source.

An other alternative consists in measuring experimentally the radiance of the source. An artificial source is then defined for the ray-tracing analysis. The shape of the artificial source corresponds to an imaginary surface that has been scanned by the detector during the characterization process (see Fig. 2-7). Each surface element (patch) of the artificial source emits rays whose direction and flux is determined in order to reproduce the measured local radiance.

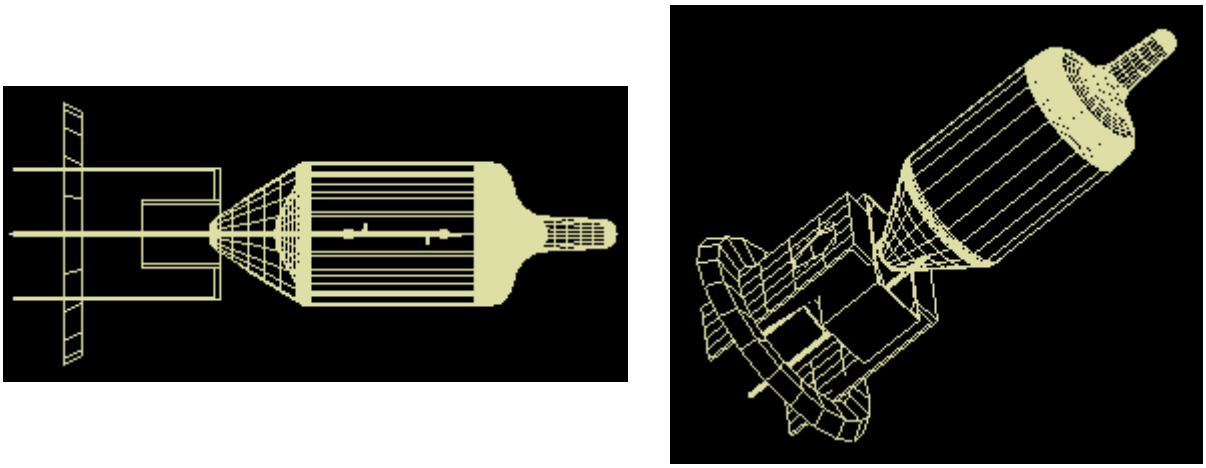

Fig. 2-6 Two different views of an H-4 headlamp bulb.

Modeled in the optical and analysis design tool ASAP ™ (courtesy of Breault Research Organization, Inc.).

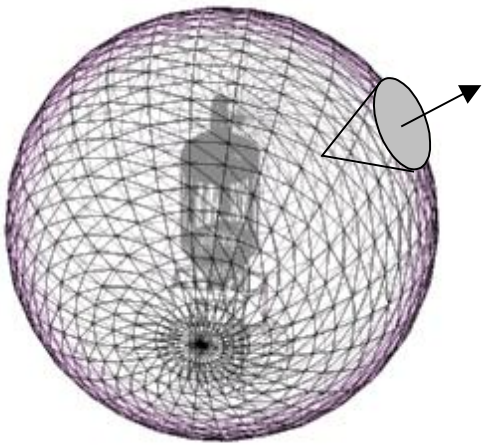

Fig. 2-7 Source defined by an radiant envelop surrounding the real source.

The radiant envelop approach is perfectly suited for the simulation of many applications. However shadowing effects due to the interactions of the reentrant rays with the source geometry are not taken into account. This can distort the results of the simulation, particularly if the source is surrounded by a reflector as shown in Fig. 2-8.

For both presented models, the simulation of the source implies the modeling of the radiance L emitted by surface elements (or patches). As illustrated in Fig. 2-9, the radiance is defined as the flux ϕ per unit projected area ($A\cos\theta$) and per solid angle ω

$$L = \frac{d^2\phi}{dA \cdot \cos\theta \cdot d\omega} \ . \qquad (2\text{-}2)$$

The units of radiance are $W\, sr^{-1}\, m^{-2}$.

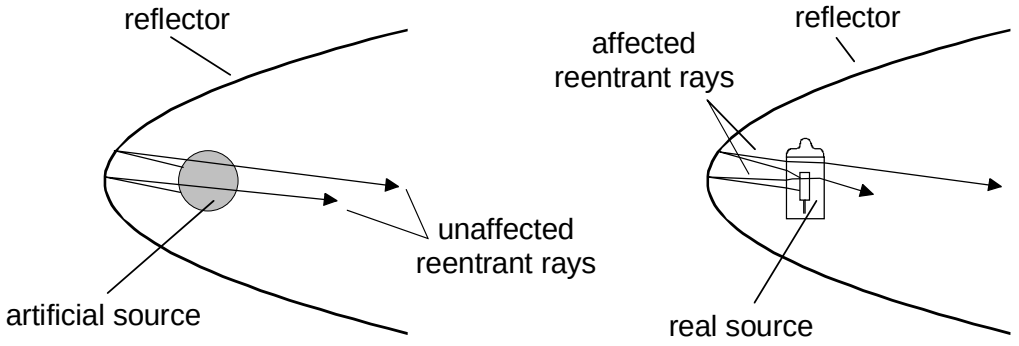

Fig. 2-8 Re-entrant rays are deviated or absorbed in the real model, but their trajectory is unmodified using the radiant envelop model.

The radiance can be simulated by generating rays in random directions and adapting their flux in accordance with the radiance in their direction of propagation. An other possibility consists in keeping the flux of the emitted rays constant and determining statistically the direction of rays in accordance with the radiance distribution. These techniques of ray generation are sometimes referred in the literature as stochastic ray-tracing [2-9].

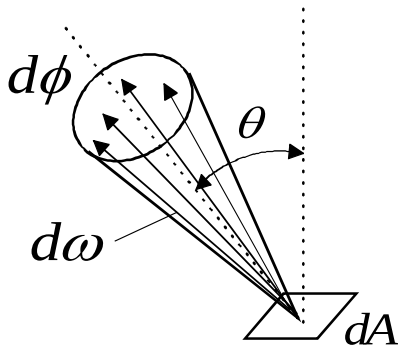

Fig. 2-9 Radiance simulated by rays emitted by the surface patch.

During a ray-tracing session, a finite number of rays are generated from the source. The number of generated rays is a critical parameter of the analysis. If the number of ray is too low, the precision of the simulation will be insufficient. In contrary, if the

number of generated rays is too high, the computation time will be prohibitive. Depending on the system configuration, the ideal number of rays to generate may vary from a few hundred to several millions. The strategy consists in starting the analysis with a reduce number of rays and to increase this number progressively until the observed power distribution on the detector(s) converges. In other words, this approach corresponds to the minimization of the signal-to-noise ratio on the detector(s), and depends directly on the detector resolution (pixel size). As the number of rays N increases, the flux ϕ_p incident on each pixel p of the detector converges towards an average value $\bar{\phi}_p$, as

$$\bar{\phi}_p = \lim_{N\to\infty}\left[\frac{1}{N}\sum_{n=1}^{N}\phi_{p_n}\right]. \qquad (2\text{-}3)$$

The ray-tracing process

The rays emitted by the source propagate straight ahead until they meet the next reflective or refractive surface. The ray-surface intersection can either be solved analytically or numerically [2-10]. The difficulty of non-sequential ray-tracing comes from the fact that the next intersected surface is not known in advance. A crude way to solve the problem consists first in calculating the possible intersections of the ray with all the surfaces of the scene, and then in selecting the shortest ray path. As a scene can be formed by several thousands of surfaces, a more efficient method is needed.

A way to speed the calculation consists in dividing the space in bonding volumes (this procedure is sometime called voxelization and the bounding volumes voxels). The ray-surface intersection algorithm is then only applied to the surfaces contained in the bounding volumes intersected by the ray path. An efficient algorithm for the calculation of the ray-box intersection is presented in Ref. [2-11]. In the example of Fig. 2-10, the ray intersects a surface in the fourth bounding volume found along the ray path. In this case, the ray-surface intersection algorithm has been applied to only six surfaces (contained in the bounding volumes 1, 2, 3 and 4).

At each intersection point, the rays change their direction of propagation by refraction, reflection, diffraction or scattering. Appendices A and B give the equations used for

the calculation of the direction of propagation. At the difference with sequential ray-tracing where only one (main) direction of propagation is considered, non-sequential ray-tracing programs take into account all the possible directions of propagation. This difference is illustrated in Fig. 2-11 for the case of a refractive surface.

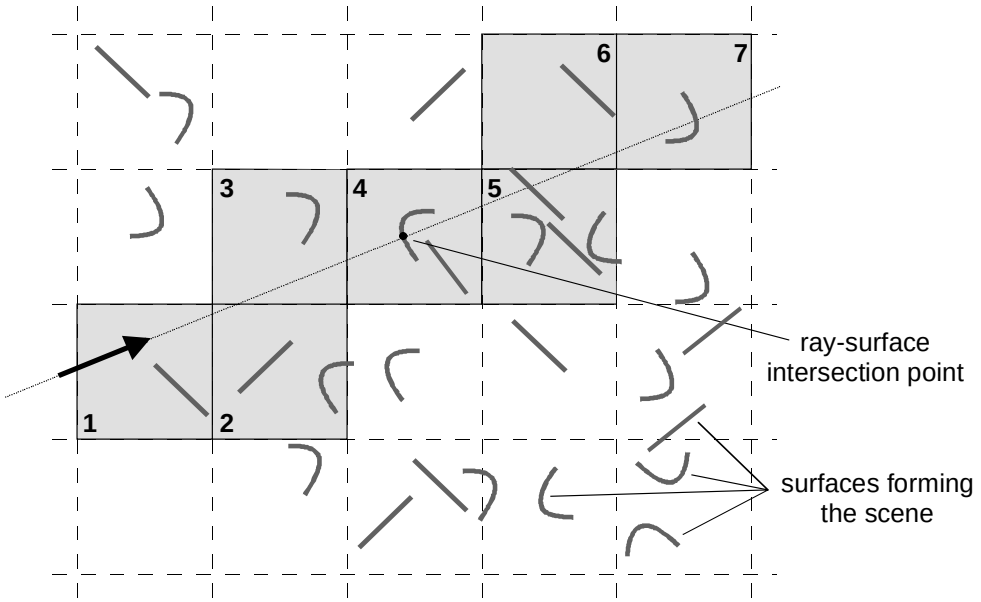

Fig. 2-10 Optimization of the ray-surface intersection algorithm by dividing the space in bonding volumes.

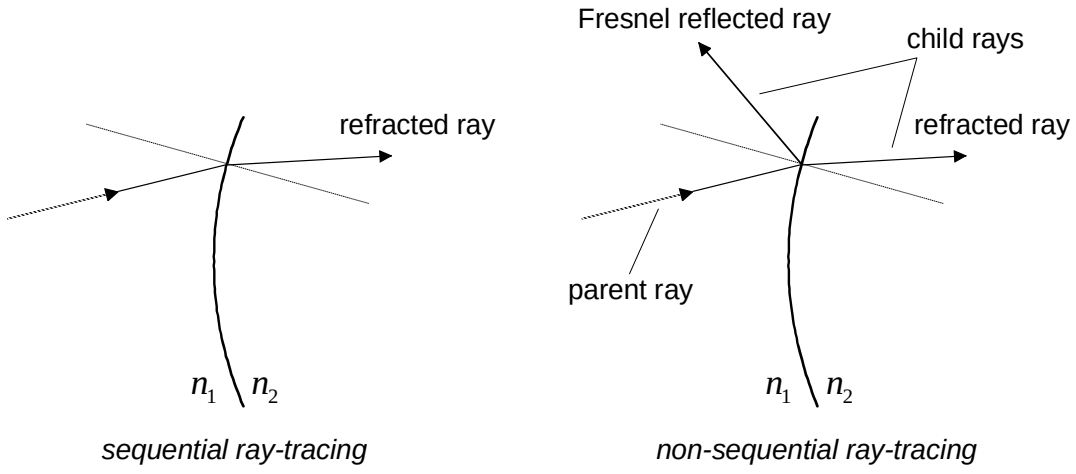

Fig. 2-11 Directions of propagation taken into account at the ray-surface intersection point for a refractive surface.

Non-sequential ray-tracing programs take into account the flux transported per ray. As shown in Fig. 2-11, the flux is spread out between reflected and transmitted rays at the

ray-surface intersection point. Moreover part of the power may be absorbed at the interface. One simulation method consists in splitting the incident (parent) ray into child rays and attributing the corresponding flux to each child ray. The *ray-splitting approach* is very intuitive. But, as the rays split at each intersection, the number of rays increases exponentially during the ray-tracing process. As the ray properties need to be stored until the ray reaches the final target (detector, or free space), the computer storage capacities may be exceeded during the ray-tracing process.

The ray-splitting method requires some care to guaranty the correctness of the simulation. The necessity to introduce a *cutoff condition* in order to avoid the endless generation of rays is illustrated in Fig. 2-12a. In this case, a few percents of the incident flux is reflected between the two surfaces. The generation of child rays is stopped when the ray flux is lower than the predefined cutoff condition. Note that, as the light used in illumination devices is incoherent, there is no interference effects to take into account in the configuration of Fig. 2-12a. In case of surface scattering, the repartition of the flux is defined by the BSDF of the given surface. The BSDF can be simulated by the statistical generation of a finite number of child rays. The number of generated child rays is called the *split ray number*; it has a value of three in the example shown in Fig. 2-12b. The choice of the cutoff condition and the split ray number is a compromise between the required precision of the simulation and the limits of the computer resources (computing time and storage capacities).

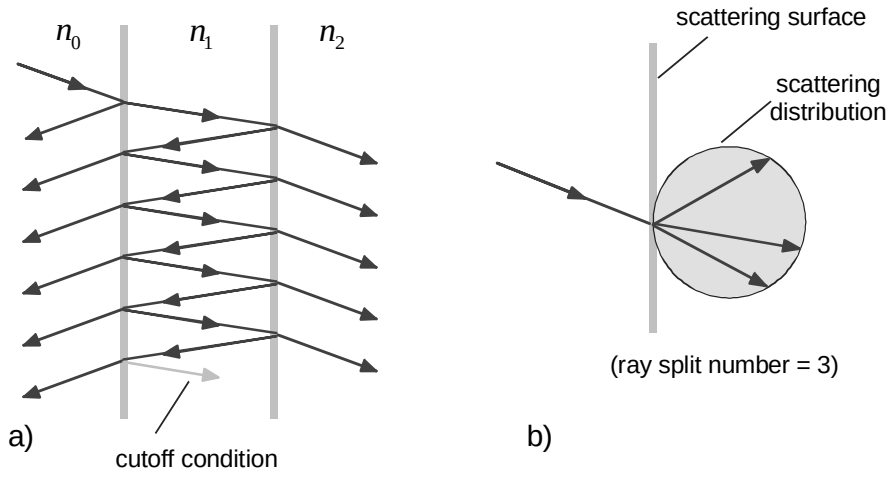

Fig. 2-12 Illustration of the parameters required by the ray splitting algorithm : a) cutoff condition, b) split ray number.

An alternative to the ray-splitting method is to consider only one direction of propagation at each interface (think to it as "one ray in, one ray out"). In this case the flux per ray is kept constant and the direction of propagation is chosen statistically. This method is sometime referred as the photon approach (a photon does not split), or more generally as *Monte Carlo ray-tracing*. The Monte Carlo method does not require the definition of any cut-off or sampling parameter. The designer only needs to increase the number of rays emitted by the source until the power distribution on the detectors converges (minimization of the signal-to-noise ratio).

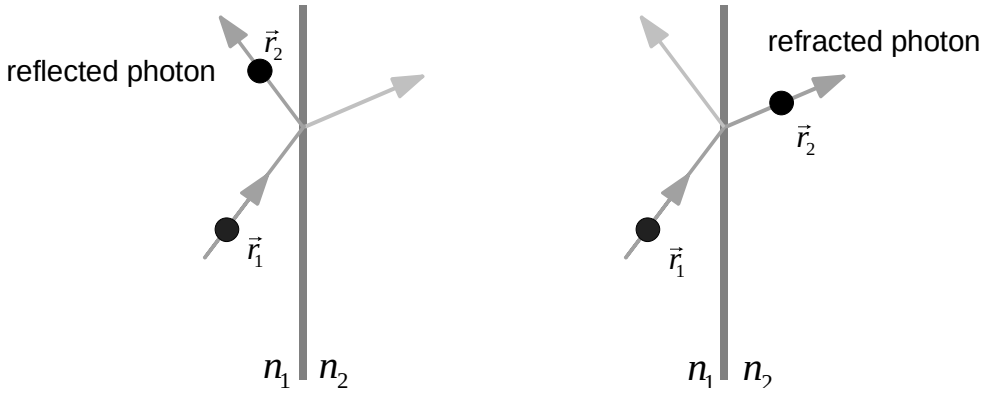

Fig. 2-13 Illustration of Monte Carlo ray-tracing at a refractive surface; the ray, or photon, is either refracted or reflected.

Table 2-1 summarizes the relations involved in the calculation of possible ray-surface interactions (see Appendices B and C for a discussion on the calculation of scattering distributions and Fresnel equations). We observe that the splitting of the flux depends on the surface properties, as well as on the direction and state of polarization of the incident ray.

Inside an absorbing media (defined by the extinction coefficient α), the ray flux ϕ varies with the ray path length z. The flux becomes

$$\phi(z) = \phi_0 \exp(-\alpha \cdot z) \,, \tag{2-4}$$

where ϕ_0 represents the initial flux of the ray. In case of Monte Carlo ray-tracing (the ray flux is kept constant), the existence or the extinction of a ray propagating through an absorbing media is determined statistically.

Surface type	Equation / Law	Interface parameters	Optical effect	
polished dielectric surface	Fresnel reflection/refraction	○ refractive indices	specular reflection and refraction	
polished metallic surface	Fresnel reflection	○ refractive index of propagation media, and (complex) refractive index of metal	specular reflection and metallic absorption	
surface coated with dielectric thin film(s)	single or multiplayer thin film calculation	○ refractive indices of surrounding medias ○ refractive indices of coatings	high specular refraction, and low specular reflection (anti-reflection coating)	
rough surface (reflective or refractive)	measured or calculated BSDF	○ refractive indices ○ statistical parameters of the surface profile	specular reflection / refraction and directive scattering	
surface coated with a volume scattering layer	measured or calculated BSDF	○ refractive indices ○ statistical distribution of molecules within the volume	specular reflection / refraction and Lambertian scattering	
surface coated with a diffraction grating (reflective or refractive)	measured or calculated grating efficiency	○ refractive indices ○ local grating period and local grating profile	specular reflection / refraction in the diffraction order directions	

Table 2-1 Possible power re-distribution at the ray-surface interface.

The ray tracing process is finished once all the rays (or photons) emitted by the source are either, intercepted by the detectors, absorbed inside the optical system, or propagated in free space to infinity. If the power distribution observed on the detector is too noisy, the number of rays emitted by the source is increased until the signal-to-noise ratio reaches acceptable levels.

Evaluation of the design

The design evaluation consists in comparing the simulated performances of the illumination device with the predefined optical requirements. Generally, the values of interest are : the distribution of the illumination on the detector(s), the direction of the illumination rays, and for some applications, the state of polarization of the illumination rays.

The illumination setup of Fig. 2-14 serves to illustrate typical analysis outputs. The irradiance map (Fig. 2-15) and intensity plot (Fig. 2-16) show the state of the illumination on the observation disk. We observe that the illumination is very directive and most of the flux is concentrated in the center of the disk.

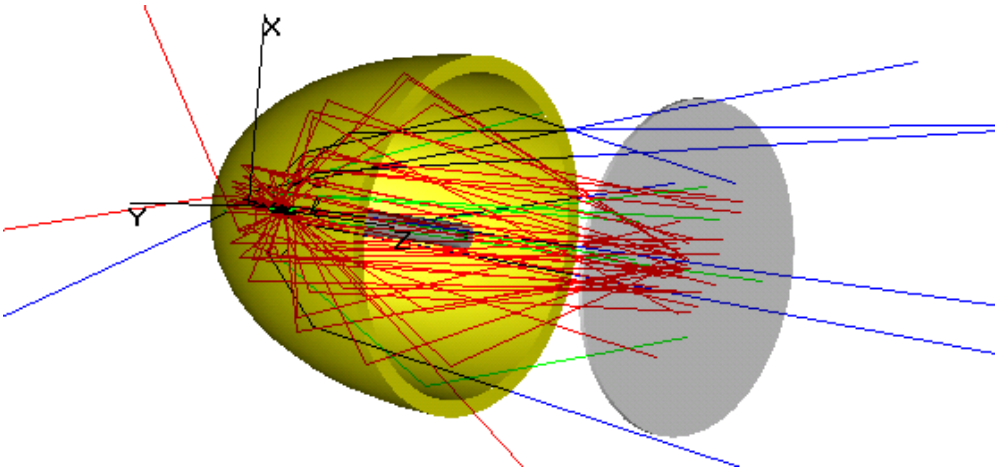

Fig. 2-14 Illumination device composed by a bulb source, a reflector, and an observation disk.
Modeled with the modeling and analysis tool TracePro ® (courtesy of Lambda Research Corp.).

Figure 2-17 illustrates the analysis of the state of polarization of rays going through a birefringence material. Actually all the rays have a linear polarization. The circular and elliptical polarizations are achieved by the superposition of several rays having a tilted

linear polarization. For instance, the analysis of the state of polarization is a critical step in optimization process of LCD back-lighting devices.

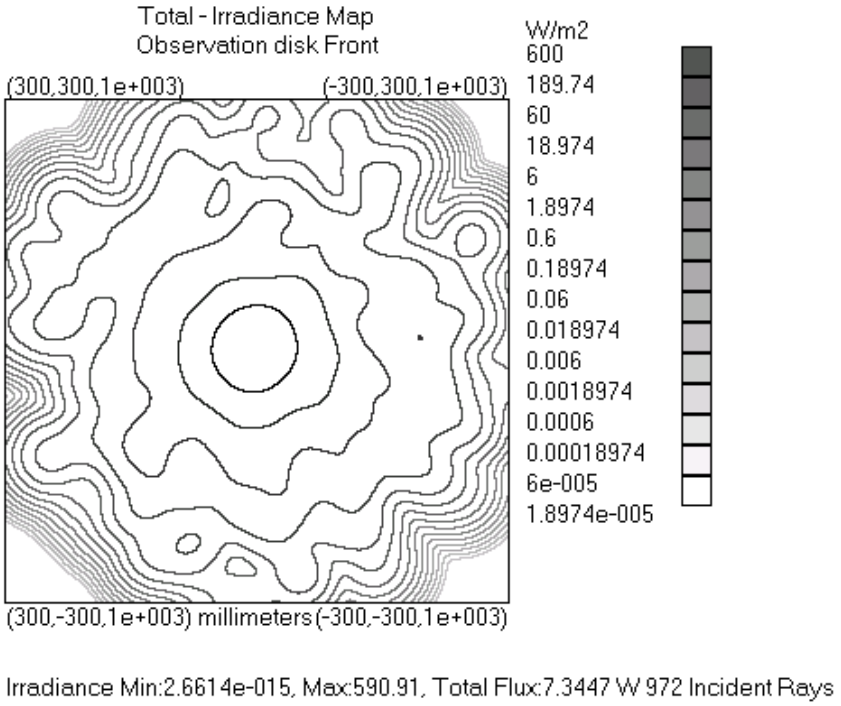

Fig. 2-15 Irradiance map as observed on the observation disk.

Modeled with the modeling and analysis tool TracePro ® (courtesy of Lambda Research Corp.).

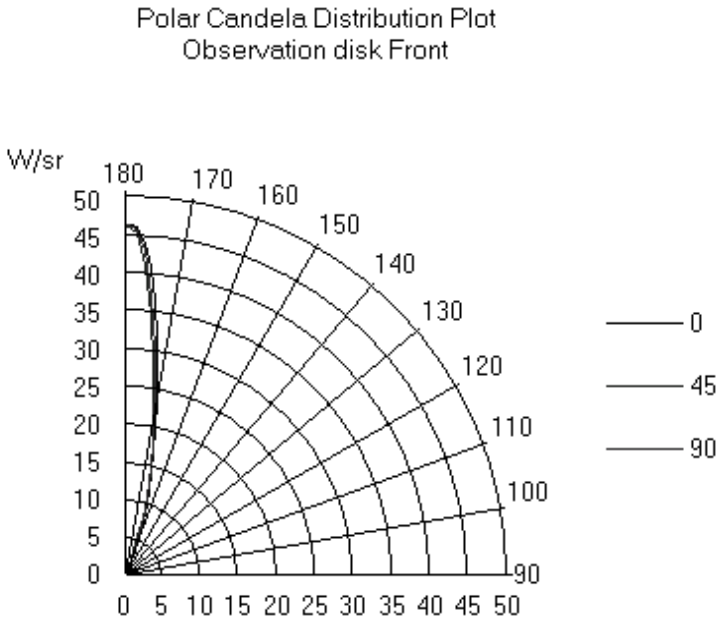

Fig. 2-16 Intensity plot as observed on the observation disk.

Modeled with the modeling and analysis tool TracePro ® (courtesy of Lambda Research Corp.).

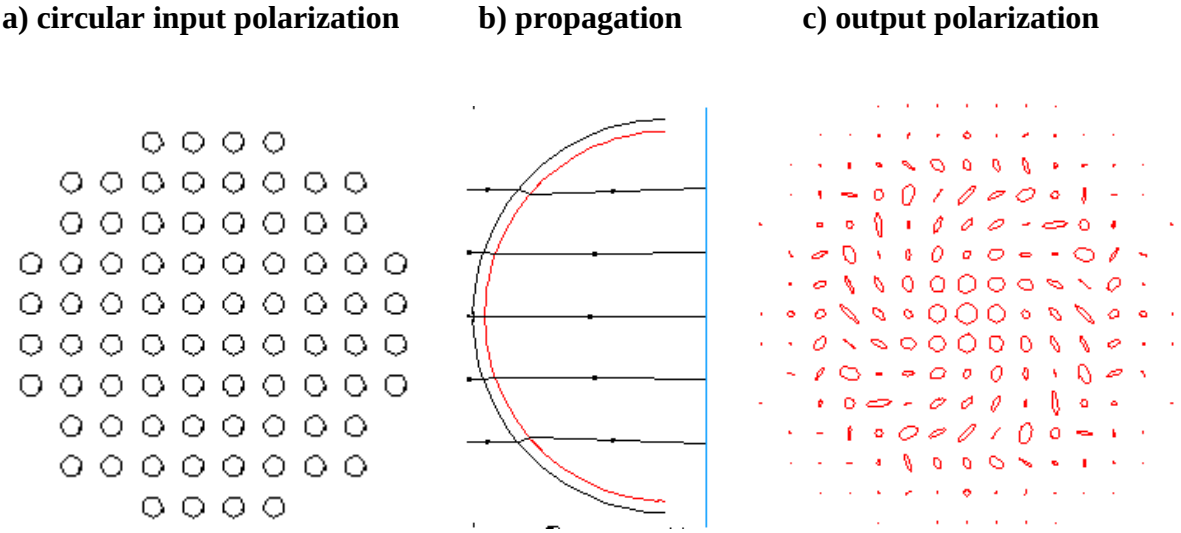

Fig. 2-17 Ray-tracing analysis of the state of polarization of a beam propagating through a birefringent material (sapphire dome).

Modeled in the optical and analysis design tool ASAP ™ (courtesy of Breault Research Organization, Inc.).

2.1.2 Global illumination

Global illumination refers to the techniques used by the computer graphics industry for the rendering of 3D scenes. The term *global illumination* means that the illumination of a surface does not only depend on light coming directly from the light sources, but also from the multiple reflections coming from the surrounding scene. Originally, global illumination has been used for the realization of virtual scenes; the emphasis being put on the aspect of the synthesized images. However, with the increase of the computer power and the evolution of computational algorithms, programs based on global illumination are slowly moving towards true simulation tools.

Strictly speaking non-sequential ray-tracing is a global illumination algorithm. However, global illumination refers generally to non exact, but computer efficient, techniques conceived for the approximate simulation of complex scenes. We show that if applied correctly, these techniques can also be valuable engineering tools for the analysis of illumination devices. This is particularly true for the calculation of complex diffusing scenes, where the amount of rays necessary for the ray-tracing analysis can quickly become prohibitive. One of the criteria slowing down the acceptance of global illumina-

tion comes from the lack of industrial tools (with the notable exception of the stray light analysis program APART© [2-12]). Actually, architecture is today the only engineering domain which makes extensive use of global illumination for the simulation of interior house lighting [2-13]. There is no doubt that new fields of application will emerge.

There is a family of global illumination algorithms which describe the exchange of radiant flux between surface elements (or patches). Thus, as shown in Fig. 2-18, the first step consists of dividing the scene in patches. This process is similar to the meshing used in finite element analysis (FEA). However, as discussed later in this chapter, the meshing criteria for global illumination differs from those of FEA. Each patch of the scene is then characterized by its emission and its BSDF. In this context, a source is simply defined by a set of non zero emission patches. There exist different algorithms which may be used for the calculation of the global illumination. The algorithm is chosen in function of the required degree of precision and its computing efficiency. The next subsections discuss the *radiance equation* method and its simplified version: the *radiosity* algorithm. Finally, once computed, the scene needs to be visualized. The fact that the viewing angle can be chosen and changed without a complete recalculation of the scene is one of the nice properties of radiosity.

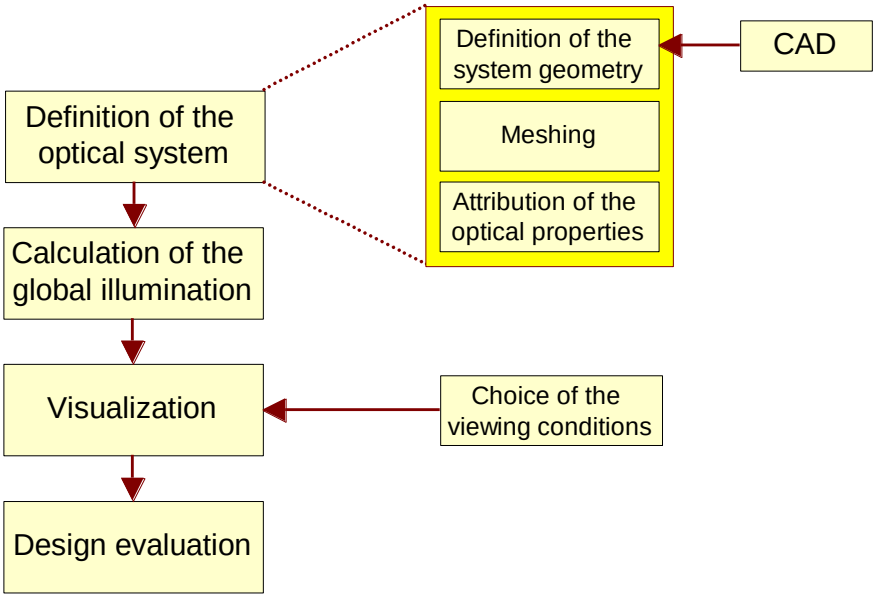

Fig.2-18 Flowchart of the analysis by global illumination algorithms.

2.1.2.1 The radiance equation

As shown in Eq. (2-2), the radiance L represents the flux by unit solid angle leaving and/or reaching a surface element. Radiance is the value used to express the exchange of flux between two surface elements, which is given by the *Fundamental Theorem of Radiometry*

$$d\phi = L_{12}\,\frac{dA_1\cos\theta_1 \cdot dA_2\cos\theta_2}{r^2}\ , \qquad (2\text{-}5)$$

where dA_1 and dA_2 are surface elements, r is the distance between the two surface elements, θ_{1_i} and θ_2 are the angles between the two surface elements and the line joining the surfaces, L_{12} is the radiance emitted by dA_1 in the direction of dA_2, and $d\phi$ is the flux incident on the surface element dA_2. Note that the flux is considered as constant within each surface element.

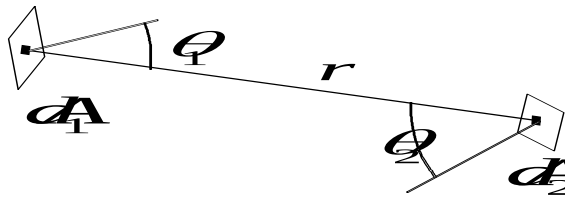

Fig. 2-19 Exchange of flux between two surface elements (patches).

The radiance has the interesting property to be invariant along the direction of propagation. Therefore, the radiance L_{12} emitted from dA_1 in direction of dA_2, is the same as the radiance L_{21} received by dA_2 from dA_1 ($L_{12} = L_{21}$).

The energy equilibrium for each patch of the scene is expressed by the *radiance equation* (also called the *global illumination equation*, see Refs 14 and 15 for a detailed discussion)

$$L(x,\theta_0,\phi_0) = L_e(x,\theta_0,\phi_0) + \int_{\Omega} \rho(x,\theta_0,\phi_0,\theta,\phi)\cdot L_i(x,\theta,\phi)\cdot\cos\theta\cdot d\omega\ . \qquad (2\text{-}6)$$

The radiance equation says that the emitted radiance L of a surface element centered in x corresponds to its proper emission L_e, plus the radiance L_i received from the surrounding scene multiplied by the BSDF ρ of the surface. The meaning of the different terms of the global illumination equation is summarized hereafter (see Fig. 2-21 for the geometrical definitions) :

- $L(x,\theta_0,\phi_0)$ is the radiance leaving point *x* in direction (θ_0,ϕ_0);
- $L_e(x,\theta_0,\phi_0)$ is the emitted radiance leaving point *x* in direction (θ_0,ϕ_0) ($L_e \neq 0$ for light sources);
- $L_i(x,\theta,\phi)$ is the incident radiance reaching point *x* from direction (θ,ϕ);
- $\cos\theta$ represents the relative orientation of the surrounding surface elements;
- Ω is a sphere (or half sphere for reflecting surface) centered at point *x*;
- $\rho(x,\theta_0,\phi_0,\theta,\phi)$ is the bidirectional scattering distribution function.

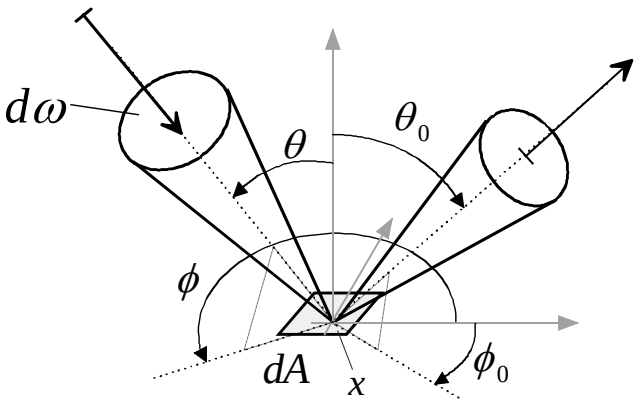

Fig. 2-20 Geometrical definitions used by the global illumination equation.

If the scene is considered as a set of patches, the radiance of the patch P_i is expressed as proper emission of the patch plus the sum of the individual contributions of the different patches of the scene. The contribution of the patch P_j on the patch P_i is expressed by an integral on P_j. The radiance equation can be rewritten as

$$L(x_i,\theta_0,\phi_0) = L_e(x_i,\theta_0,\phi_0) + \sum_j \int_{P_j} \rho(x_i,\theta_0,\phi_0,\theta,\phi)\cdot L_i(x_i,\theta,\phi)\cdot H(x_i,x_j)\cdot \gamma(x_i,x_j)\cdot dA_j \quad . \tag{2-7}$$

$H(x_i, x_j)$ is the *visibility function* between the patches P_j and P_i (takes the value 0 or 1). $\gamma(x_i, x_j)$ describes the geometrical configuration of the scene and is independent of its optical characteristics

$$\gamma(x_i, x_j) = \frac{\cos\theta_{i,j} \cdot \cos\theta_{j,i}}{|\mathbf{r}_{ij}|} \quad . \tag{2-8}$$

As shown in Fig. 2-21, $\mathbf{r}_{ij}$ represents the vector going from the patch P_i ($x_i \in P_i$) to the patch P_j ($x_j \in P_j$), $\theta_{i,j}$ is the angle between the patch P_i and the vector $\mathbf{r}_{ij}$, $\theta_{j,i}$ is the angle between the patch P_j and the vector $\mathbf{r}_{ji}$ ($\mathbf{r}_{ji} = -\mathbf{r}_{ij}$).

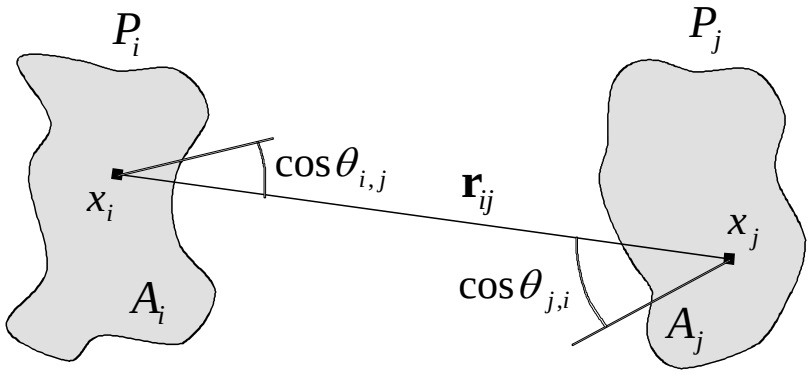

Fig. 2-21 Geometrical parameters for the determination of $\gamma(x_i, x_j)$.

The calculation problem

The radiance equation can be solved by the finite element method, as presented in Refs. [2-14] and [2-15]. However, the exact computation of Eq. (2-7) is very time consuming, making its use impractical in most cases. Different simplifications to the radiance equation have been proposed, which reduce the computation time at the expense of the precision of the simulation. The well known *radiosity* algorithm, presented in the next subsection, is a simplified version of the radiance equation for Lambertian diffusing patches. The computation time will also be minimized if the size of the patches is adapted to the local variation of the radiance. The meshing strategy is discussed in the next subsection for the radiosity case.

2.1.2.2 Radiosity

The radiance equation should not be mixed up with the radiosity algorithm extensively used in the computer graphics community (see [2-14] and [2-15]). Radiosity makes the assumption that all the surfaces of the scene are Lambertian diffusers. In spite of this crude approximation, simulations made with the radiosity algorithm give good results in many cases.

The radiosity B corresponds to the radiant exitance of a Lambertian diffusing patch. In this case, the radiance and the radiosity are related by the following equation

$$B = \int_{\Omega} L \cdot d\omega = \pi \cdot L \ . \tag{2-9}$$

Once the scene has been meshed, the exchange of radiant flux between Lambertian diffusing patches is defined by the following equation

$$B_i = \underbrace{E_i}_{\substack{\text{exitance} \\ \text{of the patch}}} + \underbrace{\rho_i \sum_{j}^{N} F_{ij} \cdot B_j}_{\substack{\text{response to the stimulation} \\ \text{of the other patches}}} \ , \tag{2-10}$$

where B_i is the radiosity of the considered patch, E_i the proper radiant irradiance of the patch (nonzero for light sources), B_j the radiant exitance of the other patches of the scene, F_{ij} the form factor between the patches i and j, ρ_i the reflectivity of the patch i, and N the number of patches of the scene.

Equation (2-10) has to be compared with the discrete form of the radiance equation (Eq. (2-7)). We observe that the radiance terms, which depend on the considered direction, have been replaced by radiant exitance and irradiance terms (scalars). Moreover the BSDF term (double directional dependency) has been replaced by the patch reflectivity (scalar).

The form factor

The form factor F_{ij} can be interpreted as the relative flux emitted by the patch P_j which is intercepted by the patch P_i. Based on the definitions given in Fig. 2-21, the form factor of the radiosity equation becomes

$$F_{ij} = \frac{1}{A_i}\int_{x_i \in P_i}\int_{x_j \in P_i} \frac{\cos\theta_i \cdot \cos\theta_j}{\pi\left|\mathbf{r}_{ij}\right|^2} H\left(x_i, x_j\right) dA_j\, dA_i \,. \qquad (2\text{-}11)$$

The meaning of the different terms of the form factor equation is summarized hereafter

- $\cos\theta_j$ Lambertian apodization of the radiant exitance of the surrounding patches;
- $\cos\theta_i$ obliquity factor;
- $\frac{1}{\pi\left|\mathbf{r}_{ij}\right|^2}$ the spherical attenuation of the propagating flux;
- $\frac{1}{A_i}\int_{x \in P_i} dA_i$ averages the irradiance over the full patch (the radiosity is considered as constant over each patch);
- $H\left(x_i, x_j\right)$ visibility function from point x_i to point x_j (takes value 0 or 1).

The calculation of the form factor can be very computer intensive. Nevertheless, some interesting properties can be used to reduce the computation time considerably. The form factor has the following properties (we let the interested reader look at Ref. [2-14] for the details)

- reciprocity : $\forall(i,j) \qquad A_i F_{ij} = A_j F_{ji}$ (2-12a)
- additivity : $F_{i(j\cup k)} = F_{ij} + F_{ik}$ (2-12b)
- conservation of energy : $\sum_{j=1}^{N} F_{ij} = 1$ (2-12c)

Equation (2-12c) is only valid in a non-absorbing closed environment for which no energy is lost. Equations (2-12) mean that unknown form factors can be derived from known ones, reducing the number of times the integral Eq. (2-11) has to be computed.

Meshing and visibility function

The calculation of the form factor is directly dependent on the meshing of the scene (number and disposition of the patches). The meshing should satisfy two main criteria : the BSDF ρ_i and the radiosity B_i are considered as constant within each patch i. In practice, the size of the patches need to be adapted to the materials and to the lighting conditions. The influence of the lighting conditions on the meshing is illustrated in Fig. 2-22. The sharp shadow cannot be reproduced exactly as the radiosity is averaged within each patch. The size of the patches is reduced along the shadow boundary in order to minimize this effect. The underlying consequence is that the meshing should be readapted if the position of the source is changed between two simulations.

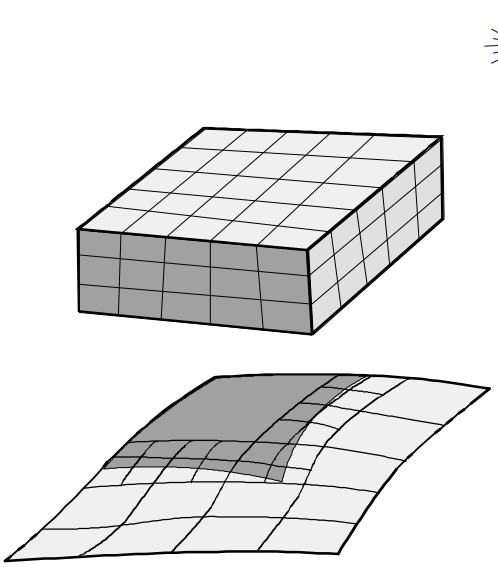

Fig. 2-22 Adaptation of the patch size to the lighting conditions. Observe the finer meshing along the shadow boundary.

The meaning of the visibility function $H(x_i, x_j)$ is illustrated in Fig. 2-23. The points x_{i1} and x_{j1} are visible to each other; thus, the visibility function takes the value 1. The points x_{i2} and x_{j2} are invisible to each other; in the case the visibility function takes the value 0.

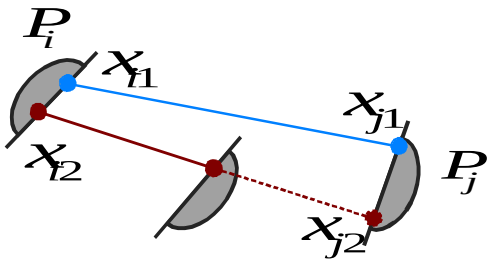

Fig.2-23 Illustration of two patches P_i and P_j partially visible to each other.

Calculation and visualization of results

The main interest of the radiosity equation (Eq. (2-10)) consists in its elegant calculation algorithms, which spare a lot of computer resources when compared to the radiance equation. Most of the resources are used for the calculation of the form factor F_{ij} (double integral, see Eq. (2-11)). The calculation time can be reduced by applying the different properties of the form factor (Eqs. (2-12)). Moreover, the form factor is independent of the optical properties of the scene. This means that different configurations of the same scene (e.g. change of the material properties) can be done without recalculating the form factor.

The radiosity (Eq. (2-9)) can be expressed in the form of a vector-matrix equation

$$\begin{pmatrix} B_1 \\ B_2 \\ \vdots \\ B_n \end{pmatrix} = \begin{pmatrix} E_1 \\ E_2 \\ \vdots \\ E_n \end{pmatrix} + \begin{pmatrix} \rho_1 F_{11} & \rho_1 F_{12} & \cdots & \rho_1 F_{1n} \\ \rho_2 F_{21} & \rho_2 F_{22} & & \vdots \\ \vdots & & \ddots & \\ \rho_n F_{n1} & \cdots & & \rho_n F_{nn} \end{pmatrix} \cdot \begin{pmatrix} B_1 \\ B_2 \\ \vdots \\ B_n \end{pmatrix}, \tag{2-13}$$

or

$$\begin{pmatrix} 1-\rho_1 F_{11} & -\rho_1 F_{12} & \cdots & -\rho_1 F_{1n} \\ -\rho_2 F_{21} & 1-\rho_2 F_{22} & & \vdots \\ \vdots & & \ddots & \\ -\rho_n F_{n1} & \cdots & & 1-\rho_n F_{nn} \end{pmatrix} \cdot \begin{pmatrix} B_1 \\ B_2 \\ \vdots \\ B_n \end{pmatrix} = \begin{pmatrix} E_1 \\ E_2 \\ \vdots \\ E_n \end{pmatrix}. \tag{2-14}$$

Equation (2-14) represents a set of linear equations of the type $\mathbf{M} \cdot \mathbf{B} = \mathbf{E}$, which has to be solved for the unknown vector $\mathbf{B}$. Different iterative techniques can be used to

solve this large set of equations. The application of different relaxation methods (Jacobi, Gauss-Seidel, Southwell, …) are discussed in Refs [2-14] and [2-15].

The physical underlying meaning of the radiosity equation is better understood if we express Eq. (2-13) as

$$\mathbf{B} = \mathbf{E} + \mathbf{R} \cdot \mathbf{B} \,, \tag{2-15}$$

where $\mathbf{R}$ is the reflectivity matrix. The radiosity vector can be found by expressing the last equation as a Neumann series (allowed because $\det(R) < 1$)

$$\mathbf{B} = [\mathbf{I} - \mathbf{R}]^{-1} \cdot \mathbf{E} = \sum_{n=0}^{\infty} (\mathbf{R})^n \cdot \mathbf{E} \,. \tag{2-16}$$

Equation (2-16) can be interpreted as the contribution of the different light sources of the scene, represented by the irradiance vector $\mathbf{E}$, which multiply the interreflection matrix $(\mathbf{R})^n$. In this case, $\mathbf{R}$ represents the contribution of one level of reflections, $\mathbf{R}^2$ the contribution of two levels of interreflections, $\mathbf{R}^3$ the contribution of three levels of interreflections, and so on. This means that the radiance equation calculates, simultaneously for all the patches of the scene, the irradiance contribution of all the surrounding patches taking into account all possible interreflections. The resulting simulation is thus independent of the point view (a virtual camera can observe the scene from any patch position).

The display of the results consists of reconstructing one or several views of the scene. The radiosities of the different patches are used as the input parameter of a shader which renders the scene to the computer screen.

The different steps of a simulation based on the radiosity algorithm are summarized in Fig. 2-24. We observe that a change in the viewing conditions only requires the computation of the visualization of the scene. The observer can move around and observe the scene from different viewing points. The changes are computed in real time. In the case where some optical properties of the scene are changed, such as the reflectivity and/or the exitance of the patches, the radiosity equation needs to be recalculated by solving the system of linear equations represented by Eq. (2-14). Despite the large size

of the matrix, nowadays, the calculation of the radiosity equation does not take more than a few minutes. This is particularly interesting for the design (and optimization) of illumination devices. The consequences of a change of the materials and the sources can be quickly simulated. Finally, a change in the geometrical configuration of requires the recalculation of the form factors. This operation can be very time consuming. However, a small change in the geometrical configuration does not necessary require a complete recalculation of the matrix.

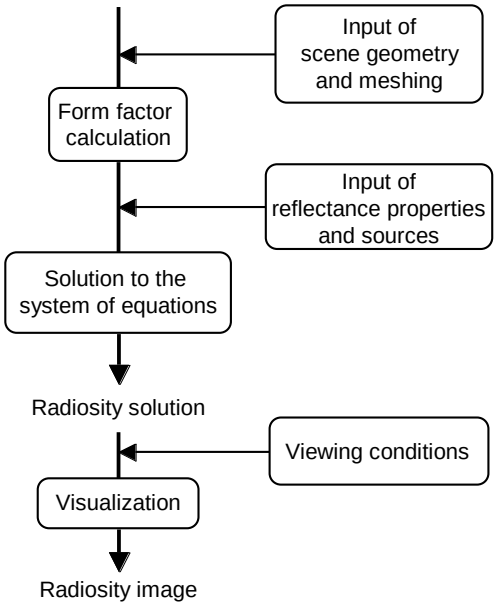

Fig. 2-24 The radiosity algorithm, as described by Sillion and Puech [2-14].

2.1.3 Discussion of the analysis methods

Three analysis methods used for the design of illumination devices, have been presented in the precedent sections: the non-sequential ray-tracing, the radiance equation (or global illumination equation), and the radiosity. These methods differ by the physical phenomenon they can describe, their precision, and their computing efficiency. Table 2-1 summarizes the characteristics of each method.

	specular	directive scattering	Lambertian scattering	diffraction	reflection	transmission	polarization	precision	computer efficiency
ray-tracing	+	±	±	+	+	+	+		
radiance equation	±	+	+	±	+	+	⌿		
radiosity	⌿	⌿	+	⌿	+	⌿	⌿		

Table 2-2 Evaluation of the basic analysis methods.

legend : + well adapted, ± more or less adapted, - badly adapted, ⌿ not supported, high, average, low

The computer efficiency of a method is strongly dependent on the configuration to analyze. This is shown in the case of the design of an illumination light pipe. Figure 2-25 illustrates schematically the situation. The light is emitted by the source **A** with a given angular spectrum and is coupled into the light pipe **B**. Within the light pipe, the light is either guided by total internal reflection (TIR), and/or coupled out from the pipe. The outcoupled portion of the light is used for the illumination of the screen **C**. The light is scattered by the screen and, finally, reaches the eye of the observer **D**. The light pipe can be designed in such a way that most of the light emitted by the source **A** reach the screen **C** (see Chapter 4 for details on the design). As all the rays participate to the functionality of the device, ray-tracing is perfectly adapted for the analysis of the propagation of the light from **A** to **C**. However, only a small fraction of the light scattered on the screen surface is going to reach the detector **D**. Ray-tracing is clearly not the more efficient approach for describing the propagation of light from **C** to **D** (most of the ray miss the detector). The radiance equation (or radiosity if the screen is a Lambertian diffuser) is a better approach for the analysis of the propagation from **C** to **D**.

Alternative methods have been developed to optimize the computation efficiency (see Refs. [2-14] and [2-15] for details). One solution consists of calculating the rays from the detector instead from the source (backwards ray-tracing). Alternatively, forwards and backwards ray-tracing may be combined, but limited to a few interreflections (bidi-

rectional ray-tracing). An efficient algorithm extensively used in computer graphics is to combine ray-tracing for the specular deviation of light, and radiosity for the diffuse reflection (two-pass method). Radiosity with directional radiance distribution may also be used for a more realistic simulation of diffusing scenes. One should be aware that most of these techniques come from the computer graphics industry, for which the aesthetic requirements prime over the correctness of the results. In other words, a nice simulation output is not the guarantee of a correct design.

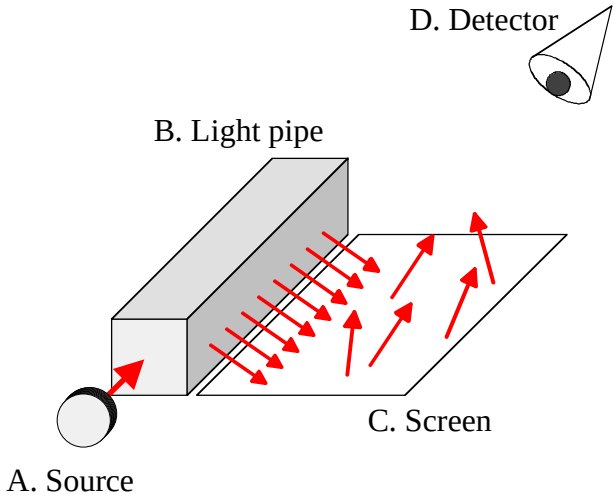

Fig. 2-25 Schematic representation of the light pipe illumination device.

Some physical phenomena are difficult to simulate with existing tools, e.g. volume scattering and fluorescence. A few Monte Carlo ray-tracing programs support volume scattering, but the related calculation are very computer intensive. Fluorescence introduces the wavelength dependency of the simulation. The simulation of polychromatic effects implies successive runs for different wavelength, resulting also in very long calculations.

However, the main limitation of all the presented methods is their lack of support of any optimization process. The next subsection presents the requirements of the optimization in the context of the illumination design; and subsection 2.3 proposes an optimization which could complement the presented analysis methods.

2.2 The optimization process

The first step of the design process is to find an initial design, which is supposed to partially fulfill the specifications of the device. The definition of the initial design is based on the designer's experience (or intuition). A first analysis will confirm or infirm the predicted results, but in most cases the design still needs some fine tuning before complying with the specifications. The optimization process is a loop where successive designs are evaluated until a design fulfilling the requirements is found (see Fig. 2-1).

The design evaluation is done looking at the root-mean-square deviation from a predefined merit function. In the case of illumination devices, the merit function can include criteria describing the distribution and efficiency of the illumination, the manufacturing constraints (feasibility and/or production cost), the electrical consumption of the device, etc. Between two iterations of the optimization process, the design is slightly modified by changing the values of a set of variable parameters. The choice of the variable parameters is closely related to the pre-defined merit function.

Contrary to the case of lens design [2-16], the optimization of illumination devices is an immature field. Beside some very specific applications (e.g. optimization of headlamp reflectors), there is no illumination design tool at the time of this writing, that implements an general optimization algorithm. The difficulty of the task comes from the large set of possible variable parameters. Moreover, the influence of a given parameter on the overall design performance is often difficult to grasp. The computing time necessary to the optimization is an other factor making traditional approaches unpractical. One single analysis done by non-sequential ray-tracing or global illumination may take several hours or days and the full optimization process may require several hundred of iterations.

Some recent commercial tools allow the automatic optimization of some specific configurations, like automotive headlamps. Generally however, the changed of the design parameters between two analysis is the responsibility of the designer.

2.3 Optical transfer blocks as a design strategy

The lack of optimization is clearly the weakness of current illumination design tools. The optimization will only become practical if the number of design parameters is reduced, as well as the computing time. A higher level of abstraction would allow a better view of the influence of a given parameter on the overall design performance. The *optical transfer block* (OTB) model constitutes an efficient approach proposed to fill some of actual limitations of illumination design tools.

The basic idea consists in describing the illumination device and the surrounding scene as a set of blocks. Each block is defined by an optical transmission function, which transforms incoming optical signals into some outgoing optical signals leaving by the block faces. This is illustrated in Fig. 2-27 for a cubic block, where one input signal i_1 produces the output signals $(o_1, o_2, o_3, o_4, o_5, o_6)$. In general, the input/output relation is described by the following vector matrix product

$$\mathbf{o} = \mathbf{T} \cdot \mathbf{i} \ , \tag{2-17}$$

where the dimensions of the vectors $\mathbf{i}$ and $\mathbf{o}$ corresponds to the number of faces of the block.

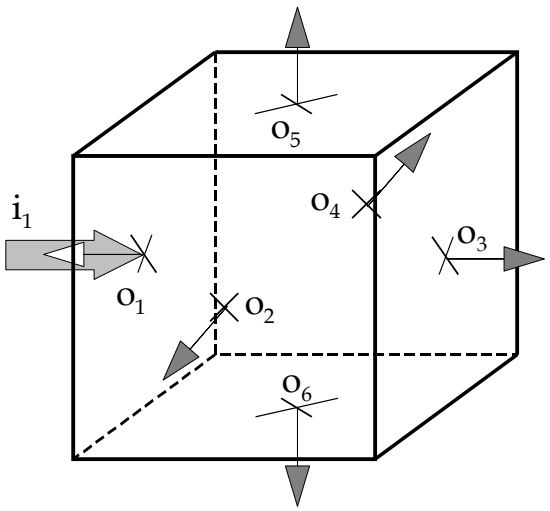

Fig. 2-26 Optical transfer block, in this case with one input signal i_1 and six output signals $(o_1, o_2, o_3, o_4, o_5, o_6)$.

At this stage, we are not interested in the physical phenomena inside the block, but only on its external optical response. The block acts as a black box. Moreover, we consider that the input and output signals are averaged for each block face. In other words, the optical characteristics of the block is described by only one input and one output signal per face.

The main interest of the OTB approach comes from the reduced set of parameters necessary to describe the block optical behavior. Moreover, complex configurations may be constructed starting from basic blocks. Ideally, the blocks could be compared to Lego® pieces, which can be connected to form bigger entities (see Fig. 2-27).

As already discussed, an illumination system is characterized by the produced distribution of light on the detector planes. The values to consider are radiometric quantities (see appendix D) and, for some applications, the polarization state. Thus, for each block face, the I/O signals may be defined by the three scalar quantities: the flux ϕ, the propagation angular spectrum ψ, and the polarization p. The block approach is valid if the I/O signals are representative of the transmission of energy through the full block face. In other words, the radiant energy is considered constant over each block face.

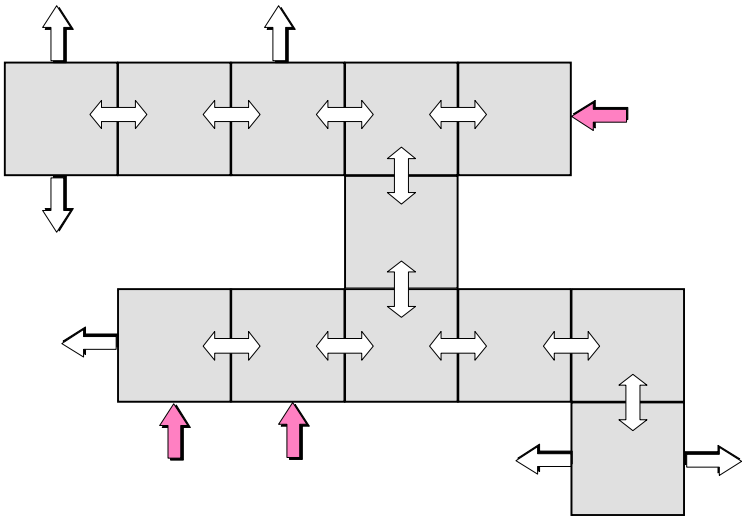

Fig. 2-27 Illustration of a system built by the assembling of OTBs.

The OTB method may not be applied to any optical configuration. Generally, an optical system cannot be simply described by the interactions of a few blocks. On the other hand, smaller blocks would improve the description of the system. In this case howev-

er, the high number of blocks would remove the main interest of the method : its simplicity. Nevertheless, the OTB method is well suited for the design of light pipes. In this case, each block describes the optical behavior of a section of the pipe. Each block is then considered as an autonomous entity whose design can be optimized locally.

The optical configurations which may be described by OTBs are rather limited. Thus OTBs do not constitute a general analysis method. However, it is perfectly possible to design and manufacture blocks which fulfill a predefined optical function. Thus the block approach constitutes a powerful design tool for the realization of sophisticated optical devices and more specifically for the realization of illumination light pipes.

The general I/O values can be applied to some very specific applications for which the lighting efficiency depends on the state of polarization. That is for example the case for the back-lighting of LCD displays. However, most applications can be build on more simple blocks, for which a reduced set of physical quantities is taken into account (see Fig. 2-28). The simpler models reduce the calculation and are simpler to connect.

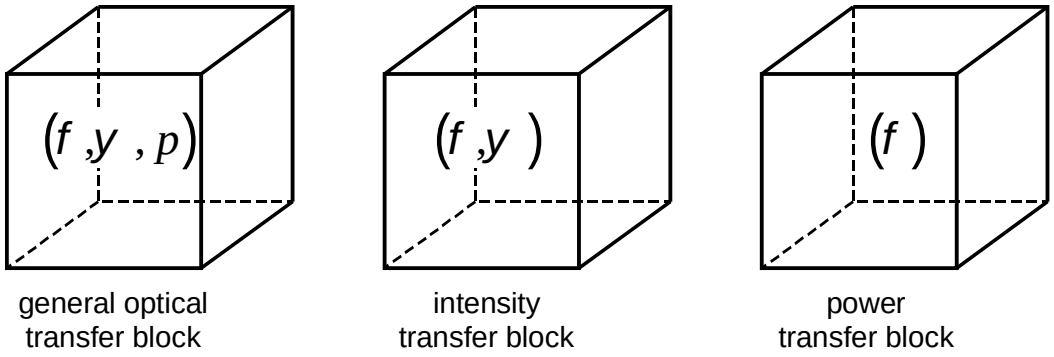

Fig. 2-28 Possible types of optical transfer blocks.

connectivity conditions

OTBs may vary in size and shape. This allow the representation of varying cross-section and curved light pipes. As for the Lego pieces, the block interconnection is only valid if some precise rules are respected. These interconnection rules are geometrical, but also based on the compatibility of the exchanged physical quantities. As illustrated in Fig. 2-29, the faces of two adjacent blocks must match perfectly in size and

position. The geometrical condition is imposed by the fact that the exchange radiant energy is constant over the full block face.

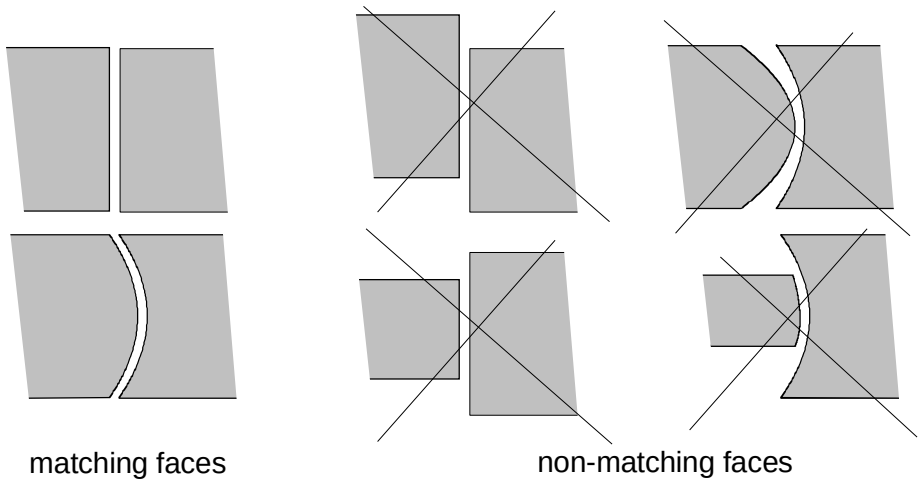

Fig. 2-29 Geometrical condition for OTB connectivity.

Moreover, each block face may have acceptance conditions which need to be respected by the adjacent blocks. These acceptance conditions could for example be the angle of acceptance of a fiber, or simply a power threshold above which the block would be destroyed due to thermal dissipation. In order to be connected, the output signals of each block have to be smaller than the acceptance conditions of the surrounding blocks.

calculation of the block assembly for the light pipe case

As shown hereafter for the single block case, the optical function of a block can be described as a vector-matrix product (i.e. a system of linear equations). The output signals (elements of the vector $\mathbf{o}$) are calculated by multiplying the input signals (elements of the vector $\mathbf{i}$) by the block transmission function (matrix $\mathbf{T}$)

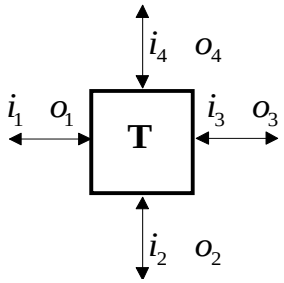

$$\mathbf{o} = \mathbf{T} \times \mathbf{i} \quad . \tag{2-18}$$

The macroscopic behavior of an illumination light pipe can be simulated by assembling several OTBs. In this case, as shown in Fig. 2-30, each block i is characterized by its block transmission function ${}^{i}T$, the fluxes entering into the block by the left l_i and by the right r_i, the outcoupled flux o_i, and the lost flux a_i (absorbed or outcoupled in a bad direction).

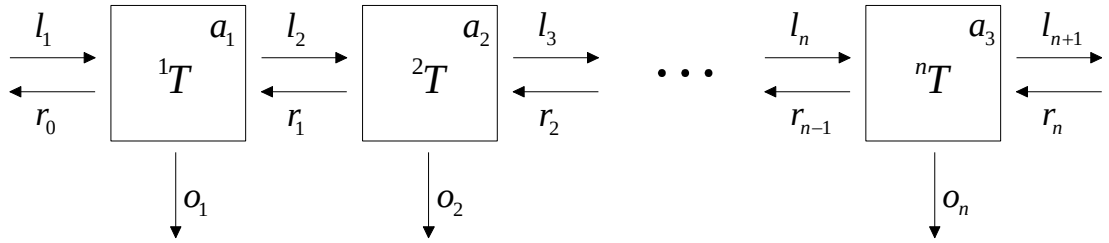

Fig. 2-30 Block assembly forming an illumination light pipe.

The balance of energy is calculated for each block i by the following equation

$$\begin{pmatrix} {}^{i}t_{11} & {}^{i}t_{12} & 0 & 0 \\ {}^{i}t_{21} & {}^{i}t_{22} & 0 & 0 \\ {}^{i}t_{31} & {}^{i}t_{32} & 0 & 0 \\ {}^{i}t_{41} & {}^{i}t_{42} & 0 & 0 \end{pmatrix} \cdot \begin{pmatrix} l_i \\ r_i \\ 0 \\ 0 \end{pmatrix} = \begin{pmatrix} l_{i+1} \\ r_{i-1} \\ o_i \\ a_i \end{pmatrix} . \tag{2-19}$$

For each block, the conservation of energy implies that

$$\begin{aligned} l_i + r_i &= l_{i+1} + r_{i-1} + o_i + a_i \\ &= \left({}^{i}t_{11} \cdot l_i + {}^{i}t_{12} \cdot r_i\right) + \left({}^{i}t_{21} \cdot l_i + {}^{i}t_{22} \cdot r_i\right) + \left({}^{i}t_{31} \cdot l_i + {}^{i}t_{32} \cdot r_i\right) + \left({}^{i}t_{41} \cdot l_i + {}^{i}t_{42} \cdot r_i\right) , \end{aligned} \tag{2-20}$$

or

$$l_i\left(1 - {}^{i}t_{11} - {}^{i}t_{21} - {}^{i}t_{31} - {}^{i}t_{41}\right) + r_i\left(1 - {}^{i}t_{12} - {}^{i}t_{22} - {}^{i}t_{32} - {}^{i}t_{42}\right) = 0 . \tag{2-21}$$

As this condition is independent of the flux entering into the block, we get the two following conditions for the block transmission function ${}^{i}T$

$$\begin{aligned} {}^{i}t_{11} + {}^{i}t_{21} + {}^{i}t_{31} + {}^{i}t_{41} &= 1 \\ {}^{i}t_{12} + {}^{i}t_{22} + {}^{i}t_{32} + {}^{i}t_{42} &= 1 \end{aligned} . \tag{2-22}$$

For a given block, the calculation of the guided, outcoupled and lost fluxes can be done independently (see Eq. 2-19). The strategy consists in calculating first the guided fluxes l_i and r_i all along the pipe, and then the fluxes o_i and a_i for each block.

The exchange of flux along the pipe is expressed by a set of linear equations which may be represented as

$$\begin{pmatrix} {}^1t_{11} & {}^1t_{12} & 0 & 0 & \cdots & 0 & 0 \\ {}^1t_{21} & {}^1t_{22} & 0 & 0 & \cdots & 0 & 0 \\ 0 & 0 & {}^2t_{11} & {}^2t_{12} & \cdots & 0 & 0 \\ 0 & 0 & {}^2t_{21} & {}^2t_{22} & \cdots & 0 & 0 \\ \vdots & \vdots & \vdots & \vdots & \ddots & \vdots & \vdots \\ 0 & 0 & 0 & 0 & \cdots & {}^nt_{11} & {}^nt_{12} \\ 0 & 0 & 0 & 0 & \cdots & {}^nt_{21} & {}^nt_{22} \end{pmatrix} \cdot \begin{pmatrix} l_1 \\ r_1 \\ l_2 \\ r_2 \\ \\ l_n \\ r_n \end{pmatrix} = \begin{pmatrix} l_2 \\ r_0 \\ l_3 \\ r_1 \\ \\ l_{n+1} \\ r_{n-1} \end{pmatrix} . \qquad (2\text{-}23)$$

The boundary conditions are given by the flux injected into the pipe at its extremities (the flux l_1 at its left extremity and the flux r_n at its right extremity). Equation (2-23) represents a set of n equations with n unknowns. The equation can be solved directly when represented in the form $\mathbf{A}\cdot\mathbf{x}=\mathbf{b}$ (see Eq. (2-24)). Note that the matrix in Eq. (2-24) is sparse and band diagonal. Different algorithms for the resolution of sparse linear systems, such as the conjugate gradient method, are discussed in [2-17, chapter 2]. The use of relaxation methods [2-17, chapter 17] may also be considered if the size of the matrix becomes too large. This is generally not the case for light pipes which are normally limited to a few hundred blocks.

$$\begin{pmatrix} 0 & 1 & 0 & 0 & 0 & 0 & \cdots & 0 & 0 & 0 & 0 \\ 0 & {}^1t_{11} & {}^1t_{12} & -1 & 0 & 0 & \cdots & 0 & 0 & 0 & 0 \\ -1 & {}^1t_{21} & {}^1t_{22} & 0 & 0 & 0 & \cdots & 0 & 0 & 0 & 0 \\ 0 & 0 & 0 & {}^2t_{11} & {}^2t_{12} & -1 & \cdots & 0 & 0 & 0 & 0 \\ 0 & 0 & -1 & {}^2t_{21} & {}^2t_{22} & 0 & \cdots & 0 & 0 & 0 & 0 \\ \vdots & \vdots & \vdots & \vdots & \vdots & \vdots & \ddots & \vdots & \vdots & \vdots & \vdots \\ 0 & 0 & 0 & 0 & 0 & 0 & \cdots & 0 & {}^nt_{11} & {}^nt_{12} & -1 \\ 0 & 0 & 0 & 0 & 0 & 0 & \cdots & -1 & {}^nt_{21} & {}^nt_{22} & 0 \\ 0 & 0 & 0 & 0 & 0 & 0 & \cdots & 0 & 0 & 1 & 0 \end{pmatrix} \cdot \begin{pmatrix} r_0 \\ l_1 \\ r_1 \\ l_2 \\ r_2 \\ \vdots \\ l_n \\ r_n \\ l_{n+1} \end{pmatrix} = \begin{pmatrix} l_1 \\ 0 \\ 0 \\ 0 \\ 0 \\ \vdots \\ 0 \\ 0 \\ r_n \end{pmatrix} . \qquad (2\text{-}24)$$

The OTBs are certainly not a practical method for the design of all optical devices. In the light pipe case however, the calculation is quite simple. We show in the next chapters that the OTB method constitutes an efficient approach for the design and the optimization of illumination light pipes.

2.4 Reviewed design process

We have presented different methods for the analysis of illumination devices. These methods differ by their precision and computing efficiency, but they all lack an efficient optimization algorithm.

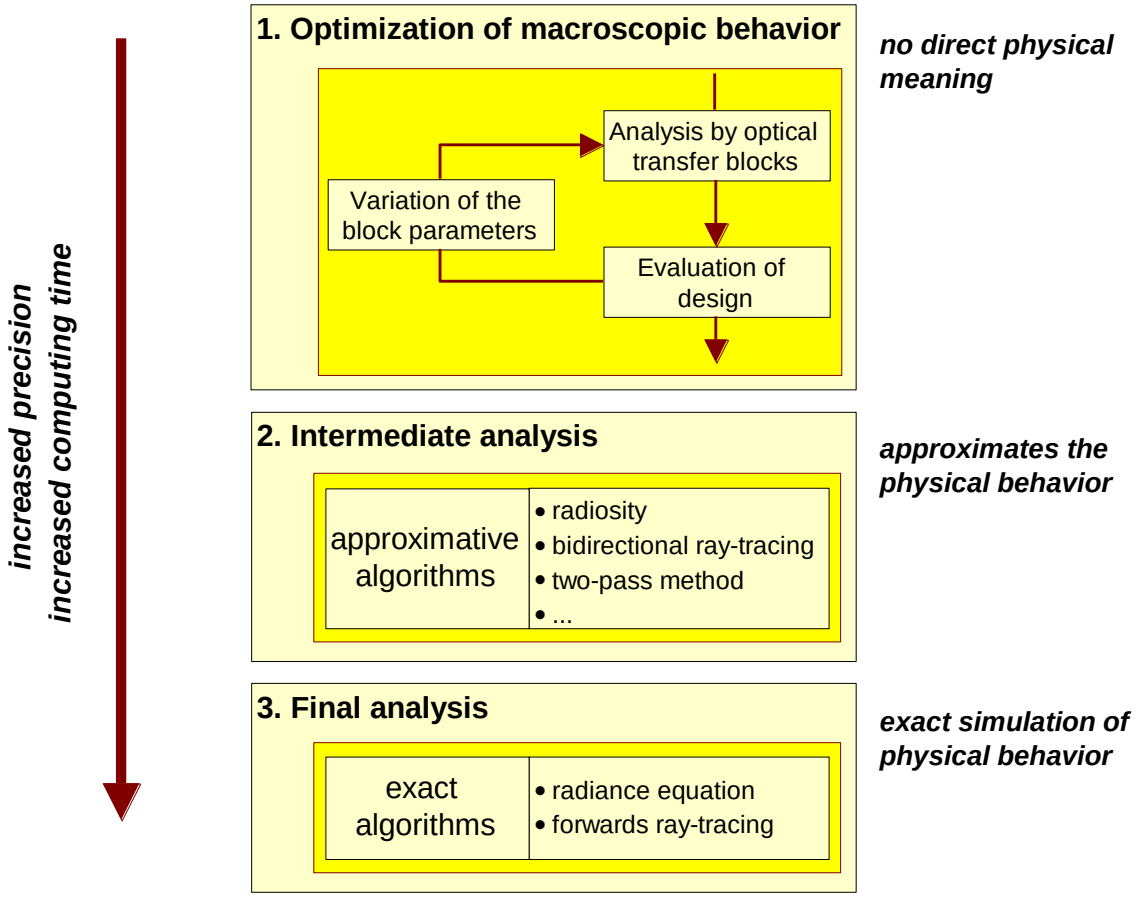

Fig. 2-32 Hierarchical design approach.

A hierarchical design approach would allow to start with a coarse description of the system. At this stage the system would be described by a reduce set of parameters and

thus would be easy to optimize. Then, by successive refinements, the precision of the simulations would be increased until the physical behavior of the illumination device is verified. Figure 2-32 illustrates the role of the introduced OTB method, as well as the presented analysis methods. We have shown however that the OTB method is too limited to be used for the analysis of general optical devices.

The OTB method is more interesting to build complex optical devices. This is particularly true for the design of illumination light pipes, which can be considered as the cascade of OTBs. The behavior of the illumination device in its surrounding environment is then verified by an analysis method.

2.5 References

[2-1] W. B. Elmer, *The Optical Design of Reflectors*, John Wiley & Sons, 1980

[2-2] W.T. Welford, *High Collection Nonimaging Optics*, Academic Press, 1989

[2-3] R. Petit, ed., *Electromagnetic Theory of Gratings*, Springer-Verlag, 1980

[2-4] H.C. van de Hulst, *Light Scattering by Small Particles*, Dover Publications, 1981

[2-5] P. Beckmann, A. Spizzichino, *The Scattering of Electromagnetic Waves from Rough Surfaces*, Artech House, 1987

[2-6] J.C. Stover, *Optical Scattering: Measurement and Analysis*, SPIE Optical Engineering Press, 1995

[2-7] J.M. Bennett, L. Mattsson, *Introduction to Surface Roughness and Scattering*, Optical Society of America, 1989

[2-8] V.N. Mahajan, *Aberration Theory Made Simple*, SPIE Optical Engineering Press, 1991

[2-9] A.S. Glassner, “An Overview of Ray Tracing”, A.S. Glassner, ed., *An Introduction to Ray Tracing*, Academic Press, 1-31 (1989)

[2-10] P. Hanrahan, "A Survey of Ray-Surface Intersection Algorithms", A.S. Glassner, ed., *An Introduction to Ray Tracing*, Academic Press, 79-119 (1989)

[2-11] E. Haines, "Essential Ray Tracing Algorithms", A.S. Glassner, ed., *An Introduction to Ray Tracing*, Academic Press, 33-77 (1989)

[2-12] R.P. Breault, A.W. Graynolds, M.A. Gauvin, "Stray Light Analysis with APART/PADE, Version 8.7", Proc. SPIE **675**, 105-125 (1986)

[2-13] R.Compagnon, B. Paule, J-L Scartezzini, "Design of new daylighting systems using ADELINE software", Solar Energy in Urban Planning and Architecure, Florence, Italy, 1993.

[2-14] F.X. Sillion, C. Puech, *Radiosity & Global Illumination*, Morgan Kaufmann Publishers, 1994

[2-15] A.S. Glassner, *Principles of digital image synthesis*, Morgan Kaufmann Publishers, 1995

[2-16] W.J. Smith, Modern Lens Design, McGraw-Hill, 1992

[2-17] W.H. Press, S.A. Teukolsky, W.T. Vetterling, B.P. Flannery, *Numerical Recipies in C, The Art of Scientific Computing*, *Second Edition*, Cambridge University Press, 1992

Chapter 3

Illumination light pipes

The optical properties of light sources are determined by material properties and technological constraints, which have little to do with the application requirements. The lighting distributions depend on the working principles of the source and on its packaging. In most cases, the source is assisted by complementary optics (e.g. lenses, reflectors, diffusers) in view to generate the desired illumination in the far-field [3-1, 3-2]. However, traditional light sources are somewhat limited for the control of the lighting distribution over short distances. Moreover, some applications require a compact packaging which may be incompatible with the overall dimensions of standard sources.

Illumination light pipes have the potential to overcome some of the limitations of traditional sources. This is perfectly demonstrated in the case of the illumination of liquid crystal displays (LCDs). Light pipes allow to deliver a uniform back-lighting with a reduce set of low consumption light sources [3-3, 3-4]. Moreover, propositions have been made, which allow to maximize the LCD lighting efficiency by means of polarizing light pipes [3-5, 3-6]. The use of light pipes for the frontal-lighting of reflective LCDs has been proposed to maximize the autonomy of personal digital assistant tools (PDAs) or portable personal computers [3-7, 3-8]. The non-obstructive frontal-lighting of watches by means of an illumination light pipe [3-9] has been extensively studied by the author and is presented in Chapter 4. Light pipes have different applications for the automotive industry. They can be used for interior car lighting [3-10], for the dashboard illumination [3-11], as compact signal lamps [3-12, 3-13], or headlamps

[3-14]. Light pipes are being used successfully in the architectural domain to replace neon and fluorescent lamps for the lighting of buildings [3-15, 3-16]. Finally, illumination light pipes are also used in the medical field for endoscopy, jaundice phototherapy, anesthesiology, transillumination, anesthesiology, cold light illumination, etc [3-17, 3-18, 3-19].

This chapter presents the design principles of illumination light pipes. More specifically, we demonstrate that the optical transfer block (OTB) method, introduced in Chapter 2, is well suited for the optimization of the light pipe design. Different light pipe concepts are evaluated in function of their optical performances and their feasibility. Finally, the possible manufacturing technologies are introduced and the limitations they impose to the design are discussed.

3.1 The light pipe concept

The light pipe principle consists in transforming a quasi-point source into an artificial extended light source. As illustrated in Fig. 3-1, the light emitted by the source is guided inside the pipe by total internal reflection (TIR). The pipe surface is selectively covered with outcoupling zones, whose function consists in extracting part of the light out from the pipe. The outcoupled light is then used for the illumination. The size and shape of the pipe, as well as the spatial distribution of the outcouplers along the pipe, are chosen in view to control the lighting distribution.

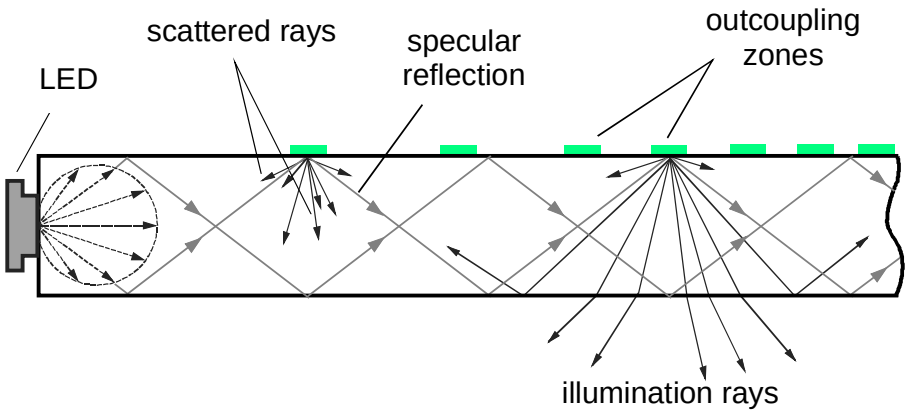

Fig. 3-1 Illustration of the light pipe principle.

The shape and dimensions of the pipe may vary depending on the desired optical function and/or the object to be illuminated. Figure 3-2 shows some basic light pipe configurations : the linear light pipe, the circular light pipe, and the plate light pipe (typically used for the back-lighting of LCDs).

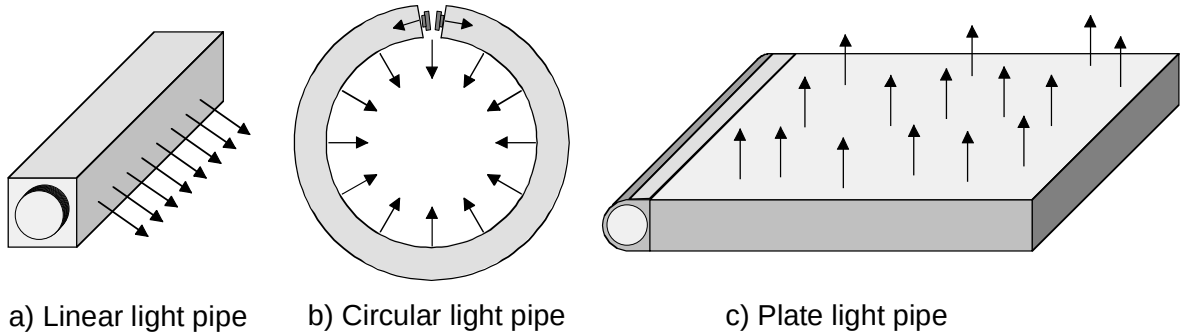

Fig. 3-2 Common light pipe configurations.

The direction of propagation of the illumination rays can be modified by the shape of the cross section. As illustrated in Fig. 3-4, this property can be used to modify the angular spectrum of the illumination (or cone of illumination). The shape of the pipe cross-section may partially be determined by technological constraints. Actually, it is generally easier to manufacture the outcouplers on flat surfaces.

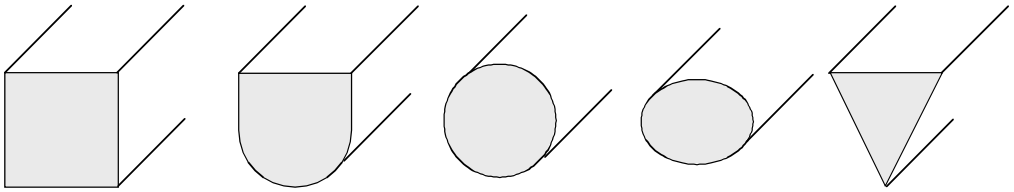

Fig. 3-3 Examples of light pipe cross-sections.

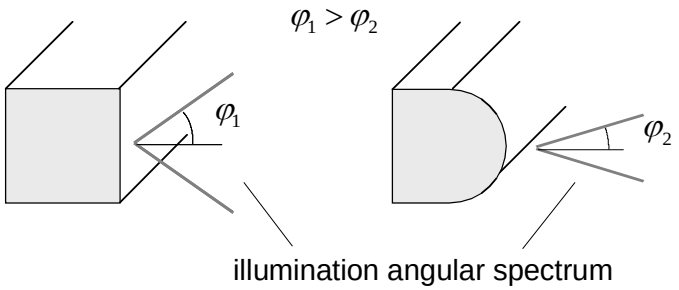

Fig. 3-4 Modification of the illumination angular spectrum by the pipe cross-section.

However, the optical function of the pipe is mostly determined by the outcoupler characteristics; that is to say, the type, the size and the position of the outcoupling zones (see Fig. 3-1). The next subsections describe and evaluate the characteristics of the different types of outcouplers. The outcouplers are classified by their working principle. The performance of the different outcouplers is mainly based on their ability to deflect the light in the desired direction (a deflection of 90° is often desired).

3.1.1 Surface scattering light pipes

It is well known that a polished light pipe transports the light by TIR without any optical losses. However, any local imperfection of the pipe surface is going to produce optical scattering [3-20]. Actually, the light is partially coupled out from the pipe by the surface roughness. The surface roughness can be generated on purpose at specific locations along the pipe by a mastered manufacturing process, such as speckle recording [3-21]. Thus, surface scattering light pipes can generate controlled lighting distributions.

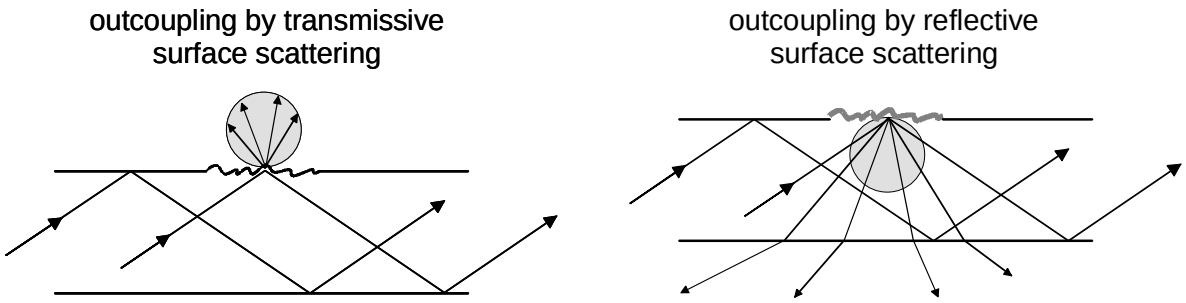

Fig. 3-5 Illumination by surface scattering.

The main drawback of the outcoupling by surface scattering is the limited control on the angular spectrum. The scattered distribution generated by polished surfaces consists generally in a distribution around the specular direction of propagation [3-22]. It has been shown however, that rougher reflective surfaces can also generate Lambertian distributions [3-23].

The scattering can also be produced at the pipe surface by the deposition of a thin layer of scattering paint [3-24]. In this case, the rays incident on the painted zones are scattered within the paint volume. However, due to the reduced thickness of the paint coating, this volume scattering phenomena is generally associated with surface scattering.

3.1.2 Volume scattering light pipes

As shown in Fig. 3-6, when the light, guided within the pipe, meets a volume scattering section, part of the light does not respect the TIR condition anymore and is coupled out from the pipe. Volume scattering is often used when the pipe cross-section is too small for the manufacturing of micro-structures on top of the pipe surface. That is for instance the case for some medical applications (endoscopy).

Volume scattering results from the deflection of light produced by particles, which are introduced into the pipe during the manufacturing process. This technology is also used for the doping of optical fibers [3-25]. The distribution of the illumination could theoretically be controlled by the modulation of the pipe doping. However, the drawing process of the pipe does not allow a precise control of the doping distribution. Therefore, it is difficult to get a uniform illumination over long distances with volume scattering light pipes.

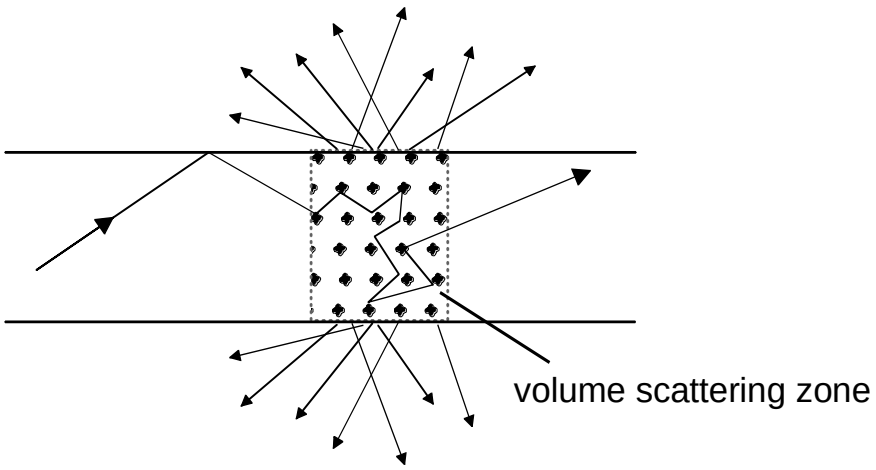

Fig. 3-6 Illumination by volume scattering.

3.1.3 Diffractive outcouplers

Diffraction gratings have the property to transform the incident rays into a set of diffracted rays (see Fig. 3-7). In the context of illumination devices, diffractive optical elements (DOEs) can be used for the correction of chromatic aberrations (bluish effect of automotive xenon headlamps), as beam splitter (controlled distribution of the light coming out of a multimode fiber in laser illuminated brake lamp [3-13]), or as a diffuser.

In the case of light pipes however, it is difficult to optimize the gratings in view to achieve a controlled distribution of the illumination. The outcoupling angles required for a normal illumination imply grating periods in the wavelength range. In this case, the grating works in the electromagnetic regime. Due to the resonance nature of the electromagnetic regime [26], strong variations of the diffraction efficiencies η_p (flux in the different diffraction orders) are observed for small variations of the angle of incidence α and of the wavelength λ. In the case of the light pipe, the light reaches the grating with a broad angular spectrum. Moreover, the light sources used for the illumination are generally polychromatic.

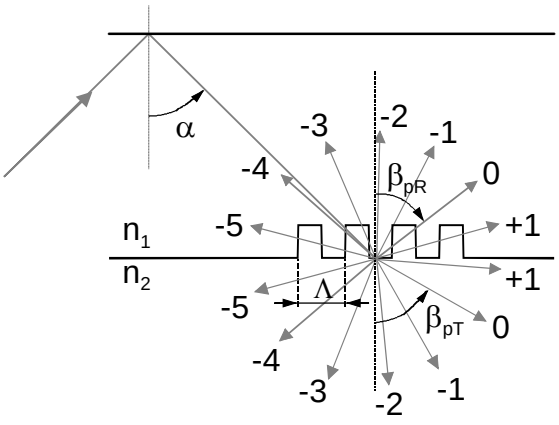

Fig. 3-7 Illumination by diffractive outcouplers.

3.1.4 Variable cross-section light pipes

The outcoupling can be done by a variation of the pipe cross-section. As shown hereafter, the variation of the cross-section can either be continuous or discontinuous.

Figure 3-8 illustrates the discontinuous cross-section approach. The prism angle is chosen in order that the light incident on the prisms is coupled out from the pipe. The amount of flux coupled out is then directly proportional to the variation of the pipe cross-section. The guided flux I_{i+1} at the $i+1^{th}$ section of the pipe is defined as

$$I_{i+1} = \frac{d_{i+1}}{d_i} I_i \ , \tag{3-1}$$

where I_i is the guided flux at the i^{th} section of the pipe, and d_i and d_{i+1} are the sizes of the respective cross-sections. The locally outcoupled flux is then defined as

$$\phi_i \propto I_i \left(1 - \frac{d_{i+1}}{d_i} \right) . \tag{3-2}$$

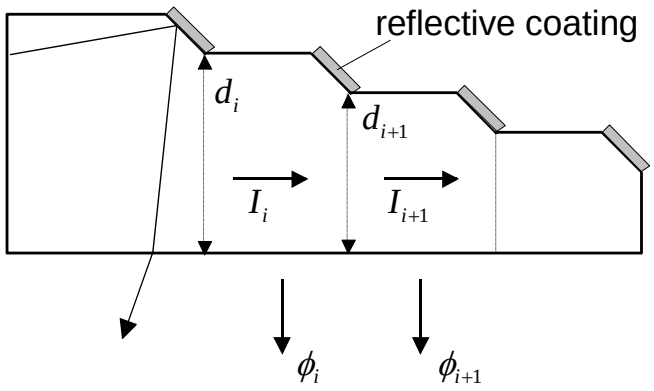

Fig. 3-8 Discontinuous variable cross-section light pipe.

For the discontinuous case, the reflective outcoupling micro-prisms do not influence the angular spectrum of the guided rays. That is not the case for the continuous case shown in Fig. 3-9. The propagation angle α_i of the guided rays is changed at each intersection with the oblique face (see Fig. 3-9). When the propagation angle α_i becomes smaller than the critical angle α_c, the ray does not respect the TIR condition anymore, and is therefore coupled out.

If the pipe surface has a slope angle φ; for and incident angle α_{i-1}, the new propagation angle α_i is defined as

$$\alpha_i = \alpha_{i-1} - 2\varphi \ . \tag{3-3}$$

If the media surrounding the pipe has a refractive index n_1, and the pipe a refractive index n_2, the critical angle is defined as

$$\alpha_c = \sin^{-1}\left(n_1/n_2\right) . \tag{3-4}$$

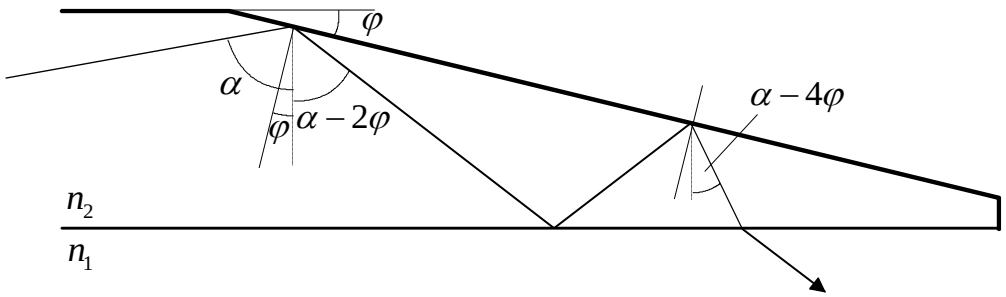

Fig. 3-9 Continuous variable cross-section light pipe.

Variable cross-section light pipes couple out the guided light coming from one direction only (from left to right in the examples of Figs. 3-8 and 3-9). Symmetric configurations can be done by joining two pipe has shown in Fig. 3-10. In this case, a minimal cross-section $d_{\min}$ is imposed in order to avoid any mechanical break of the pipe.

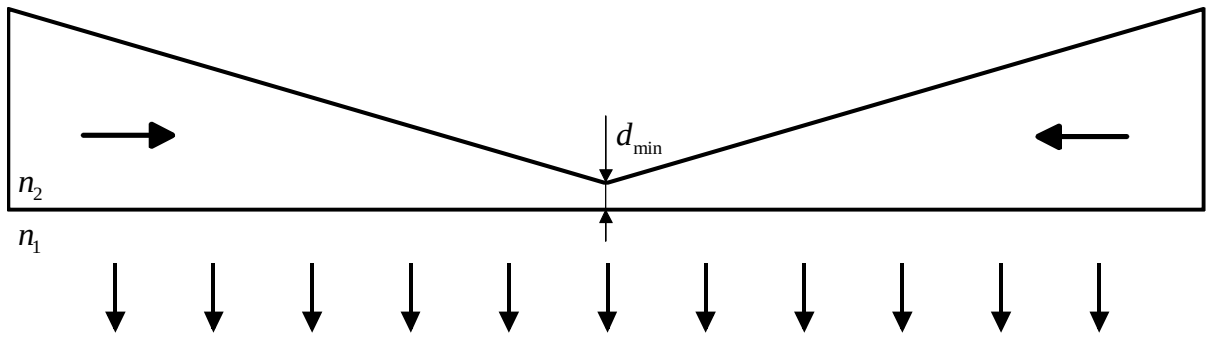

Fig. 3-10 Symmetric variable cross-section light pipe.

3.1.5 Refractive outcouplers

The basic principle of light pipes is based on the propagation of flux by TIR. This happens if the incident angle of the rays α is greater than the critical angle α_c (see Eq. (3-4)). The principle of refractive outcouplers consists in placing discontinuities along the

pipe surface in order to locally exceed the TIR condition ($\alpha < \alpha_c$). In this case, as illustrated in Fig. 3-11, the light escapes from the pipe by refraction. The outcoupling angle β is calculated by Snell's law as

$$\beta = \sin^{-1}\left[\frac{n_1}{n_2}\sin(\alpha - \rho)\right] + \rho \ , \tag{3-5}$$

where α is the incident angle, ρ the inclination of the refractive surface, n_1 the refractive index of the media surrounding the pipe, and n_2 the refractive index of the pipe.

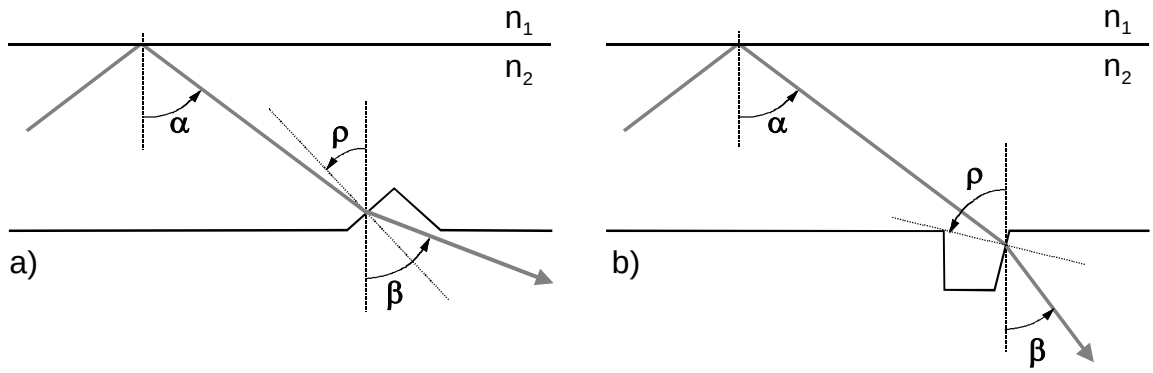

Fig. 3-11 Examples of refractive outcoupling by discontinuities on the pipe surface.

Figure 3-12 shows the outcoupling angle β achieved for different orientations ρ of the refractive surface, in the case where $n_1 = 1.0$ and $n_2 = 1.49$ (refractive index of PMMA). The gray region covers the angles of incidence α which correspond to the cone of propagation inside the pipe. The cone has an aperture of $42.2°$ which results from the coupling of a Lambertian source at the pipe entrance.

We observe that most of the outcoupled rays leave the pipe at grazing angles ($45 < \beta < 90$). That is not practical for most lighting configurations which require an illumination normal to the pipe ($\beta = 0$). Therefore, refractive outcouplers are assisted by a correction plate (see Fig. 3-13), whose rule is to achieve the desired main direction of illumination.

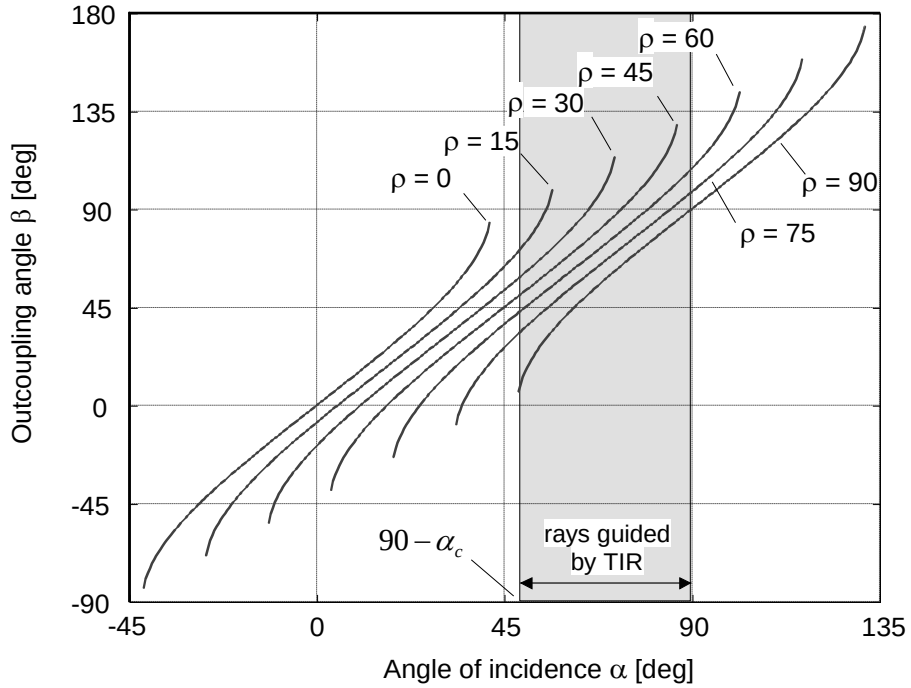

Fig. 3-12 Outcoupling angles achieved by refraction for different orientations of the refractive surface.

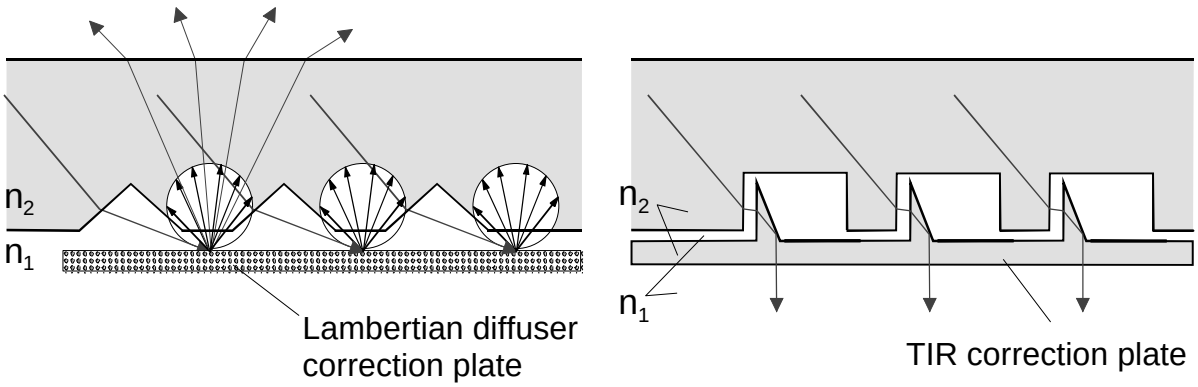

Fig. 3-13 Correction of the illumination angle with external correction plates.

The shape of the refractive discontinuity can vary. For instance, instead of prism like shapes, lenslets can be used in order to combine the decoupling and beam shaping functions [3-27]. But the main drawback of refractive outcouplers remains : the necessity to use a correction plate to avoid a grazing direction of illumination.

3.1.6 Reflective outcouplers

As for the refractive case, reflective outcouplers use discontinuities along the pipe surface which deviate the direction of propagation of the guided rays. The deviated rays are coupled out from the pipe and are used for illumination. Two kinds of reflective outcouplers are described in the next subsections : the coated micro-prisms and the TIR micro-prisms. Other outcoupler shapes can be selected. However, all reflective outcouplers share the same working and design principles.

3.1.6.1 Coated micro-prisms

As illustrated in Fig 3-14, reflective micro-prisms located along the pipe surface deviate part of the guided rays. These rays are used for illumination purpose.

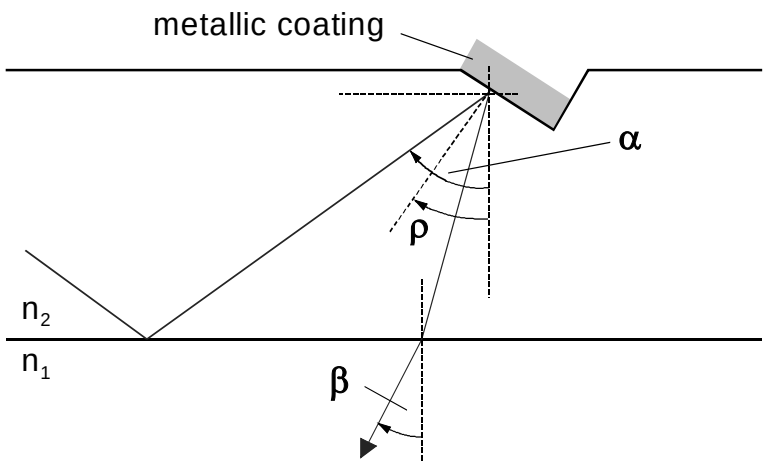

Fig. 3-14 Outcoupling produced by a reflective micro-prism.

The direction of illumination is defined by the angle α of the incident rays and the prism orientation ρ. The outcoupling angle β is determined by

$$\beta = \sin^{-1}\left[\frac{n_1}{n_2}\sin\left(-\alpha + 2\rho\right)\right]. \qquad (3\text{-}6)$$

The graph of Fig. 3-15 shows the outcoupling angle β achieved for different orientations ρ of the prism, for the case where $n_1 = 1.0$ and $n_2 = 1.49$ (PMMA). The gray re-

gion covers the angles of incidence α, which correspond to the cone of propagation inside the pipe resulting from the coupling of a Lambertian source at the pipe entrance.

When compared with the refractive case, where the outcoupled light leaves the pipe at grazing angles, the reflection case is much more flexible. Actually, for a given angle of incidence α, any outcoupling direction β can be selected by choosing the right prism orientation ρ.

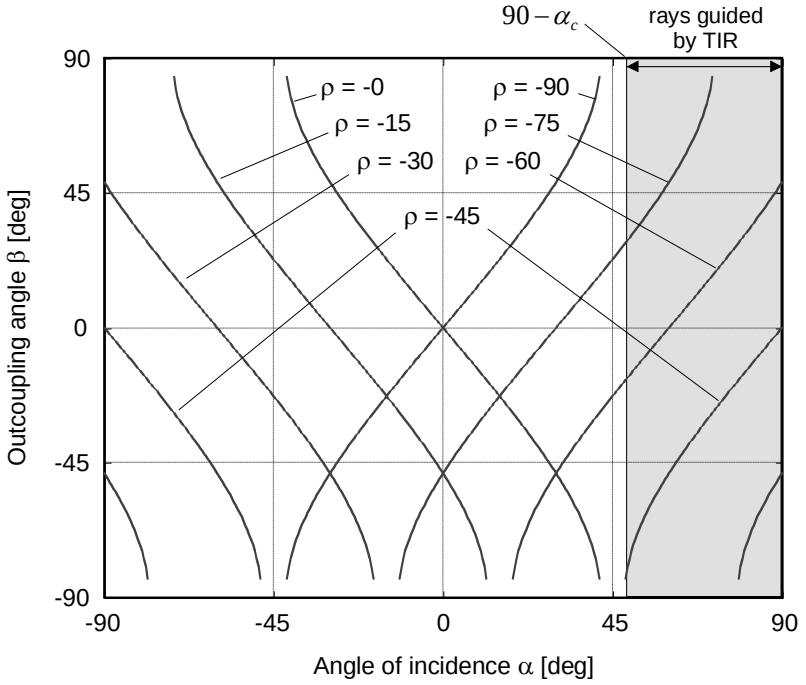

Fig. 3-15 Outcoupling angles achieved by reflection for different orientations of the reflective micro-prism.

Shadowing

The flux coupled out from the pipe is a function of the prism size and of the prism density along the pipe. However, for a given angle of propagation α, there is a prism density limit above which the outcoupled flux remains constant. Actually, as illustrated in Fig. 3-16, the shadowing limits the outcoupling efficiency of the prisms. Obviously, the effects of shadowing increase for grazing incidence angles ($\alpha \to 90°$).

A way to completely suppress the shadowing is to design variable cross-section light pipes (see Fig. 3-8 and 3-9). Nevertheless, the variable cross-section approach is lim-

ited to the light pipes which allow a relatively strong variation between the maximum and minimum dimensions of the cross-section. The question is to know if shadowing can be avoided, or at least reduced, for a micro-prism light pipe having a constant cross-section.

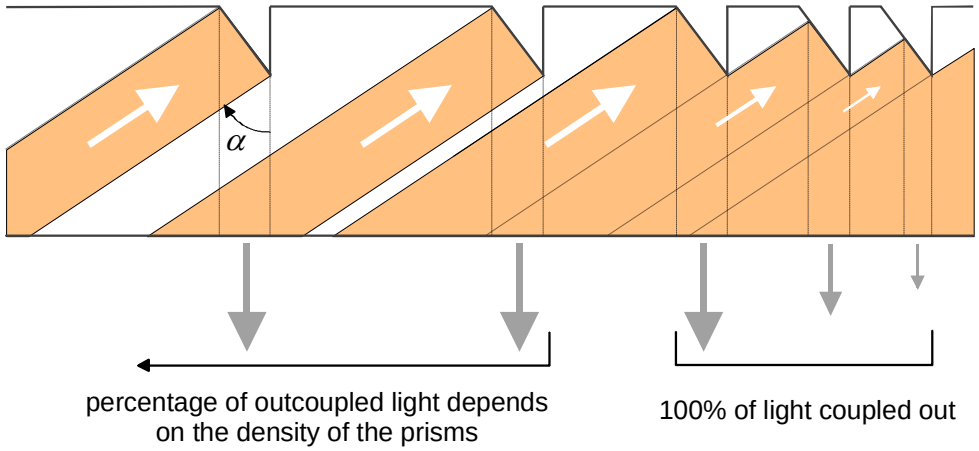

Fig. 3-16 Influence of the shadowing effect for a given angle of incidence α.

We analyze first the light propagation in a standard light pipe for which all the light propagates by TIR. As shown in Fig. 3-17, the pipe has a cross-section of dimension Y. Let us consider a plane at the position z_0. Each point of the plane z_0 can be considered as a point source, which emits the light in the $+z$ direction. For each point, the angular spectrum of the propagating light is defined by a cone, whose half angle has a value φ (in any case $\varphi \le |90 - \alpha_c|$). We observe the distribution of the angular spectrum after the propagation to the plane at position z_1. It is easy to demonstrate that all points of plane z_1 are equally illuminated by a cone of half angle φ. For the demonstration, we have chosen the position z_1, which corresponds to the minimum distance, where all points of plan z_0 contribute to the illumination of all points of plane z_1.

$$z_1 = z_0 + Y/\tan\varphi \ . \qquad (3\text{-}7)$$

The propagation can also be simulated by backward ray-tracing starting from the observation plane z_1. In this case, the reflection on the pipe surface can be replaced by the backward propagation to an enlarged virtual plane at position z_0

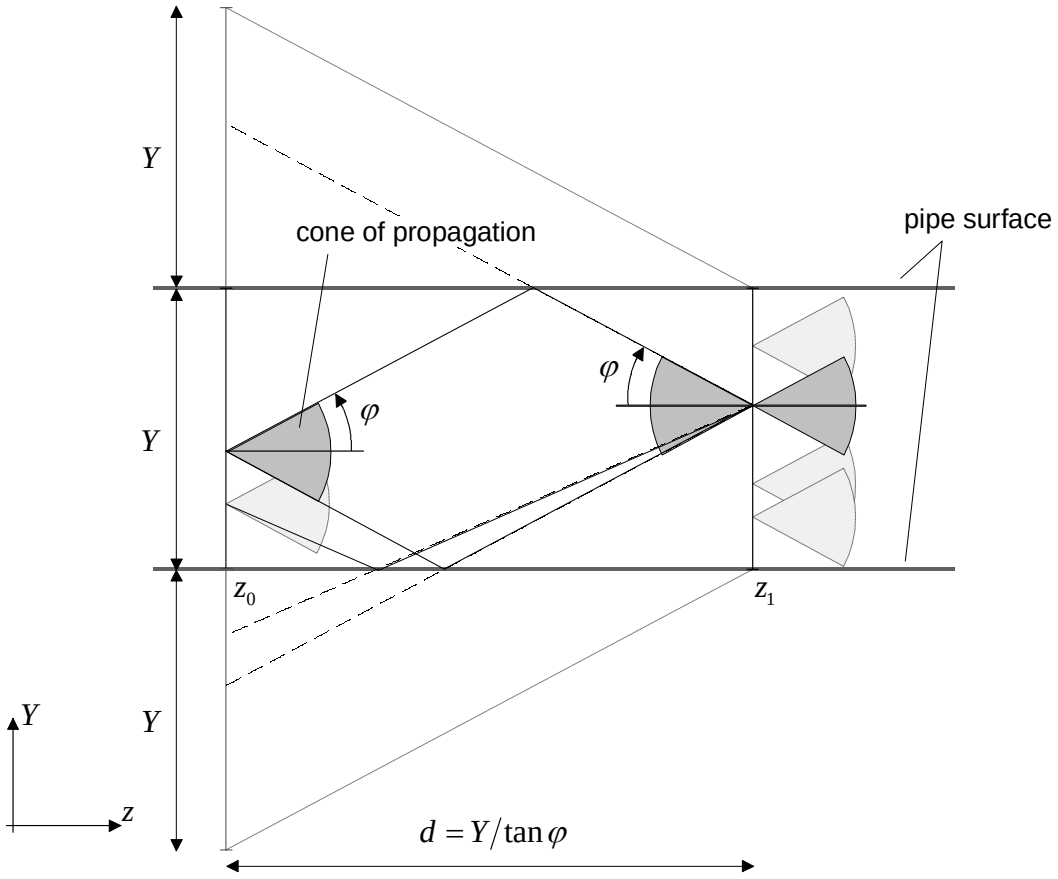

Fig. 3-17 Propagation between two sections of the light pipe.

Our goal is to analyze the influence of shadowing, if reflective (or obstructive) micro-prisms are placed between the two planes z_0 and z_1. In the example of Fig. 3-18, three micro-prisms (labeled by 1, 2, 3) of depth P_y are placed at three arbitrary positions. As expected, we observe that the angular spectrum and the irradiance in plane z_1 depend on the position (y-coordinate). In the presented example, there is even a region which does not receive any light (complete shadow).

The intuitive solution to reduce the shadowing is to choose smaller prisms. This approach is illustrated in Fig. 3-19, where the prisms have the same position as in Fig. 3-18, but their size has been reduced to 60%. As expected, the angular spectrum for most of the points in plane z_1 is enlarged. The light can even propagated between the prisms producing some discontinuities in the propagation angular spectrum. Moreover, the zone of complete shadow has been considerably reduced.

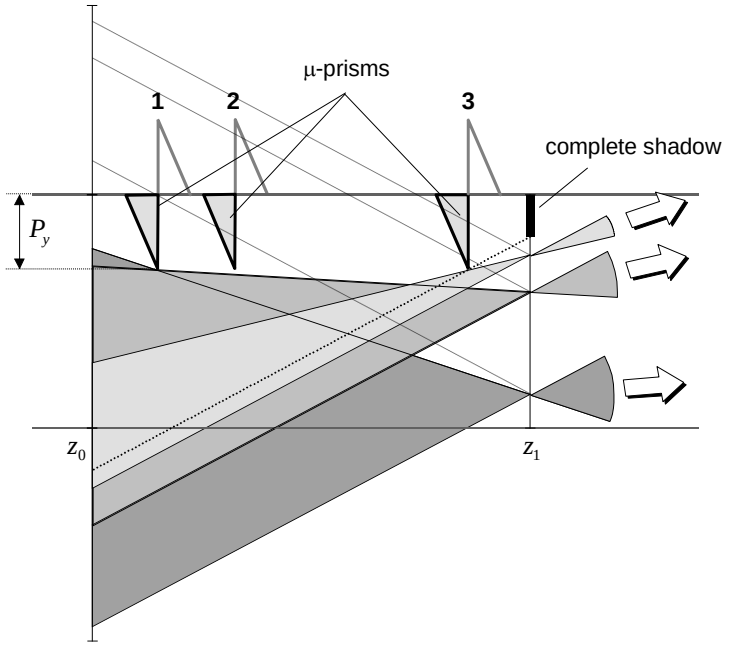

Fig. 3-18 Influence of the shadowing on propagation of the flux and the angular spectrum.

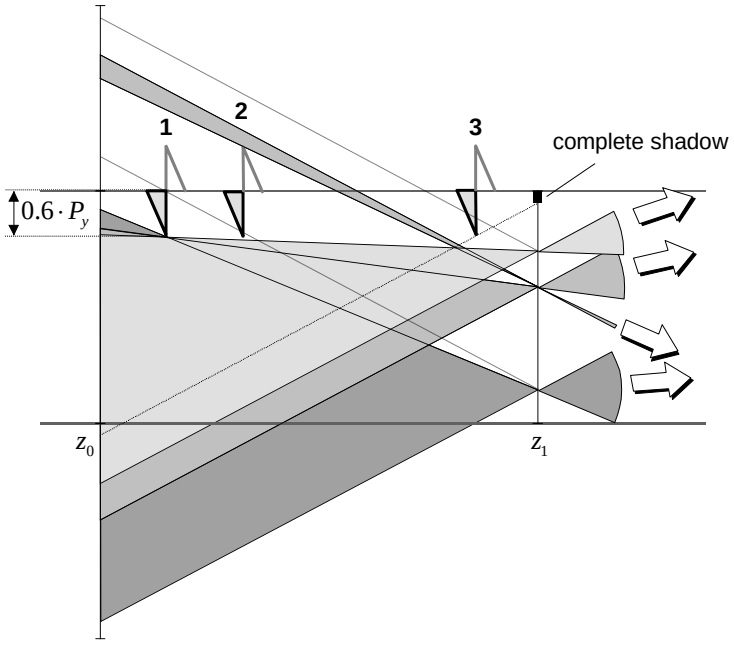

Fig. 3-19 Reduction of the shadowing effect by reduced prism size.

Nevertheless, we should be aware that the pipe lighting efficiency η is proportional to the prism surface density Γ along the pipe surface, which is

$$\eta(z) \propto \Gamma(z) = \nu_p(z) \cdot P_z \quad , \tag{3-8}$$

where ν_p is the local spatial frequency of the prisms, and P_z is the prism size in the z-direction. Thus, the reduction of the prism size does not only reduce the shadowing effect, but also the lighting efficiency of the pipe.

The way to reduce the shadowing, while keeping the outcoupling efficiency constant, is to reduce the prism size and to increase proportionally the prism spatial frequency (see Fig. 3-20). The advantage of using very small prisms, also called micro-prisms, becomes obvious. Typically, the size of the micro-prisms may vary between $10\,\mu m$ and $200\,\mu m$.

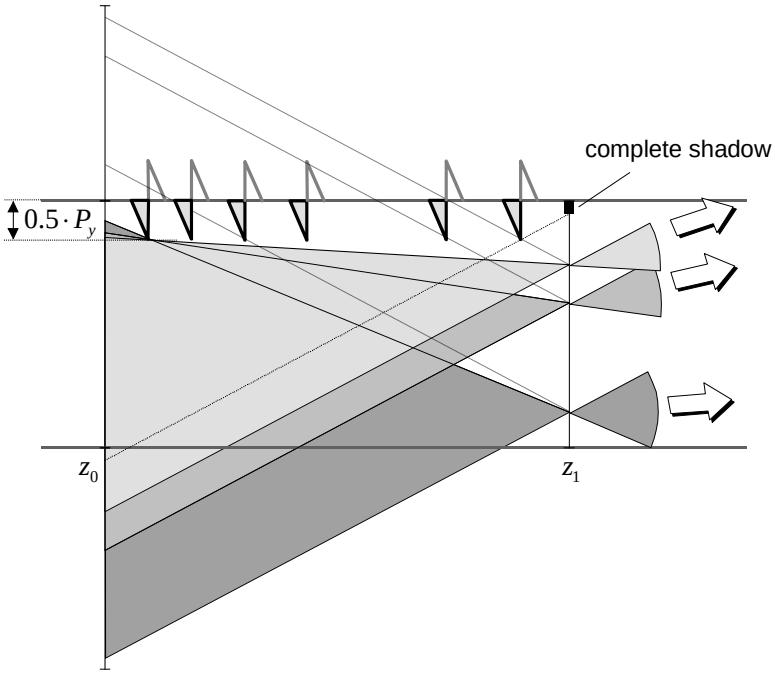

Fig. 3-20 Reduction of the shadowing effect by a reduction of the prism size and a proportional increase of the prism spatial frequency.

Actually, it is not the absolute size of the prisms which influence the shadowing, but rather the ratio between the prism depth P_y and the size of the prism cross-section Y. Experience has shown that the condition

$$\frac{Y}{P_y} \geq 20 \tag{3-9}$$

has to be fulfilled.

The model which has been presented describes the propagation between two planes of the pipe in the yz-plane. The model only gives a partial view of the influence of the geometrical parameters on the shadowing effect. The analysis of the light propagation within the pipe is a 3D problem, which has to be analyzed numerically with non-sequential ray-tracing programs. Figure 3-21 shows the propagation angular spectrum for different positions along the light pipe. The pipe has a cross section of $5 \times 5 mm$, and the prisms placed on the top face of the pipe have a depth of $85 \mu m$. We see that, as the light propagates inside the pipe, the angular spectrum is only (slightly) truncated in the vertical direction. This result is not surprising since the prisms do not influence the rays which propagate in the horizontal xz-plane.

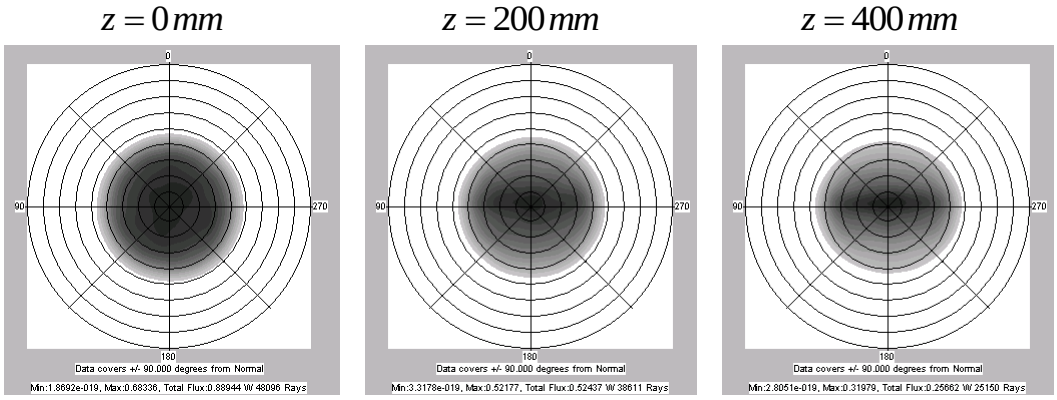

Fig. 3-21 Propagation angular spectrum at different positions of a micro-prism light pipe.

Technological considerations

Reflective micro-prisms require the deposition of a thin metallic coating. This operation can either be done on the prism working face only (Fig. 3-22a), or on the full face which contains the prisms (Fig. 3-22b). The selective deposition of the metallic layer on the prism working face is relatively expensive. Nevertheless, this approach has the advantage that the metallic absorption (see Appendix C) only affects the outcoupled rays. On the other hand, the metallic evaporation on the full face is simpler and cheaper. In this case, the metallic absorption affects the outcoupled rays (once) and the guided rays (at each reflection on the top face of the pipe). The resulting cumulative optical losses can lower significantly the efficiency of the light pipe.

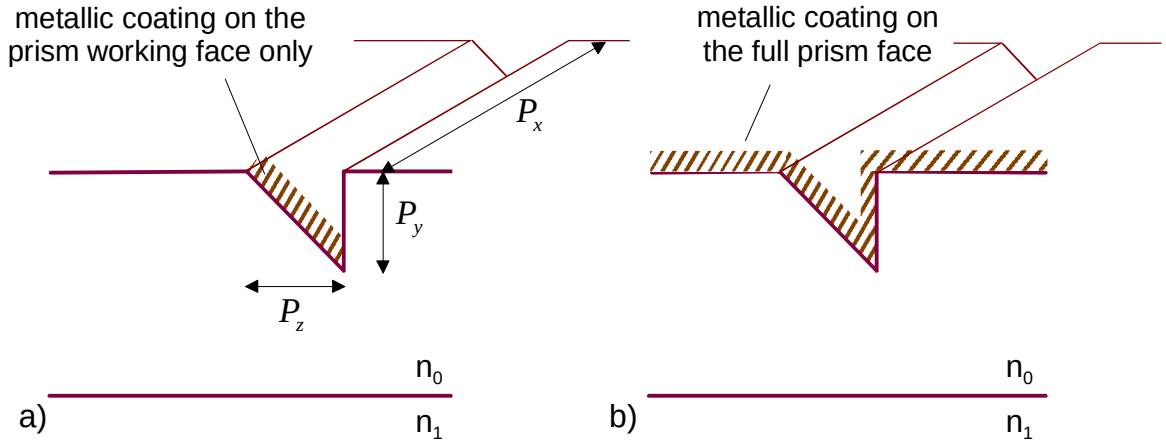

Fig. 3-22 Possible coating configurations for reflective micro-prism light pipes.

For instance, the ray-tracing analysis of two similar light pipes shows the differences produced by the two coating configurations. As shown in Fig. 3-23, the analyzed light pipe has a length of $500\,mm$ and a square cross-section of $5\times5\,mm$. The top pipe surface is covered by 60 micro-prisms of constant dimension ($P_x = 5000\,\mu m$, $P_y = 83\,\mu m$, $P_z = 100\,\mu m$). When only the prisms are Al-coated, 57.8% of the light injected into the pipe is coupled out for illumination purposes. The lighting efficiency decreases to 36.2% if the full prism face is Al-coated.

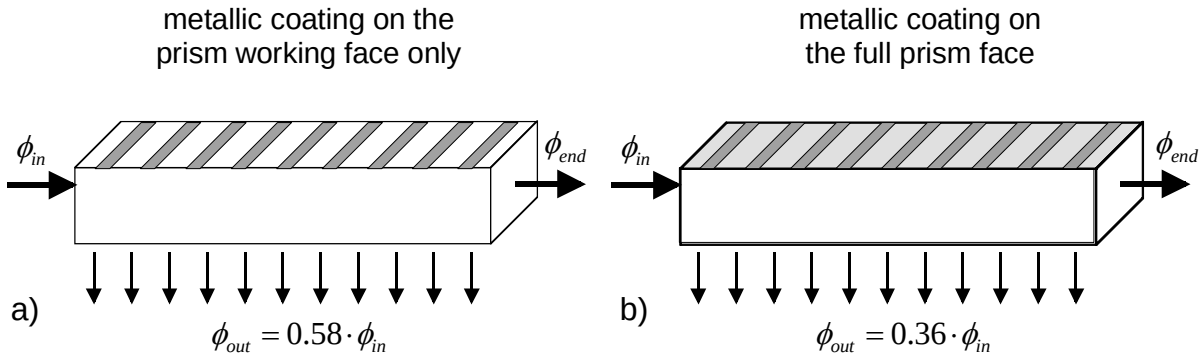

Fig. 3-23 Dependence of the lighting efficiency on the coating configuration.

3.1.6.2 TIR micro-prisms

As discussed, the big advantage of reflective micro-prism outcouplers over their refractive counterparts comes from their capacity to deviate the light in any direction. However, reflective micro-prisms require the deposition of a reflective metallic coating. This operation may be too expensive depending on the application requirements. Furthermore, optical losses by metallic absorption may become critical if the metallic coating is deposited on the full prism face.

TIR micro-prisms have the advantage that they do not require any coating. Moreover, TIR does not generate optical losses. However, as shown in Fig. 3-24, TIR only occurs for the rays reaching the prism with a relative incident angle α_r greater than the critical angle α_c, which means

$$\alpha_r = |\alpha - \rho| > \alpha_c \ . \tag{3-10}$$

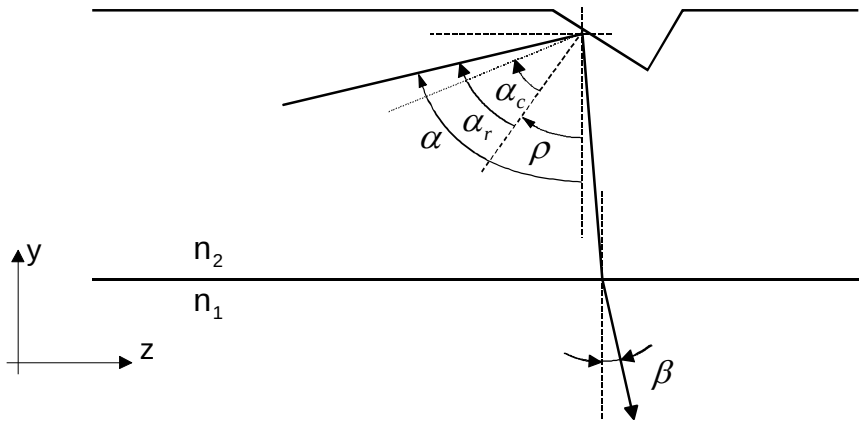

Fig. 3-24 Outcoupling produced by TIR (total internal reflection).

The configuration of Fig. 3-24 has the drawback, that a non negligible portion of the rays falling on the prism does not respect the TIR condition ($\alpha_r \leq \alpha_c$). Consequently, part of the light is coupled out from the pipe by refraction as illustrated in Fig. 3-11a. The analysis of the light propagation within the pipe is a 3D problem which can best be analyzed numerically. In fact, most of the rays fall obliquely on the prisms (out of the yz-plane) and are coupled out from the pipe by TIR. This phenomenon is con-

firmed by the analysis of a light pipe example (same geometry as the one described in section 3.1.6.1). The simulations show that 44.8% of the energy injected into the pipe is coupled out by TIR. The light outcoupled by refraction through the top face represents only 17.2% of the energy injected into the pipe.

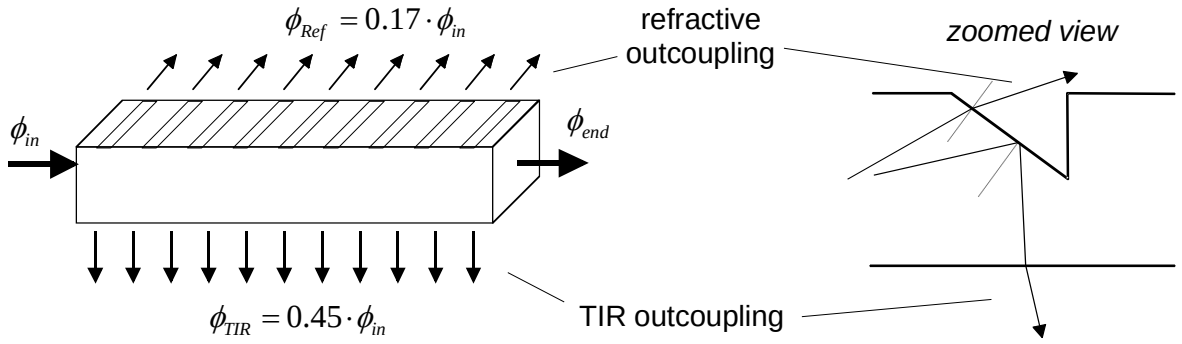

Fig. 3-25 Combination of TIR and refractive outcoupling.

It is interesting to note that the TIR configuration has a higher outcoupling efficiency than the fully coated prism face configuration. That is to say, the losses due to metallic absorption of the configuration of Fig. 3-23b are higher than the losses by refraction of the configuration of Fig. 3-25. However, since a part of the incident rays are refracted, the angular spectrum achieved by TIR is not as uniform as in the coated micro-prism case. This is illustrated in Fig. 3-26, where we see that some directions are missing in the TIR case. The angular spectrum of the outcoupled rays becomes asymmetric.

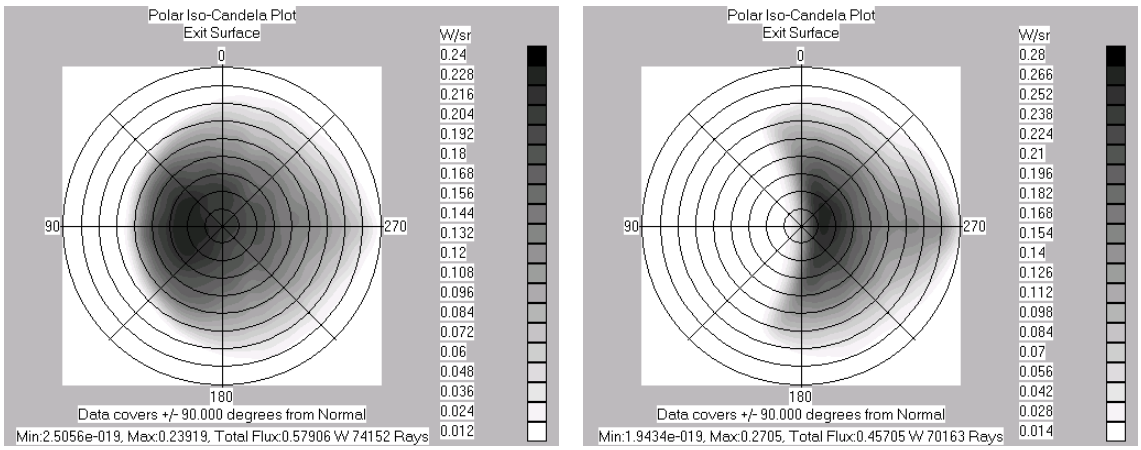

Fig. 3-26 Angular propagation spectrum for the rays coupled out by coated micro-prisms (left), or TIR micro-prisms (right).

Figure 3-27 shows an alternative configuration for which all the rays are coupled out by TIR [3-28]. In this case, the resulting outcoupled propagation spectrum becomes symmetric around the normal to the pipe. A additional advantage of this configuration is the fact that there is no shadowing effect. Nevertheless, this shape is very difficult to manufacture. Moreover, the configuration is not suited for the low cost manufacturing by injection molding as the prism shape is unpractical for the molt removal.

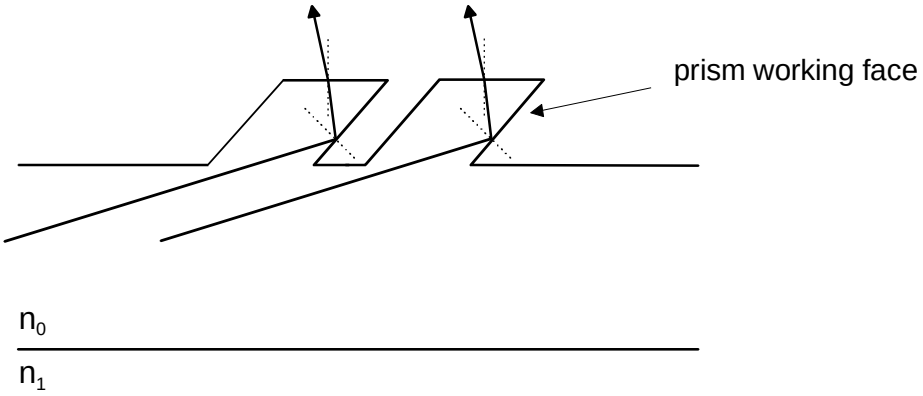

Fig. 3-27 TIR micro-prism light pipe avoiding shadowing effects.

3.2 Design of illumination light pipes

The goal of illumination light pipes is to transform quasi-point sources (e.g. LEDs) into artificial extended light sources. Such lighting devices allow the control of the spatial distribution of the light emitted by the source. As for any other light source, illumination light pipes may be assisted by complementary elements (e.g. surrounding correction plates as shown in Fig. 3-13). The first design step is to find an optical system, which potentially fulfills the requirements of the considered application. Then, the exact role of the light pipe within the system has to be identified. This step typically defines the distribution of the outcoupled flux along the pipe and the direction of illumination. In some cases, as the illumination of LCDs, the state of polarization of the outcoupled rays may also be specified.

Once the optical function of the light pipe is defined, the design of the pipe consists of selecting the type of outcoupler and in determining the repartition of the outcouplers

along the pipe surface. Technological constraints, such as the feasible feature size and the manufacturing costs, need to be taken into account during the full design process. Finally, the design is validated by the analysis of the full optical system (including the surrounding optics, the mounting, and the detectors).

The next sections details the different steps leading to the design of light pipes. In particular, we demonstrate the utility of the OTB method for the calculation of the outcoupler spatial density along the pipe.

3.2.1 Specifications

The illumination light pipes have to deliver a specified lighting distribution, or irradiance $\left(W\,m^{-2}\right)$ on a target (e.g. a display, a detector, …). For the lighting of LCDs, the requirements are more demanding, since the efficiency of the device depends on the direction and on the state of polarization of the illumination. For signal lamps, where the light goes directly from the source to the detector (e.g. the eye), we are interested in maximizing the amount of rays reaching the detector (placed in the far-field). In this case, the optical specifications of the device are given in terms of radiance $\left(W\,sr^{-1}\,m^{-2}\right)$. Moreover, depending on the application, further requirements may limit the volume available for the lighting device. Finally, the choice of the light source(s) may also be limited by the electrical consumption constraints.

The flexibility of the light pipe approach allows to comply with the requirements for a large set of applications. The shape and the size of the pipe may be imposed by the available space. The designer can choose the type and the disposition of the outcouplers. Some technological requirements may limit the choice.

In order to illustrate the design concept, we choose a simple light pipe configuration, whose specifications are described hereafter. However, more complex configurations can be calculated based on the same design principles.

As illustrated in Fig. 3-28, the light pipe consists of a PMMA parallelepiped, which has the following geometrical parameters :

- length : $L_z = 500\,mm$,
- square cross-section : $L_x = L_y = 5.0\,mm$.

The light is injected at one end of the pipe by an LED, which has the following optical characteristics :

- emission type : Lambertian,
- surface of emission : $200 \times 200\,\mu m^2$,
- peak wavelength : $\lambda_{peak} = 650\,nm$,
- spectral line half width : $\Delta\lambda_{1/2} = 20\,nm$.

Based on experimental measurements, molded PMMA has an absorption coefficient of $1 dB/m$ at $650\,nm$, which corresponds to an extinction coefficient of

$$\alpha_{PMMA} = 2.303 \cdot 10^{-4}\, mm^{-1} .$$

The optical requirements of the pipe are :

- distribution of the outcoupled energy : uniform along the pipe,
- direction of illumination : in the –y direction,
- shape of the illumination : symmetric around the y-axis,
- lighting efficiency : to maximize,
- polarization of illumination rays : irrelevant.

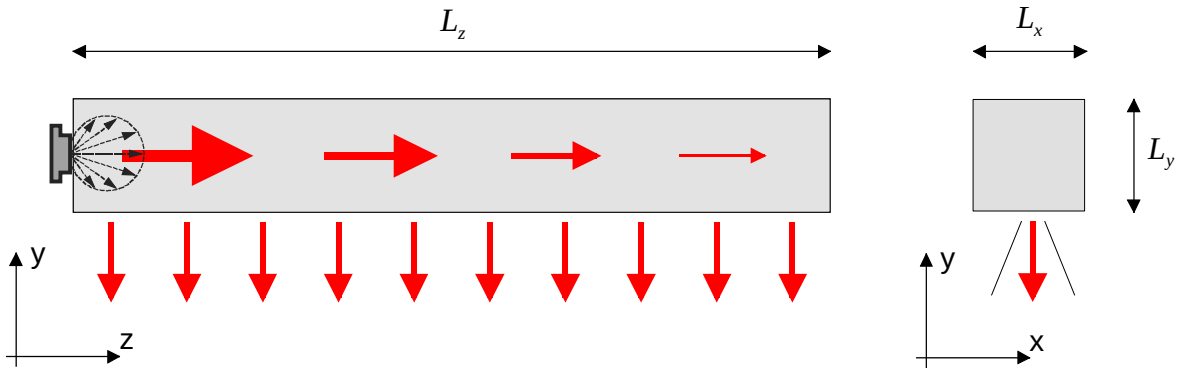

Fig. 3-28 Illustration of the specified light pipe configuration.

3.2.2 Selection of an outcoupler

The optical function of the illumination light pipe is partially determined by its geometry (shape and size), which has been fixed by the specifications. However, the type and the disposition of the outcouplers along the pipe are the main parameters. As discussed hereafter, the selection of the outcoupler is based on optical and manufacturing criteria.

Optical properties which determine the choice of an outcoupler :

- the control on the outcoupling direction,
- the outcoupling efficiency.

Manufacturing parameters to take into account for the selection of an outcoupler :

- the minimal and/or the maximal geometry feature size,
- the production costs.

The weight which is given to each selection criteria depends on the application requirements. But, we have to keep in mind that the device has to be fabricated, and therefore the limits of the technology should not be exceeded. The possible technologies for the manufacturing of illumination light pipes are briefly discussed in section 3.3

In the case of the light pipe specified in the last section, the illumination has to be normal to the pipe (symmetric vs. the y-axis). Based on the considerations done in section 3.1, three kinds of outcouplers can deliver a uniform illumination normal to the pipe : the Lambertian scattering paint (surface scattering), the TIR micro-prisms, and the metallic coated micro-prisms.

Light pipes using scattering paint as outcoupler have been designed and realized successfully [3-24]. The paint is easy to fabricate and apply. This makes it very practical for the simple realization of prototypes. However, the paint is not well adapted to the industrialization process, where reproducibility, high volume and low cost manufacturing are essential criteria.

TIR micro-prisms have the advantage that they do not require any coating. However, in order to get a uniform outcoupled angular spectrum, TIR micro-prism light pipes require a geometrical configuration which is unpractical to manufacture (see Fig. 3-27 in section 3.1.6.2).

Finally, despite the required coating, metallic reflective micro-prisms represent the best suited outcouplers for the present configuration. The next sections present the detailed design steps including the determination of the prism geometry and the calculation of the prism repartition on top of the pipe surface.

3.2.3 Control of the lighting distribution

The problem related to the control of the lighting distribution is illustrated schematically in Fig. 3-29. The light is emitted by the source *A* with a given angular spectrum and is coupled into the light pipe *B*. The light is either guided by total internal reflection (TIR), or coupled out from the pipe when intersecting an outcoupler. Finally, the light reaches the target *C* with a given flux and angular spectrum.

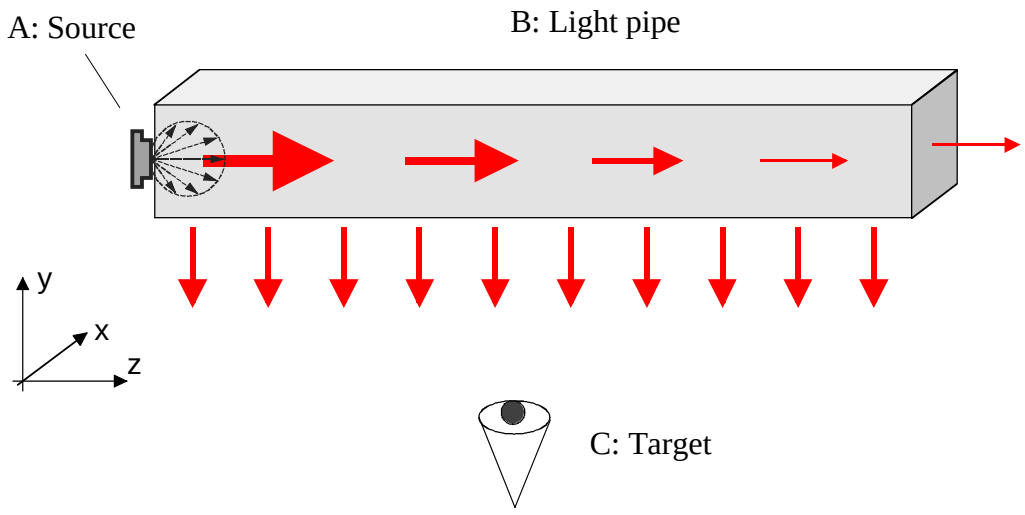

Fig. 3-29 Schematic representation of a light pipe illumination device.

The specifications fixed in section 3.2.1 require that the light pipe delivers a constant irradiance or radiant exitance $\left(W\,m^{-2}\right)$ along the bottom face, and a symmetric angular

spectrum. Moreover, the overall lighting efficiency of the device has to be maximized. The next sections detail the design steps.

3.2.3.1 Determination of the prism geometry

In the case of the selected reflective micro-prism configuration (Fig. 3-30), the orientation ρ of the prism working face determines the direction of the reflected rays and, therefore, the direction of the illumination. The prism size P_z establishes the amount of energy outcoupled by a single prism. We discussed hereafter how to define the different parameters of the prism geometry.

Determination of the prism angle

In our case, the specifications require to have a symmetric illumination normal to the pipe (in the –y direction). The pipe shape being fixed, the prism angle ρ is the only parameter which influences the direction of illumination.

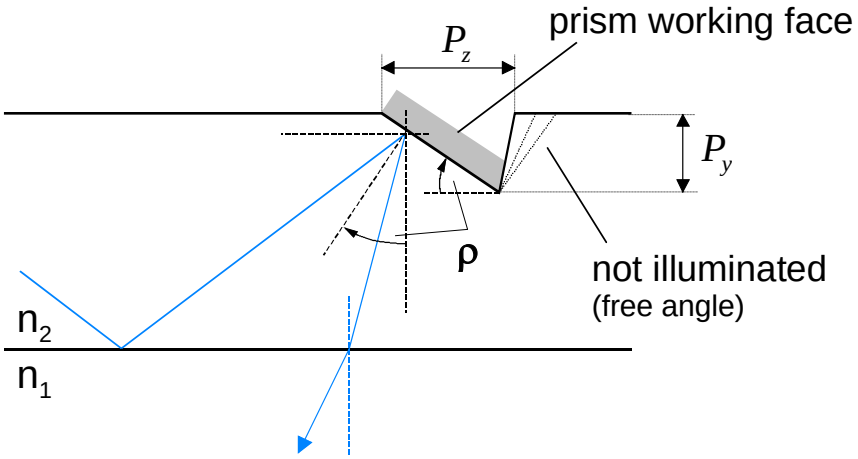

Fig. 3-30 Parameters of the prism geometry.

As shown in Fig. 3-31, the angular spectrum emitted by the source is represented by the cone of propagation whose half angle has a value θ_s. After coupling into the pipe, the light propagates inside the pipe under a cone of aperture θ_s'. In principle, only the superior half of the cone reaches the prisms. In the yz-plane, the rays reflected by the prism propagate inside the pipe under a cone of aperture θ_p'. Outside the pipe, this corresponds to a cone of illumination whose half angle has a value θ_p.

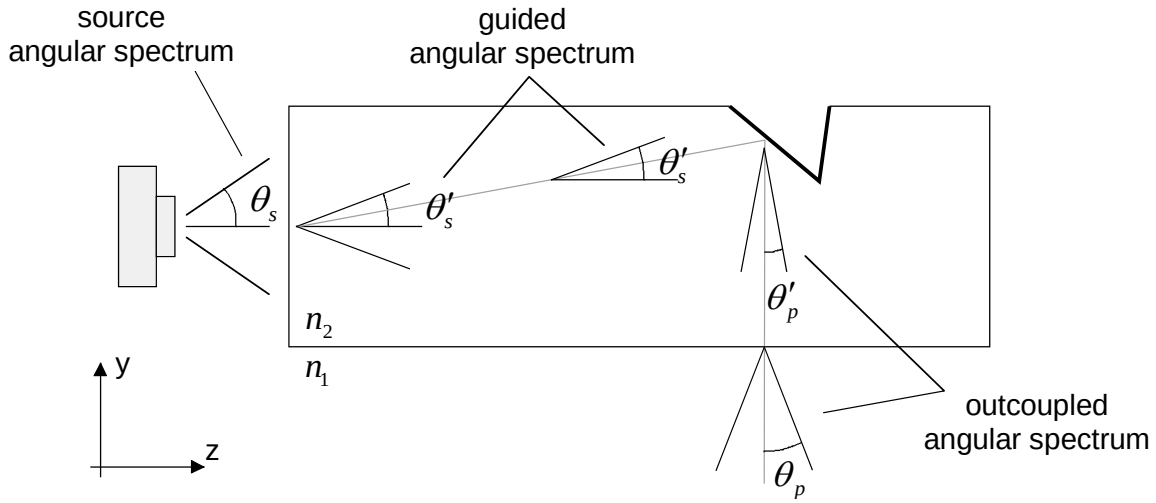

Fig. 3-31 Illustration of the angular spectrum propagation, in the yz-plane.

For the specified configuration, the angular distribution emitted by the source is Lambertian. Thus, in air, the half angle of emission has a value of $\theta_s = 90°$. After coupling into the PMMA pipe ($n_2 = 1.49$), the cone of propagation is defined by Snell's law as

$$\theta'_s = \sin^{-1}\frac{1}{n_2} = 42.16° \ . \tag{3-11}$$

Note that the last equation is only true if there is an air gap between the source and the pipe. The air gap configuration has the advantage that all the rays coupled into the pipe are guided by TIR.

We consider that only the upper part of the guided cone illuminates the micro-prisms. The prism angle ρ is chosen in order that the average direction of propagation is coupled out perpendicularly to the pipe surface. For simplification, we consider that the average direction of propagation has value of $\theta'_s/2$ (see Fig. 3-32). In this case, the prism angle becomes

$$\rho = \frac{\pi}{4} - \frac{\theta'_s}{4} = 34.5° \ . \tag{3-12}$$

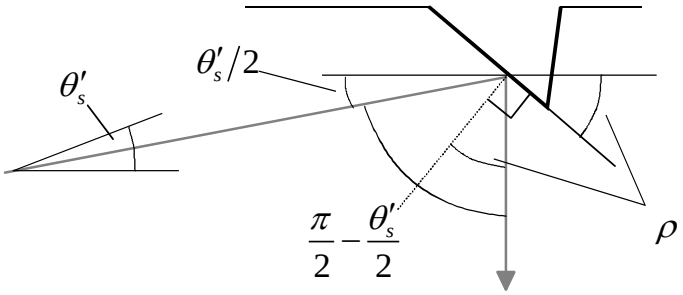

Fig. 3-32 Geometrical derivation of the prism angle.

The geometrical derivation of the prism angle is approximate. The outcoupling has been analyzed in the yz-plane, but the process happens in the 3D space. The effects produced by the out of plane rays should be taken into account. Moreover, for low prism spatial frequencies, part of the rays reach the prisms after reflection on the top face of the pipe (see Fig. 3-33). This effect results in a broader and asymmetric illumination angular spectrum. Figure 3-34 presents a geometrical turnaround which allows to avoid the unwanted asymmetric outcoupling.

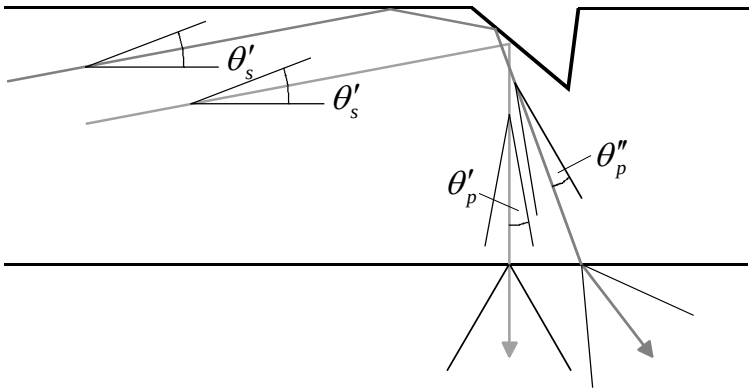

Fig. 3-33 Asymmetric outcoupling after reflection on the top face of the pipe.

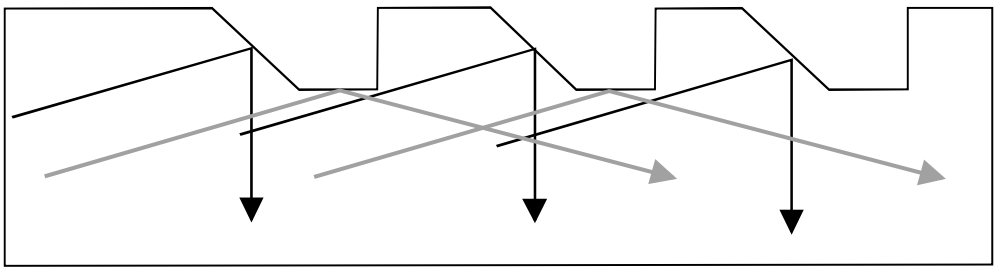

Fig. 3-34 Geometrical turnaround avoiding oblique outcoupling;
the rays reflected by the pipe top face do not reach the prisms.

An optimized prism angle is found iteratively by successive ray-tracing analysis. This approach takes into account the 3D configuration of the pipe as well as the apodization of the source (the flux carried by the rays is not equal in all directions). Figure 3-35 shows the outcoupled angular spectrums for the analytical solution ($\rho = 34.5°$) and for the numerically optimized prism angle ($\rho = 42.5°$).

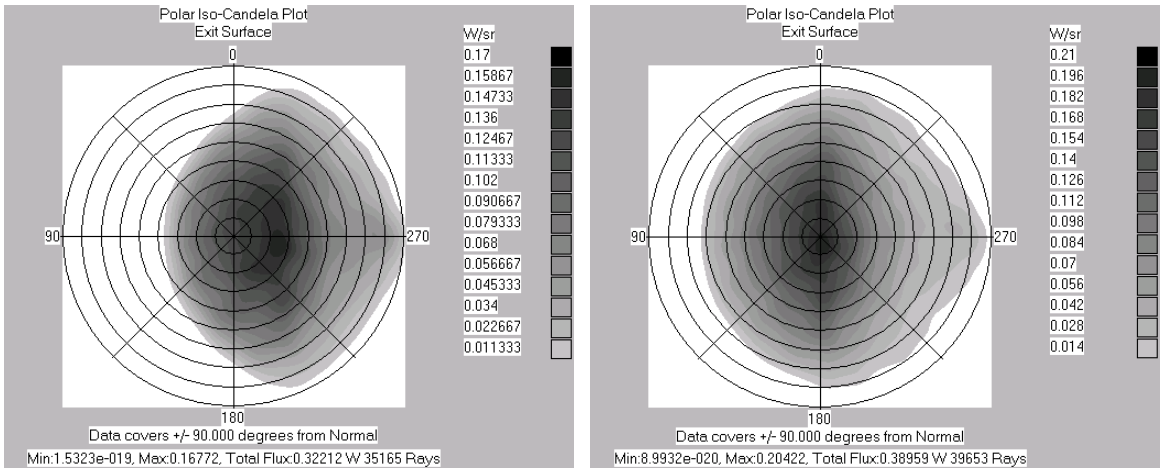

Fig. 3-35 Outcoupled angular spectrum for two different prism angles: $\rho = 34.5°$ *(left), and* $\rho = 42.5°$ *(right).*

We see that even the optimized outcoupled angular spectrum is not perfectly symmetric. This asymmetry is mainly due to the asymmetrical nature of the half cone incident on the micro-prisms. A perfectly symmetric illumination angular spectrum could be achieved by a Lambertian scattering outcoupler (e.g. the scattering paint), or by a symmetric micro-prism light pipe (see Fig. 3-36).

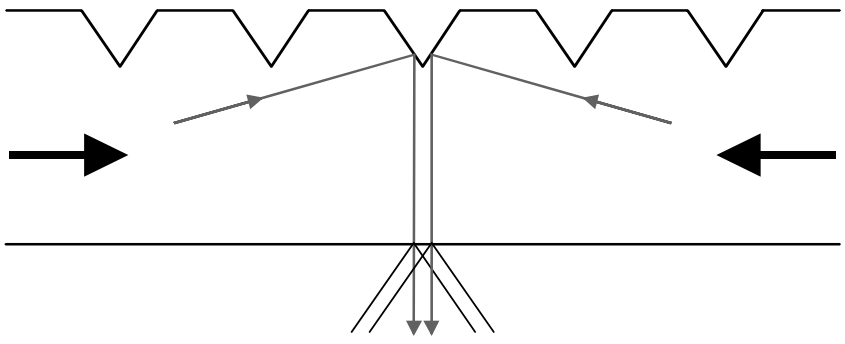

Fig. 3-36 Symmetric outcoupled angular spectrum produced by a symmetric micro-prism light pipe..

Determination of the prism size

We have shown in section 3.1.6 that the shadowing effect can be minimized when the prism depth P_y is small compared to the pipe cross-section Y. See Fig. 3-30 for the definition of the geometrical parameters. An indicative criteria, based on experience, fixes the maximal prism depth in function of the prism cross-section to

$$P_y \leq \frac{Y}{20} \ . \tag{3-13}$$

As shown in the next section, small prism sizes allow to have a smoother repartition of the prisms on top of the pipe surface. This way, near-field discontinuities can be avoided. On the other hand, the micro-prisms should not be too small in order to avoid diffraction effects. Given the large angles of incidence, the prism size should be $P_z \geq 10\,\mu m$ for the visible.

Beside the design considerations, the choice of the prism size is also based on the limitations and the costs of the technology. Typically, the prism depth is chosen in the $10\,\mu m \leq P_y \leq 200\,\mu m$ range. The realization of micro-prisms in the range of $25\,\mu m$ to $100\,\mu m$ is a technological challenge, because these dimensions are large for photolithographic technologies and small for the traditional diamond turning approach. The strengths and limits of the different technologies are discussed in section 3.3.

In the case of the specified light pipe (see section 3.2.3.1), a lateral prism size of $P_z = 100\,\mu m$ is chosen. With a prism angle of $\rho = 42.5°$, this corresponds to a prism depth of $P_y = 91.6\,\mu m$. These dimensions can be realized by diamond turning. Other technologies, like laser micro-machining, may also be considered.

3.2.3.2 Calculation of the outcoupler spatial density

The design principle of illumination light pipes consists in balancing, all along the pipe, the amount of energy which is transported by TIR, and the energy which is coupled out from the pipe for illumination purposes. As illustrated in Fig. 3-1, the illumination rays result from the deflection produced on the rays reaching the outcouplers distributed on the pipe surface. Thus, locally, the outcoupled flux $I_{out}(z)$ is propor-

tional to the guided flux $I(z)$ multiplied by the outcoupler surface density (or fill-factor) $\Gamma(z)$, viz.

$$I_{out}(z) \propto \Gamma(z) \cdot I(z) \ . \qquad (3\text{-}14)$$

As part of the light is coupled out, the guided flux $I(z)$ decreases along the pipe. The design task is to find the outcoupler distribution on the pipe surface which delivers the required illumination. In the example of Fig. 3-37, where the illumination flux has to be constant ($I_{out}(z) = cst$), the outcoupler density $\Gamma(z)$ increases along the pipe in order to compensate the decrease of the guided flux $I(z)$.

Application of the optical transfer block (OTB) method

For the delivery of a uniform illumination, the distribution of the outcouplers along the surface could be calculated analytically. We show hereafter that the more general OTB approach described in Chapter 2 is perfectly adapted for this task. Moreover, the OTB method can be applied to non-uniform lighting distributions.

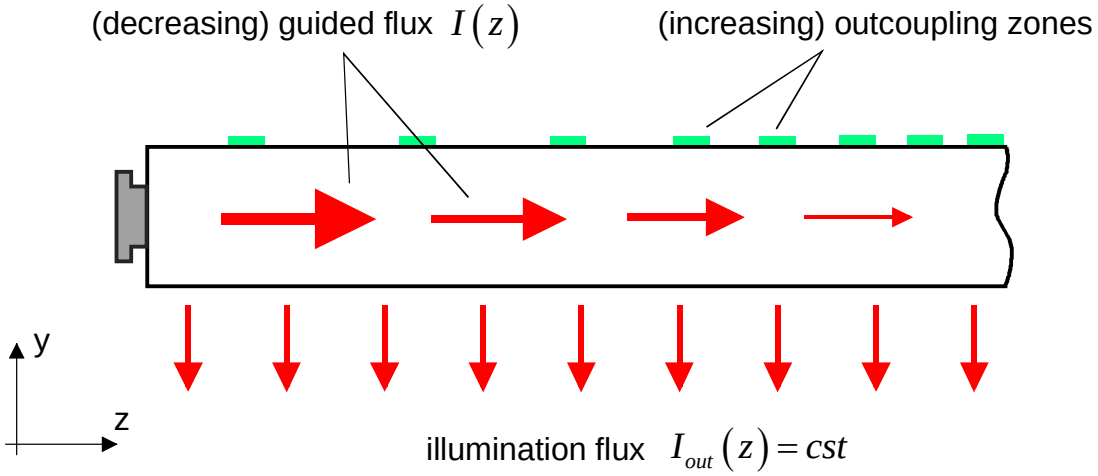

Fig. 3-37 Dependency of the illumination flux on the guided flux and on the outcoupler density.

The OTB method describes the transfer of the flux along the pipe by appropriately chosen volume elements, or blocks (see Fig. 3-38). The method gives a good estimation of the macroscopic behavior of the light pipe with a reduced set of parameters. Once the energy characteristics of each block have been calculated, the research of the

best outcouplers distribution is made easier. A further analysis, with the help of a non-sequential ray-tracing program, is necessary for the final fine tuning of the design.

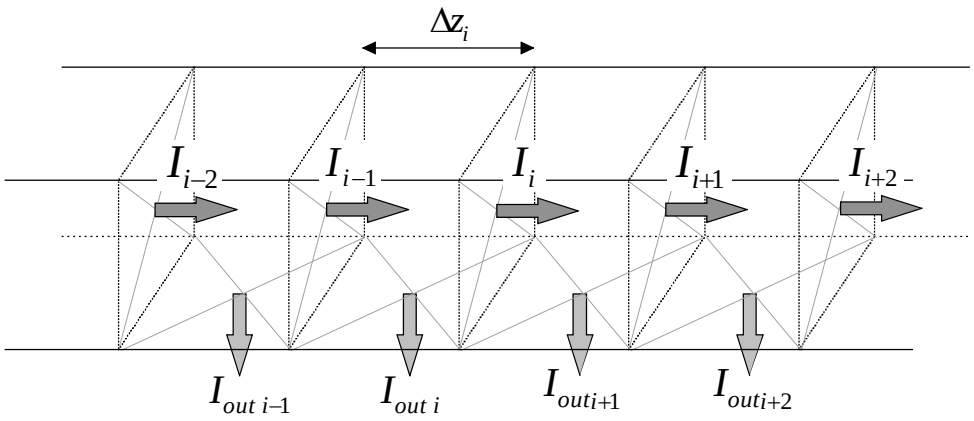

Fig. 3-38 Analysis of the flux propagation by power transfer blocks.

The inner nature of each block does not matter in a first approach. As illustrated, we are only interested in the transfer of the flux along the pipe. Thus, the model does not have to take into account the variations of the angular spectrum or polarization effects.

The OTB assumes that the flux is constant inside the boundaries of each block face. Figure 3-39 presents the repartition of the flux at different positions inside the pipe. We observe a near-field effect at the proximity of the source. Nevertheless, the distribution of the flux becomes quickly uniform ($z > 2.5\ mm$). In other words, the OTB approach should not be used to analyze the light pipe behavior at the proximity of the pipe. For our configuration, the near-field effect affects only a very small portion of the pipe. Therefore the OTB should be applied successfully.

We describe hereafter the design of a uniform illumination light pipe by the OTB method. As illustrated in Fig. 3-40, each block i is characterized by its length Δz_i, the flux I_{i-1} of the guided rays at the block entrance, and the (constant) outcoupled flux I_{out}. The following assertions are made : the pipe material has an absorption coefficient α and the split between guided and outcoupled rays happens at the entrance of each block.

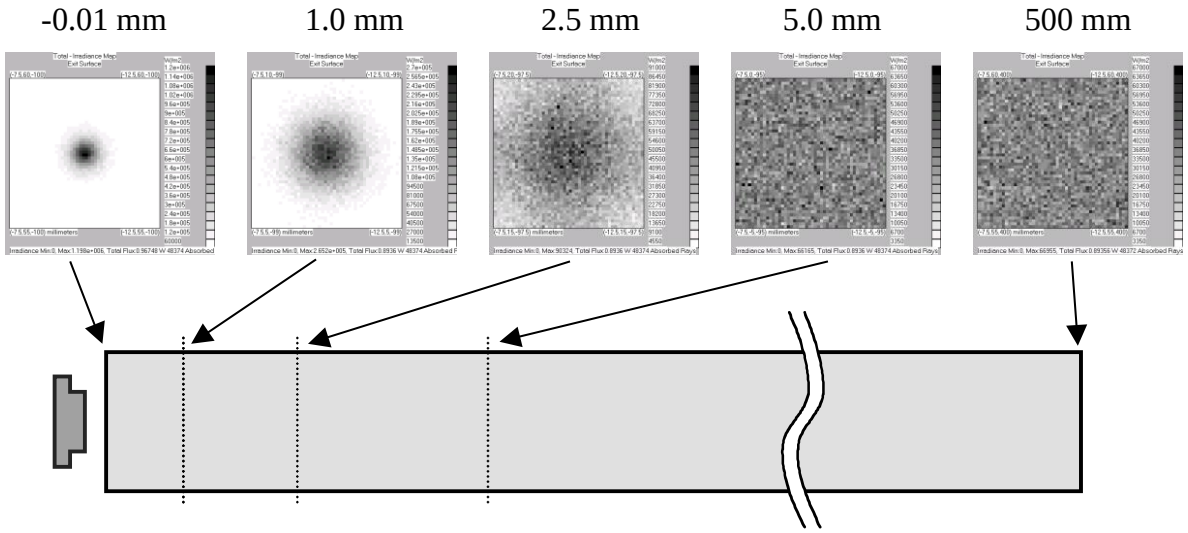

Fig. 3-39 Flux distribution for different sections along the (polished) light pipe.

For each block, the conservation of energy implies

$$I_{i-1} = I_i + I_{out} + A_i \ , \tag{3-15}$$

where A_i is the energy absorbed inside the i^{th} block.

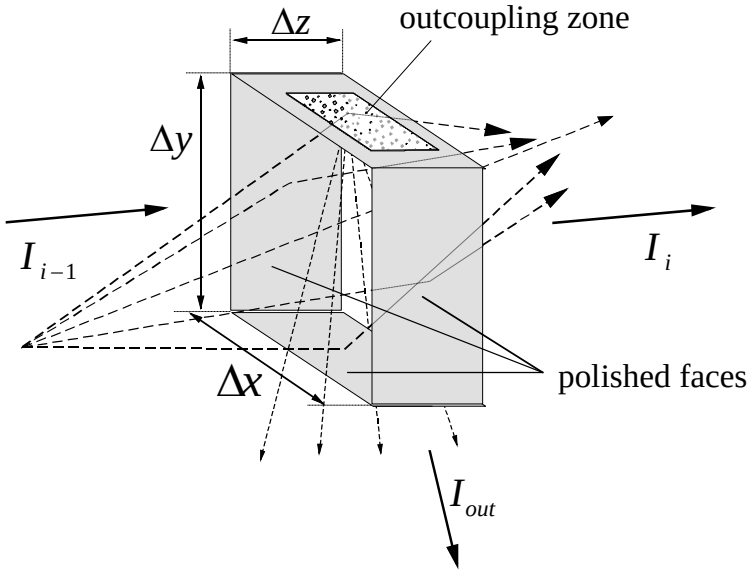

Fig. 3-40 Detailed view of the i$^{\text{th}}$ *light pipe block.*

The absorption can be decomposed as

$$A_i = A_{out_i} + A_{g_i} \ , \tag{3-16}$$

where, A_{out_i} is the energy lost by the outcoupled rays inside the pipe, and A_{g_i} is the absorption of the guided rays within a block.

A_{out_i} is proportional to the outcoupled flux I_{out_i} ($A_{out_i} = \beta_i \cdot I_{out_i}$). Considering that each block has the same geometry and that the outcoupled flux is constant, A_{out_i} becomes

$$A_{out_i} = A_{out} = \beta\, I_{out}, \quad \forall i \ . \tag{3-17}$$

The absorption on the outcoupled rays A_{out} can be originated by absorption at the surface (e.g. metallic absorption) and/or absorption in the pipe volume. This last component can be neglected for blocks having small cross-sections.

The flux of the outcoupled rays before absorption is defined as

$$\tilde{I}_{out} = I_{out} + A_{out} = I_{out}\left(1+\beta\right) = cst \ . \tag{3-18}$$

For each block, the absorption of the guided rays can be written as

$$A_{g_i} = I_i\left[\exp\left(\alpha \cdot \bar{s}\right) - 1\right] , \tag{3-19}$$

where $\bar{s}$ is the average path length of the guided rays inside each block.

Taking into account Eq. (3-19), the energy balance inside a block becomes

$$I_i = I_{i-1} - \tilde{I}_{out} - A_{g_i} = \left(I_{i-1} - \tilde{I}_{out}\right) \cdot \exp\left(-\alpha \cdot \bar{s}\right) \ . \tag{3-20}$$

I_0 being the intensity at the pipe entrance, it is easy to demonstrate recursively that

$$I_i = I_0 \cdot \exp\left(-i \cdot \alpha \cdot \bar{s}\right) - \tilde{I}_{out} \sum_{j=1}^{i} \exp\left(-j \cdot \alpha \cdot \bar{s}\right), \quad i \in \{1..b\} \ , \tag{3-21}$$

where *b* is the total number of blocks.

An outcoupling coefficient χ_i is defined as

$$\chi_i = \frac{\tilde{I}_{out}}{I_{i-1}} \ . \tag{3-22}$$

Substituting Eq. (3-21) into Eq. (3-22), the outcoupling coefficient for each block along the pipe becomes

$$\chi_i = \begin{cases} \dfrac{\tilde{I}_{out}}{I_0} & \text{for } i = 1 \\ \dfrac{1}{\dfrac{I_0}{\tilde{I}_{out}} \cdot \exp\left[-(i-1)\cdot\alpha\cdot\bar{s}\right] - \sum_{j=1}^{i-1}\exp\left(-j\cdot\alpha\cdot\bar{s}\right)} & \text{for } i \in \{2..b\} \end{cases} . \tag{3-23}$$

The boundary condition requires that the guided intensity at the end of the pipe must be greater than zero. If the pipe is subdivided into *m* blocks, the maximum outcoupled power per block becomes

$$\tilde{I}_{out_{\max}} = \frac{\exp\left(-m\cdot\alpha\cdot\bar{s}\right)}{\sum_{j=1}^{m}\exp\left(-j\cdot\alpha\cdot\bar{s}\right)} \cdot I_0 \ . \tag{3-24}$$

The outcoupling coefficient χ_i of each block being known, the design of the light pipe can be finalized. The outcoupling coefficient χ_i is related to the block outcoupler density by the following relation

$$\chi_i = \Gamma_i \cdot S_i \cdot K \ , \tag{3-25}$$

where K is the outcoupling coefficient of the used outcoupler, and S_i is the surface of the i^{th} block.

For micro-prism light pipes, the outcoupling coefficient K is function of the shape of the prisms. If the prism shape is kept unchanged all along the pipe, the outcoupling coefficient K is constant. The outcoupling coefficient K is determined numerically with a the help of a non-sequential ray-tracing program.

If the prism spatial frequencies ν_p is high, the shadowing effect influences the outcoupling coefficient $K(\nu_p)$. In this case, the numerical determination of the outcoupling coefficient $K(\nu_p)$ should be repeated for different prism spatial frequencies.

Encoding schemes

Equation (3-23) defines the outcoupler surface density Γ_i for each block i in view to get a uniform illumination along the pipe. The geometrical definition of Γ_i is given by

$$\Gamma_i = \frac{S_{o_i}}{S_i} \ , \tag{3-26}$$

where S_{o_i} is the surface covered by the outcoupler for the block i. Usually, the block size is kept constant along the pipe; in this case S_i is constant. Using Eqs. (3-25) and (3-26), we get the design condition for each block i in view to get a uniform illumination light pipe

$$S_{o_i} = \frac{\chi_i \cdot S_i}{K} \ . \tag{3-27}$$

The final step of the design consists in covering the surface of each block with the outcoupler respecting the condition given by Eq. (3-27).

In the case of the micro-prism light pipe (specified in section 3.2.1), the prism cross-section is kept constant all along the pipe (see Fig. 3-41).

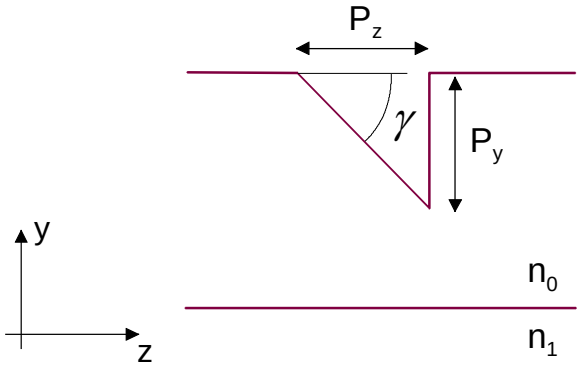

Fig. 3-41 Prism cross-section parameters (constant all along the pipe).

For each block, the variation of the surface S_{o_i} covered by the prisms is achieved by changing the prism dimension P_x and/or the prism density along the z-direction. As illustrated in Fig. 3-42, we have considered two prism encoding schemes. The first approach (Fig. 3-42a) keepings all the dimensions of the prisms constant all along the

pipe. The modulation of the prism surface density is achieved by the variation of the prism spatial frequency vs. the z-axis. The second method (Fig. 3-42b) tends to keep the prism spatial frequency constant and to only vary the prism dimension vs. the x-axis P_x. When the prism size reaches the size of the pipe cross-section, the prism spatial frequency is doubled and the encoding process goes on. A more general encoding scheme where the spatial frequency and the prism dimensions vary simultaneously could be considered for the generation of more complex lighting distributions.

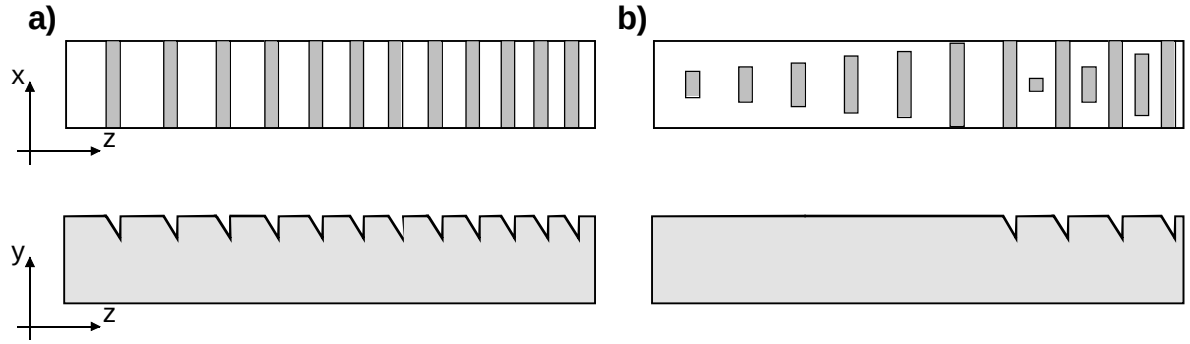

Fig. 3-42 Prism encoding schemes :
a) variable spatial frequency with constant prism size along the x-axis,
b) variable prism size along the x-axis with constant spatial frequencies.

The two encoding schemes shown in Fig. 3-42 have been applied to design the specified light pipe. The distribution of the outcoupled flux along the pipe has been simulated by ray-tracing for both configurations (see Fig. 3-43). The graphics illustrate the flux distribution close to the outcoupling face of the pipe (near-filed measurement).

The average outcoupled flux is almost uniform along the pipe. However strong local variations are observed for the variable frequency case (left). This is a near-field effect due to the large distance between the prisms at the beginning of the pipe (separation between the first two prism : $18.7\,mm$). Thus, each peak at the beginning of the pipe corresponds to the contribution of a single prism. As the distance between the prisms decreases along the pipe, the contribution of the prisms overlap and the peaks vanish (see Fig. 3-44). In the fixed frequency case, the prisms at the beginning of the pipe are separated by only $2\,mm$, and thus no near-field effect is observed. The near-field effect can also be avoided for the variable spatial frequency case, if a smaller prism size

is chosen. In this case, the prism spatial frequency can be proportionally increased. However, as the cones of illumination overlap when the light moves away from the pipe, the near-field effect is not necessary disturbing.

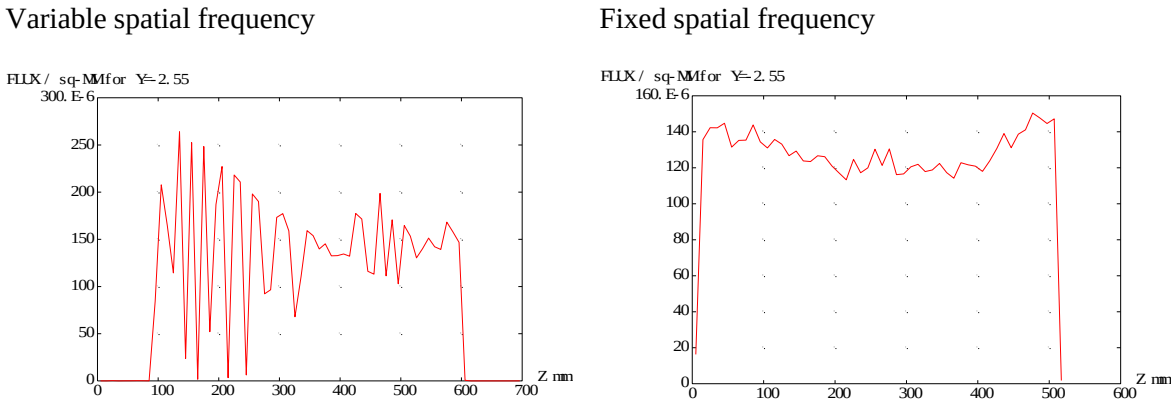

Fig. 3-43 Distribution of the illumination for the two encoding schemes; for the constant longitudinal prism size of : $P_z = 100\,\mu m$.

The variable prism size configuration (Fig. 3-42b) is technologically more demanding. Indeed, it is easier to manufacture prisms through the full face of the pipe (Fig. 3-42a), than to etch prisms having lateral faces. Depending on the considered manufacturing technology, this can be a decisive advantage in favor of the variable spatial frequency encoding scheme.

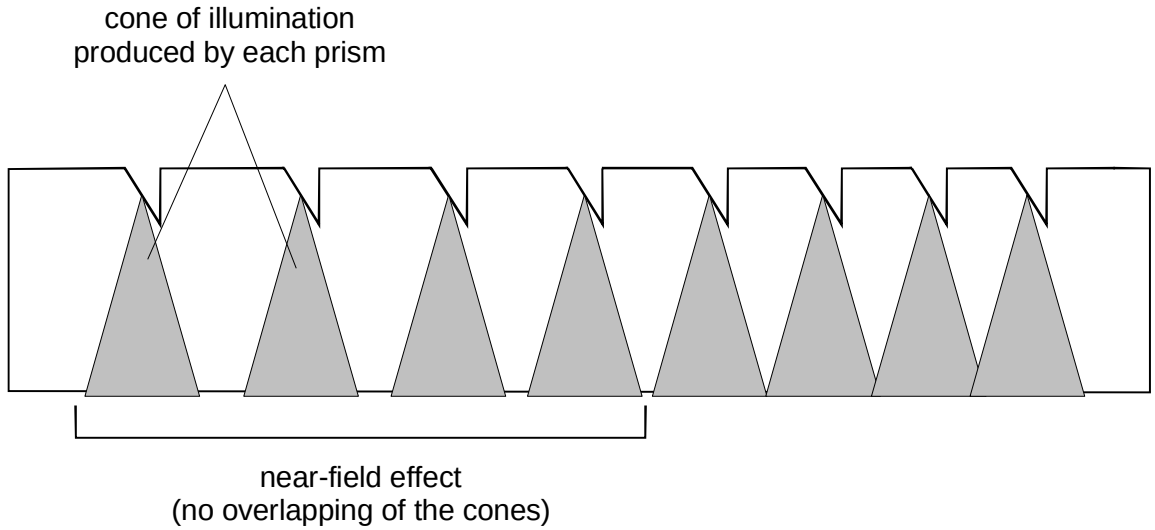

Fig. 3-44 Illustration of the near-field effect.

3.2.4 Lighting efficiency

Usually, one of the requirements of illumination devices is to maximize the amount of energy reaching the optical target (object or detector to be illuminated). The origin of the optical losses is presented hereafter. Ways to maximize the lighting efficiency of illumination light pipes are proposed.

The optical efficiency of the illumination light pipe is defined by

$$\eta = \frac{\phi_o}{\phi_s} \ , \tag{3-28}$$

where ϕ_s is the flux emitted by the source, and ϕ_o the flux coupled out from pipe and used for the illumination. In this context, the optical losses are all the interactions which prevent the light from being coupled out from the pipe, in direction of the optical target.

The physical origins of optical losses are listed hereafter :

- absorption inside the pipe material,
- Fresnel reflection/refraction,
- metallic absorption.

At a wavelength of $\lambda = 650nm$, measurements have shown that the absorption of molded PMMA may vary considerably. We consider an average value of $1dB/m$. This means that the absorption inside PMMA can be neglected for small light pipes. In the case of a $500mm$ long light pipe, the percentage of energy lost by absorption at the end of the pipe corresponds to

$$1 - \frac{I_1}{I_0} = 1 - 10^{-\frac{0.5}{10}} = 10.88\% \ , \tag{3-29}$$

where I_1 is the flux reaching the end of the pipe, and I_0 is the guided flux at the entrance of the pipe.

Fresnel reflection happens each times the light meets a jump of refractive index. The reflectivity depends on the angle of incidence of the rays as shown in Appendix C. In the case of the light pipe, losses by Fresnel reflection happen for the air-to-PMMA and PMMA-to-air interfaces. A few percent of energy are lost at the LED-to-pipe interface, as well as when the light is coupled out from the pipe. Overall Fresnel losses contribute to a reduction of 10 to 15% of the lighting efficiency.

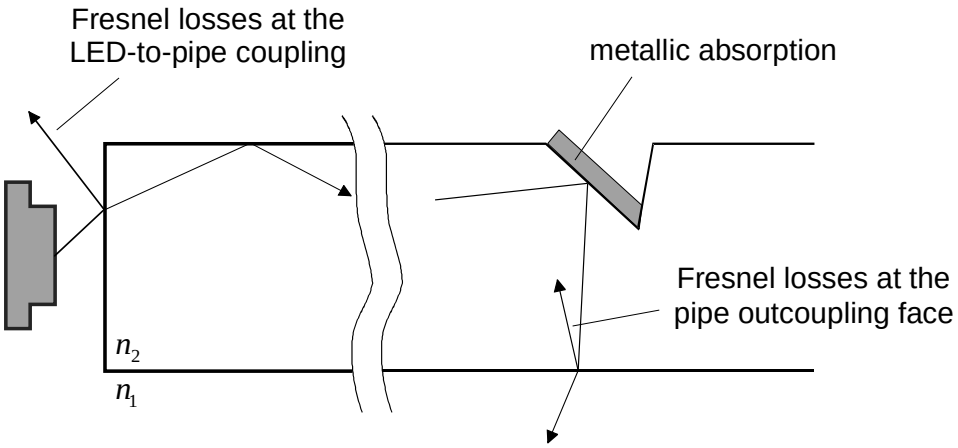

Fig. 3-45 Illustration of the losses produced by Fresnel reflection/refraction and metallic absorption .

The losses by metallic absorption are generated every time when the light reaches a coated surface. As shown in Appendix C, the metallic absorption for an Al-coated surface varies from 0 to 17%, depending on the angle of incidence. As discussed in section 3.1.6.1, if possible, metallic reflection should not be used for the guiding of the rays, but only for outcoupling purposes. Figure 3-23 illustrates the influence of the coating configuration on the light pipe lighting efficiency.

Losses having a physical origin can hardly be avoided. Some losses may have their origin in a poorly designed light pipe. For instance, in the case of the linear light pipe, the light reaching the end of the pipe is lost (see Fig. 3-46). The flux ϕ_{end} could be recycled by back reflection into the light pipe (Fig. 3-47a), or by direct outcoupling generated by a progressive diminution of the pipe cross-section (Fig. 3-47b).

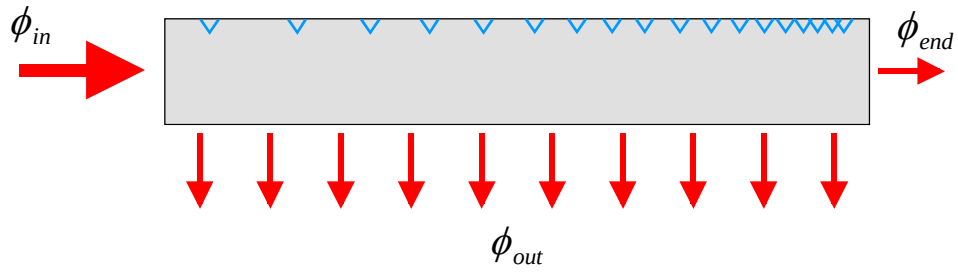

Fig. 3-46 Energy lost at the end of the pipe (flux ϕ_{end}).

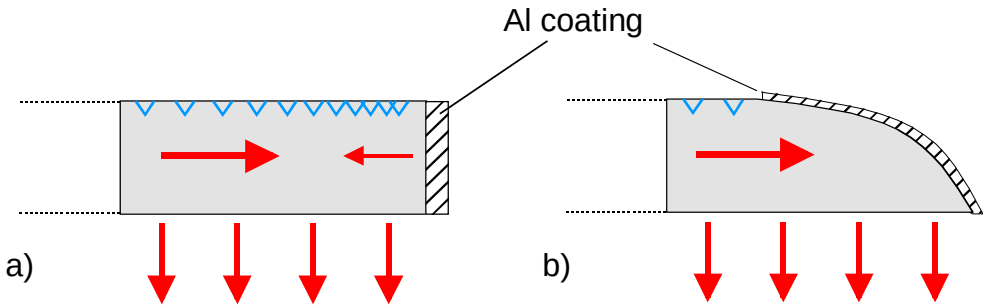

Fig. 3-47 Two alternative designs for recycling of the flux reaching the end of the pipe.

3.2.5 Tolerancing

The design of any device needs to take into account the imperfections (or deviations from the ideal design) which are going to be introduced by the manufacturing process. The optical performances of a good design should only vary slightly, if the manufacturing tolerances are respected.

The perturbations introduced by the manufacturing process depend on the accuracy of the technology. Most of the variations are geometrical. If the fabrication of the pipe is done by replication, special care has to be taken during the fabrication of the master (or molt) in view to avoid the systematic reproduction of manufacturing errors.

Each tolerancing parameter and its influence on the performances of the lighting device is discussed hereafter.

The pipe geometry

The primary function of a light pipe is to transport the light without losses by TIR. A good manufacturing process should keep this behavior intact.

We have shown in section 3.1.4, that if the cross-section of the pipe varies (see Fig. 3-8b), the angular spectrum inside the pipe is influenced, and part of the light may be coupled out. Nevertheless, these macroscopic variations of the pipe cross-section can easily be avoided by the manufacturing. In other words, the accuracy of the dimensions of the pipe is not very critical.

Depending on the used manufacturing technology, some undesired surface roughness can be introduced. In this case, part of the guided light is coupled out from the pipe by surface scattering [3-20], producing optical losses. The transport of energy by TIR requires a surface quality close to the optically polished surfaces. In other words, the heights of surface irregularities have to be small compared with the wavelength (approximately $10\,nm$ for the visible).

The micro-prism geometry

The prism shape influences the direction of propagation of the outcoupled rays. Thus, as illustrated in Fig. 3-48, a variation of the prism angle ρ changes the illumination angular spectrum. A tolerance of $\pm 2°$ around the optimal prism angle ($\rho = 42.5°$) is acceptable. These requirements can easily be achieved by most of the fabrication processes.

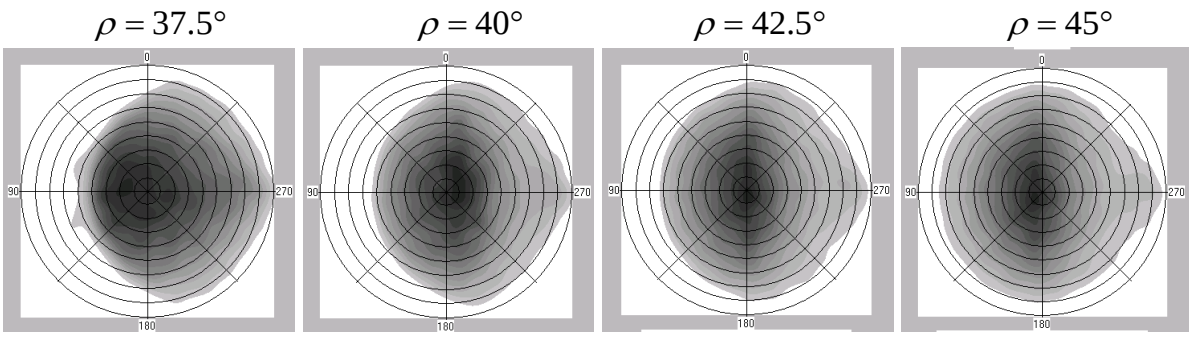

Fig. 3-48 Angular spectrum of the outcoupled rays in function of the prism angle ρ.

As illustrated in Fig. 3-49, the geometry of the prisms can be affected by the manufacturing process. In particular, the effective prism size P_z' may be modified, thereby influencing the local outcoupling coefficient χ_i and the distribution of the illumination. A fine tuning of the design may be required once the influence of the manufacturing has been characterized experimentally.

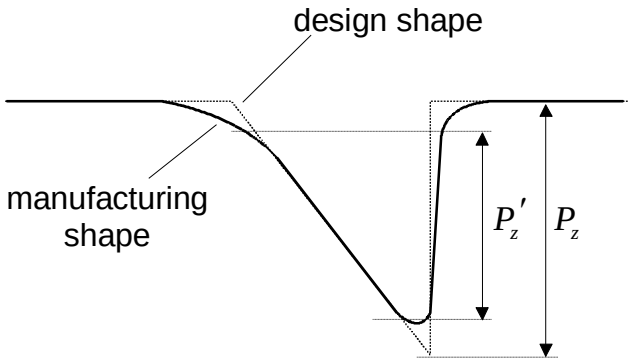

Fig. 3-49 Variation of the prism shape between design and manufacturing.

Position of prisms along the pipe

The position of the prisms along the pipe determines the distribution of the illumination. However, the tolerances in the prism positioning are not very demanding. The manufacturing tools can address the position of the prisms with a precision of a few microns. This generally corresponds to a small fraction of the local prism spacing and therefore does not influence the optical properties of the pipe.

Absorption coefficient of molded PMMA

A variation on the absorption coefficient α could be introduced by variations in the injection molding process. Measurements have shown that, at $650nm$, the attenuation of molded PMMA may vary from $0.5dB/m$ to $2dB/m$. Such variations may slightly influence the uniformity of the illumination for long light pipe ($>1m$). However, the influence of absorption can generally be neglected.

3.2.6 Ray-tracing analysis

We have shown in Chapter 2, that different analysis methods can be used for the analysis of illumination devices. Non-sequential ray-tracing is the most commonly used technique. Nevertheless, ray-tracing is not very well adapted for the simulation of complex scenes, because it suffers from the waste of computer resources.

However, ray-tracing is perfectly well adapted for the analysis of the illumination light pipe. Actually, all the rays emitted by the source are coupled into the pipe. Inside the pipe, the rays interact with the pipe surfaces, where they are either reflected or coupled out from the pipe by the outcouplers. Thus, all rays participate to the light pipe behavior, and therefore there is no waste of resources during a ray-tracing simulation. Nevertheless, the analysis of the light pipe represents only one step of the design process. Depending of the light pipe function, it may be required to simulate the interaction of the light leaving the pipe with the surrounding scene. In this case, the use of other methods like the radiance equation or the radiosity may be necessary. A further limitation of non-sequential ray-tracing (and of all illumination simulation tools) is the lack of automatic optimization. Therefore, we have used the OTB method to determine the distribution of the outcouplers on the pipe surface. In this context, ray-tracing is a complementary tool, which allows the validation and the fine tuning of the design achieved with the OTB method.

In order to illustrate the different steps of a ray-tracing session, we present hereafter the analysis of the micro-prism light pipe specified in section 3.2.1.

Definition of the system geometry

The light pipe geometry is relatively simple. It can be directly defined within most of non-sequential ray-tracing programs, which have some CAD capabilities. However, the use of a parametric solid modeling program allows the rapid modification of the design parameters (i.e. the position, the size, and the shape of the prisms) and therefore simplifies the tolerancing analysis.

Attribution of the optical properties

The pipe material (PMMA) is defined by its index of refraction, and its absorption coefficient at the analysis wavelength. The metallic coating (Al) is defined by its complex refractive index, which is also wavelength dependent. Micro-roughness parameters may also be introduced in order to simulate the imperfections introduced by some technological processes.

Definition of the detectors

The detectors are planes which record the position, the direction and the flux of the intersecting rays, allowing to analyze the irradiance $\left(W\,m^{-2}\right)$ and the intensity $\left(W\,sr^{-1}\right)$. For the ray-tracing process, the detectors are placed at positions where the analysis of the spatial and angular distribution of light serves for the evaluation of the design performances. Figure 3-50 illustrates the positioning of the main detectors used during the ray-tracing analysis. The longitudinal detector is placed very close to the pipe (a few microns). It allows to control the uniformity of the illumination as well as the direction of the illumination. The transversal detector is moved at different positions inside the pipe. It allows to see the evolution of the angular spectrum of the guided rays.

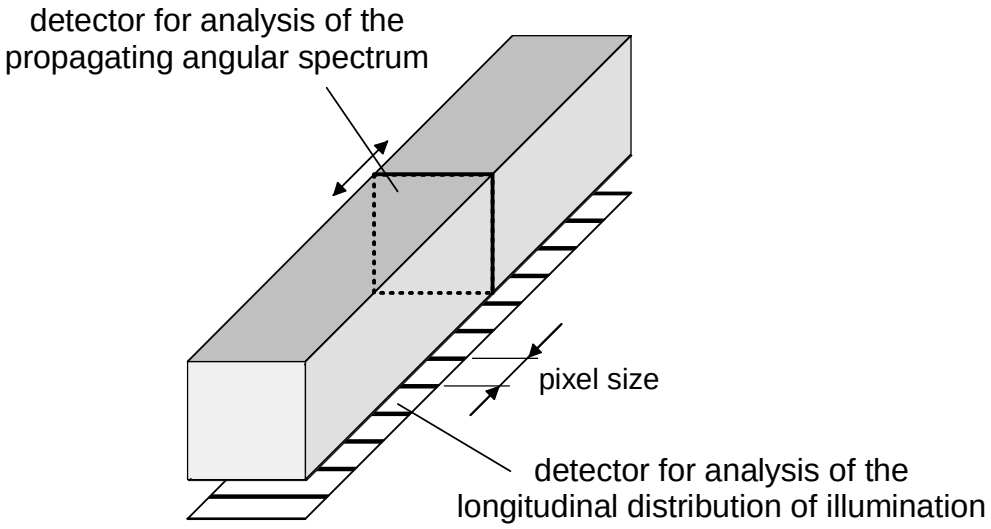

Fig. 3-50 Positioning of the detectors for the ray-tracing analysis.

The pixel size (or resolution) of the detectors has to be defined. The resolution is determined in function of the application (i.e. resolution of a CCD camera). This parame-

ter also influences the precision of the simulation and, indirectly, the number of rays necessary to reach an acceptable signal-to-noise ratio.

Definition of the source

Non-sequential ray-tracing programs allow the precise definition of the sources. In our example, the LED has an surface of emission of $200 \times 200\,\mu m^2$, an Lambertian emission behavior, and a central wavelength of $\lambda = 650\,nm$.

The number of rays emitted by the source needs to be defined before starting any simulation. This parameter determines the signal-to-noise ratio on the detectors and the computing time. For the specified example, $10'000$ to $500'000$ rays have been emitted by the source; corresponding to computing times of 1 to 12 hours on a 350 MHz Pentium II computer.

At this point, it should be noted that the computing time does not only depend on the number of rays to trace, but also on the number of intersections to calculate and on the ray-tracing cutoff conditions (see below). In other words, the computing time also depends on the complexity of the geometrical configuration (in this case, the number of prisms on the pipe surface).

Ray-tracing

As explained in section 2.1.1.2, two parameters need to be defined before the ray-tracing process : the ray split number (only necessary for the simulation of scattering) and the cutoff condition. These parameters will influence the precision of the simulation, as well as the computing time. The general strategy is to make the first simulations with conservative values (i.e. a low split number and a high cutoff condition), which imply low computing times. Then, the ray-tracing process is repeated with a new set of parameters. The results of the simulations are compared and the process is repeated until a convergence of the results is achieved.

In the case of our example micro-prism light pipe, no split number is defined (there is no scattering surface), and the cutoff condition has been set to 1%. This means that only one Fresnel reflection is taken into account during the simulation.

Evaluation of the design

The detectors record the flux and the direction of the incident rays and thus allow to analyze the irradiance and the angular spectrum at different positions. The study of the distributions on the detectors has two goals. First, it should determine if the simulated design fulfils the specified requirements. Moreover, if the requirements are not fulfilled, the analysis has to deliver the necessary information in view of the optimization of the design. For instance in the case of a micro-prism light pipe, an asymmetric angular spectrum of the outcoupled rays indicates that the prism angle ρ has to be adapted (see section 3.2.5).

In the case of the specified micro-prism light pipe, two main requirements have to be fulfilled : the illumination has to be uniform all along the pipe and the illumination angular spectrum has to be symmetric and normal to the pipe. Note that due to the sensitivity of the human eye [3-29], a variation of 10 to 20% of the illumination along the pipe is still considered as uniform.

The distribution of the illumination along the pipe has been simulated for the two different encoding schemes (see Fig. 3-43). The strong variations observed in Fig. 3-43a are due to a near-field effect, which disappear when the observation is done at a larger distance from the pipe. The configuration of Fig. 3-43b shows that the uniformity of the illumination fulfills the uniformity criteria (the peak-to-valley variation represent roughly 15%). It should be noted that both designs result directly from the approximate OTB method. The ray-tracing simulation suggests how the designs can be optimized. Actually, Fig. 3-43b shows that the prism spatial frequency can be slightly increased at the center of the pipe, in order to equalize the illumination along the pipe.

Figure 3-48 shows the illumination angular spectrum for different prism angles. In this case, the ray-tracing simulation allows the selection of the optimal prism angle, which cannot be defined with precision analytically.

3.3 Fabrication

The choice of a fabrication method depends on the size and the shape of the pipe, the quantity of samples to manufacture, and the allowed cost of production. But, above all, the technology is determined by the characteristics of the selected outcoupler.

We briefly review hereafter the possible manufacturing methods which can be used for each type of outcoupler. Some of these technologies are traditional, and thus perfectly mastered. Other technologies are specially developed for the manufacturing of micro-optical elements. Some of these techniques are still in their infancy and their real limits (and potential) are still under investigation.

Volume scattering outcouplers

Volume scattering is produced by the interaction of the light with the particles (molecules) inside the media. As shown in Fig. 3-6, the outcoupling can be produced by volume scattering zones within the light pipe. In this case, the scattering media is produced directly at the manufacturing stage of the light pipe. These techniques are similar to those used for the realization of doped fibers or GRIN lenses. Volume scattering light pipes are relatively expensive to produce. But it may be the only valid approach for very small cross-section light pipes, as those used for endoscopic applications [3-19]. Actually, the micro-machining of very small surfaces is unpractical and an endoscopic fiber has a typical diameter of a few hundred of microns.

The scattering media can also be deposited on top of the pipe surface, under the form of a scattering paint layer. Scattering paint light pipes [3-24] present the advantage that they are very easy to realize. The hands of some automotive dashboards represent the best known example of painted light pipes. However, painting does not represent a suitable solution for light pipes requiring a precise and reproducible mass production.

Surface scattering outcouplers

It is well know that rough surfaces produce scattering. The surface micro-roughness is generally an undesired parameter resulting from the machining and/or imperfect pol-

ishing. In the case of surface scattering light pipes, the surface micro-roughness is not a manufacturing defect, but a desired property.

In order to get reproducible BSDFs, the surface micro-roughness has to respect some statistical properties (i.e. random distribution). Mechanical manufacturing tools tend to produce directive micro-grooves, which produce anisotropic scattering. Optical diffusing surfaces can be produced by the recording of speckles into a photoresist layer deposited on top of the pipe surface [3-21]. As the speckle size can easily be controlled, the surface profile can be smoothly modulated. Once one surface scattering light pipe is realized, it can be reproduced at low cost by injection molding [3-30] or embossing [3-31].

Micro surface relief outcouplers

Refractive, reflective, and diffractive outcouplers are all micro-relief optical elements. Therefore, they share the same manufacturing constraints. The selection of the manufacturing technology depends on the shape and size of the micro-structure, on the material, and on the allowed fabrication cost. An extended review of the technologies for the manufacturing of micro-optics is presented in [3-32]. We discuss hereafter the possible technologies for the realization of micro-prism light pipes.

Micro-prism light pipes are products which have generally to be manufactured in large quantities. Therefore, the cost of production is one of the first criteria for the selection of the manufacturing technology. Moreover, the manufacturing process has to fulfill the specified tolerances, which define the acceptable variation of the prism geometry and the acceptable surface roughness.

The low cost manufacturing of micro-prism light pipes is a two steps process, a master is first realized and then the mass production is done by replication. The replication process implies the use of polymer light pipes (e.g. PMMA). The replication is either done by injection molding [3-30] or embossing [3-31].

Different technologies may be used for the realization of the master micro-prism light pipe. The choice of the technology mainly depends on the prism geometry, and on the minimal and maximal feature sizes. The strengths and limits of the different technolo-

gies for the fabrication of micro-prisms is still under investigation. First results show that diamond turning and laser ablation [3-33] are good candidates for the manufacturing of relatively large micro-prisms ($>50\,\mu m$). Technologies like laser beam writing [3-34] and gray-tone mask [3-35, 3-36] have also a good potential for the realization of small micro-prisms ($<20\,\mu m$). Alternative techniques, such as electro-erosion, wet etching of silicon, mass transport smoothing [3-37] have been applied with success to the realization of micro-prisms. However, the former technologies have constraints that limit them to specific configurations.

The development of the different technologies is going on in order to master the manufacturing of prisms having a depth in the $20\,\mu m$ to $50\,\mu m$ range. An other challenge consists in finding a technology able to realize small prisms ($<20\,\mu m$), with large prism angles ($\rho > 45°$), and a reduced surface roughness.

The next table summarizes the general characteristics of the different technologies. The values should only be taken as indicative.

technology	prism depth min.	prism depth max.	maximum prism angle	surface roughness
diamond turning	$50\,\mu m$	∞	70°	average
laser ablation	$20\,\mu m$	∞	70°	average
laser beam writing	$2\,\mu m$	$20\,\mu m$	50°	average
gray-tone mask	$2\,\mu m$	$20\,\mu m$	50°	good
wet etching of silicon	$2\,\mu m$	∞	fixed	good
electro-erosion	$50\,\mu m$	∞	70°	poor
mass transport smoothing	$2\,\mu m$	$20\,\mu m$	40°	good

Table 3-1 Main characteristics of the possible technologies for micro-prisms

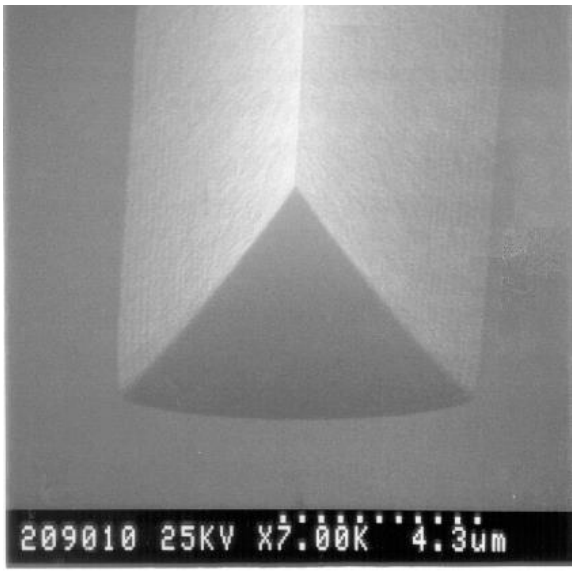

Fig. 3-49 Photoresist micro-prism manufactured from a gray-tone mask.
(courtesy of Fraunhofer - Institute für Siliziumtechnologie, D-25524 Itzehoe)

3.4 References

[3-1] W. T. Welford, R. Winston, *High Collection Nonimaging Optics*, Academic Press, San Diego, 1989

[3-2] W. B. Elmer, *The Optical Design of Reflectors*, John Wiley & Sons, New York, 1980

[3-3] M. Shinohara, et al. "Vector Radiation Coupling Method for High Efficiency and High Uniformity Lightguide", Proc. of the Diffractive Optics and Micro-Optics Conference, OSA Technical Digest Series Vol. **10**, 189-191 (1998)

[3-4] Y. Oki, "Novel Backlight with High Luminance and Low Power Consumption by Prism-on-Light-Pipe Technology", SID Digest, 157-160 (1998)

[3-5] M. Suzuki, J. Mamiya, et al., "Improvement of Backlighting Method by Means of Light Pipe Polarizer", Proceedings of the 16th International Display Research Conference, 229-232 (1996)

[3-6] M. Suzuki, Y. Oki, "A Backlighting Unit with Polarization Recycle by Stacked Transparent Plates", SID AsiaDisplay Digest, (1998)

[3-7] T. Funamoto, et al., “A Front-lighting System Utilizing A Thin Light Guide”, SID AsiaDisplay Digest, (1998)

[3-8] H. J. Cornelissen, M. J. J. Donna, H. Greiner, “Frontlights for Reflective LCDs Based on Lightguides with Micro-Grooves”, 1999 SID International Symposium Digest of Technical Papers, **30**, 912-915 (1999)

[3-9] J.-C. Poli, J. Grupp, J. M. Teijido, H. P. Herzig, *Dispositif d'illumination uniforme du cadran d'un appareil d'affichage,* Europ. Patent EP860755A1 (1998)

[3-10] D. Decker, “CELIS – a concept for high-quality car interior lighting with light-guide technology”, SAE Technical Paper Series, **960488** (1996)

[3-11] D. J. Lamb, et al., “The Use of Aspheric Surfaces in Waveguide Illumination Systems for Automotive Display”, SAE Technical Paper Series, **980874** (1998)

[3-12] M. Poppendieck, D. Brown, “Control of Light Output from Plastic Optical Fiber with Optical Elements”, SAE Technical Paper Series, **960491** (1996)

[3-13] J. T. Remillard, et al., “Diode laser illuminated automotive brake lamp using a linear fanout diffractive optical element”, Proc. of the Diffractive Optics and Micro-Optics Conference, OSA Technical Digest Series Vol. **10**, 192-194 (1998)

[3-14] B. J. Cassarly, et al., “Distributed Lighting Systems: Uniform Light Delivery”, SAE Congress, March 1995

[3-15] I. R. Edmonds, et al., “Daylighting enhancement with light pipes coupled to laser-cut light-deflecting panels”, Lighting Res. Technol., **27**, 27-25 (1995)

[3-16] I. R. Edmonds, J. Reppel, P. Jardine, “Extractors and emitters for light distribution from hollow light guides”, Lighting Res. Technol. **29**, 23-32 (1997)

[3-17] A. Katzir, *Lasers and Optical Fibers in Medicine,* Academic Press, 1993

[3-18] J. Spigulis, D. Pfafords, “Clinical Potential of Side-Glowing Optical Fibers” Proc. SPIE **2977**, 84-88 (1997)

[3-19] H. van den Bergh, “On the Evolution of Some Endoscopic Light Delivery Systems for Photodynamic Therapy”, Endoscopy **30**, 392-407 (1998)

[3-20] M. Nieto Vesperinas, J. A. Sánchez Gil, "Light scattering from a random rough interface with total internal reflection", J. Opt. Am. A, **9**, 424-436, (1992)

[3-21] P. F. Gray, "A method of forming optical diffusers of simple known statistical properties", Optica Acta **25** (8), 765ff (1978).

[3-22] J. E. Harvey, A. Kotha, "Scattering Effects from Residual Optical Fabrication Errors", Proc. SPIE **2576**, (1995)

[3-23] M. Nieto-Vesperinas, "Random rough surfaces that produce a Lambertian distribution of radiant intensity", Opt. Lett., **8**, 165-167 (1982)

[3-24] J. M. Teijido, H.P. Herzig, R. Dändliker, J. Grupp, J.-C. Poli, "Design of a non-conventional illumination system using a scattering light pipe", Proc. SPIE **2774**, 747-756 (1996)

[3-25] A. Bjarklev, *Optical Fiber Amplifiers: Design and System Applications*, Artech House, Boston, 1993

[3-26] M. G. Moharam, et al., "Formulation for stable and efficient implementation of the rigorous coupled-wave analysis of binary gratings", J. Opt. Soc. Am A **12**, 1068-1076 (1995)

[3-27] J. M. Teijido,. H.P. Herzig, R. Dändliker, J. Grupp, "Illumination light pipe using micro-optics as diffuser", Proc. SPIE **2951**, 146-155 (1996)

[3-28] S. M. Zimmerman, et al., *Illumination system employing an array of microprisms*, United States Patent 5555109 (1996)

[3-29] E. F. Zalweski, "Radiometry and Photometry", *Handbook of Optics, volume II*, Chapter 24, McGraw-Hill, New-York, 1995

[3-30] R. A. Malloy, *Plastic part design for injection molding*, Hanser Publishers, Munich, 1994

[3-31] M. T. Gale, "Replication", in H. P. Herzig, ed., *Micro-Optics: Elements, Systems, and Applications*, Taylor and Francis, London, 1997, pp. 153-177.

[3-32] H. P. Herzig, ed., *Micro-Optics: Elements, Systems, and Applications*, Taylor and Francis, London, 1997

[3-33] P. Topart, et al., “Excimer laser fabrication and optical properties of polymer prismatic microstructures”, proc. SPIE, **3739**, 186-194 (1999)

[3-34] M. T. Gale, “Direct Writing of Continuous-relief Micro-optics”, in H. P. Herzig, ed., *Micro-Optics: Elements, Systems, and Applications*, Taylor and Francis, London, 1997, pp. 87-126.

[3-35] K. Reimer, et al., “One-level gray-tone lithography mask data preparation and pattern transfer”, proc. SPIE, **2783**, 71-79 (1996)

[3-36] K. Reimer, et al., “Fabrication of Microrelief Surfaces using a One-Step Lithography Process”, proc. SPIE, **3226**, 2-10 (1997)

[3-37] T. A. Ballen, J. R. Leger, “Mass-Transport Fabrication of Off-Axis and Prismatic Gallium-Phosphide Optics”, Appl. Opt. **38**, 2979-2985 (1999)

Chapter 4

An application example : the front-side watch lighting device

This chapter illustrates the full potential of illumination light pipes at the example of the frontal illumination of a watch dial. The concepts presented hereafter are protected by two patents [4-1, 4-2], owned by Asulab S.A. (2074 Marin, Switzerland).

The frontal lighting of watches is a challenging problem for different reasons. For aesthetic motivations, the illumination of the dial has to be as uniform as possible. Moreover, the device has to fit into the mechanical design of existing watches. The electrical consumption used for the illumination should be as low as possible, in order to preserve the lifetime of the watch battery. Moreover, the production cost of the lighting device (including the source, the driving electronics, and the optics) should fall in the $1 to $2 range.

There is no commercially available light source able to fulfill these requirements. The uniformity of the illumination could be partially achieved with a set of well orientated sources placed around the dial. But the multi-source approach is incompatible with the electrical and price requirements. The aim is to develop a low consumption extended light source, which surrounds the watch dial.

Recent advances in the field of electro-luminescent light sources [4-3] allow to generate a uniform emission over large surfaces. The geometry of the emitting surface can be customized for each application. In particular, an electro-luminescent ring surround-

ing the watch dial could be developed. Nevertheless, the relatively low lighting efficiency and the non-directive nature of the electro-luminescent sources are drawbacks for the watch application.

LEDs (light-emitting diodes) fulfill the electrical and mechanical requirements. However, LEDs have a very small surface of emission, which is a priori incompatible with the required uniformity of illumination. The solution is to inject the light emitted by the LED into a light pipe which surrounds the dial. Thus, the light is transported by the pipe all around the watch and can be selectively coupled out from the pipe for the illumination of the dial.

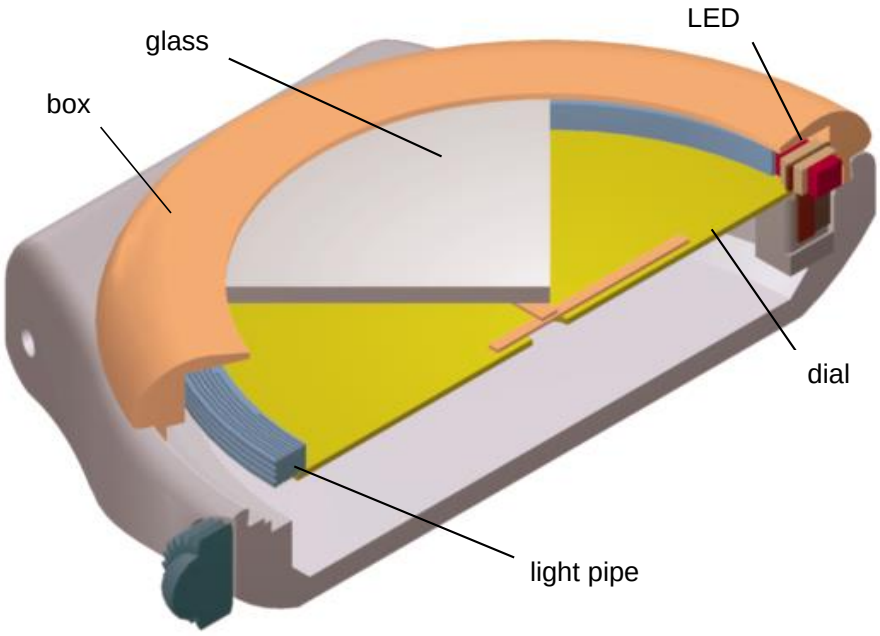

Fig. 4-1 Basic setup of the watch frontal-lighting device based on a scattering light pipe.

The relative positioning of the main watch elements (glass, dial, pipe, box) is illustrated schematically in Figs. 4-1 and 4-2. The lateral positioning of the pipe with respect to the dial implies the use of a directional illumination light pipe. As illustrated in Fig. 4-2, if the illumination delivered by the pipe is non-directive, part of the emitted rays would leave the watch without touching the dial. These rays act as dazzling rays, reducing the signal-to-noise ratio, as well as the lighting efficiency of the device.

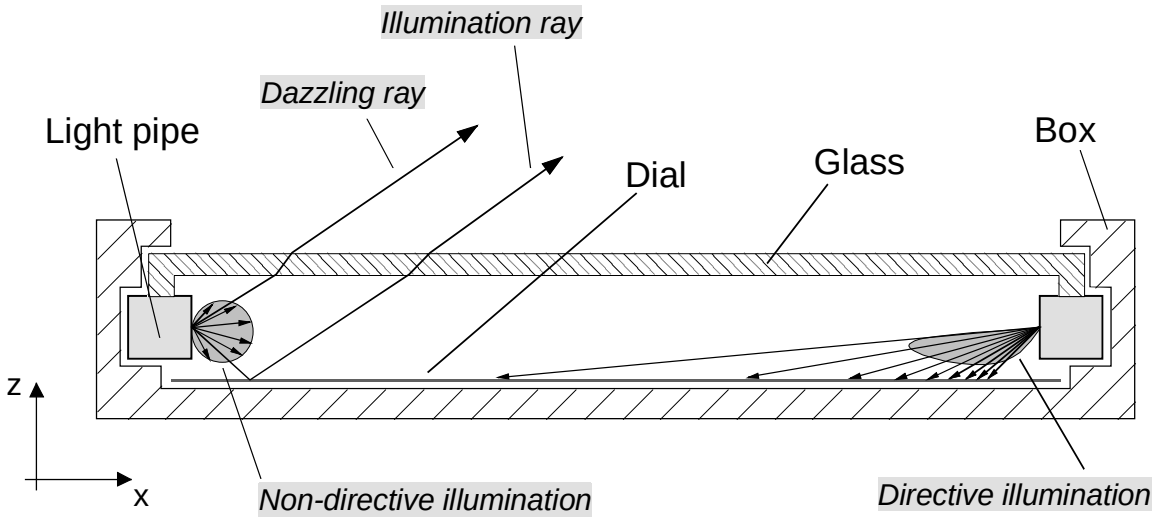

Fig. 4-2 Schematic cross-section of the watch. Illustration of badly adapted non-directive illumination, and efficient directive illumination.

As demonstrated in Chapter 3, reflective micro-prisms are the best outcoupler candidate in order to generate a directive illumination. The design of the illumination light pipe consists in determining the prism geometries, and the repartition of the prisms along the pipe. The design of the LED-to-pipe coupler also needs special care. The goal is to avoid a local discontinuity of the lighting distribution. These different design steps are discussed hereafter.

The LED-to-pipe coupling

In order to avoid any discontinuity in the distribution of the illumination, the pipe needs to cover the full circumference of the dial. As illustrated in Fig. 4-3, the LED must be placed perpendicularly to the pipe. The design of the LED-to-pipe coupler is described hereafter.

A good LED-to-pipe coupler has to fulfill the following requirements :

- to minimize the dazzling rays (going directly from the LED to the eye),
- to equally balance the flux between the two branches of the pipe,
- to minimize any illumination discontinuity of the dial,
- to minimize the coupling losses,
- to maximize the allowed mounting (positioning) tolerances.

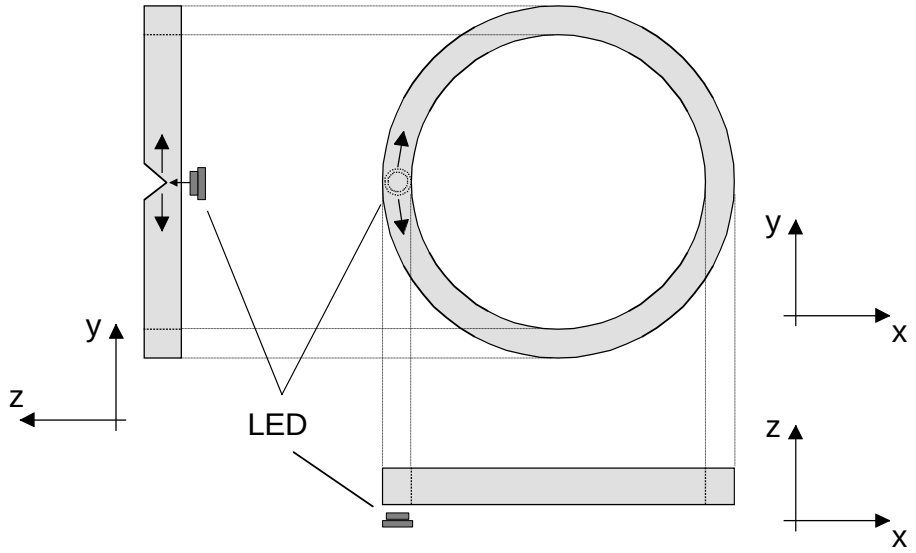

Fig. 4-3 Selected pipe / source arrangement for a circular watch.

As illustrated in Fig. 4-4 (yz-view), the light emitted by the LED has to be coupled equally into the two branches of the pipe. Moreover, a good LED-to-pipe coupler has to avoid the generation of dazzling rays. Figure 4-4 (xz-view) shows that, if an air gap is let between the source and the pipe, all the rays inside the pipe respect the TIR condition. Therefore there are no dazzling rays leaving the pipe in direction of the eye.

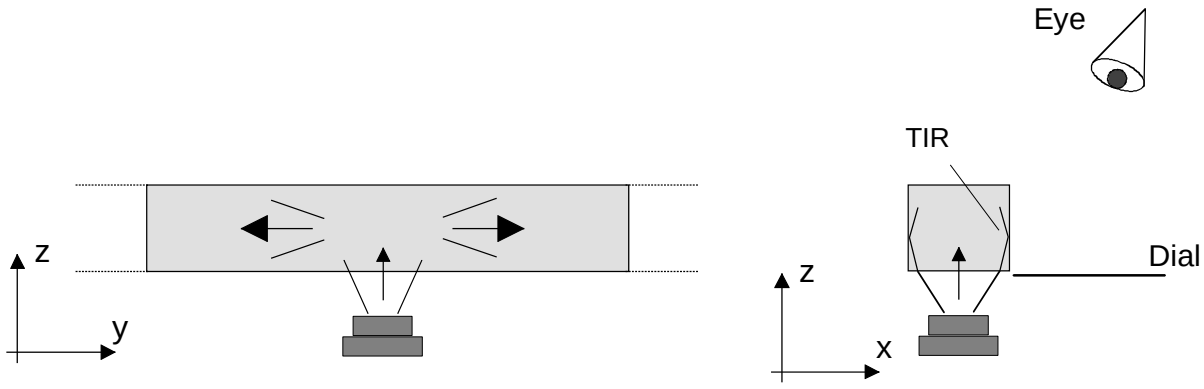

Fig. 4-4 Balanced coupling of the light into the two branches of the pipe (left); the TIR condition avoids the generation of dazzling rays (right).

The coupling into the two branches of the pipe could be done by a reflective micro-prism as illustrated in Fig. 4-5. However, in order to keep manufacturing costs as low as possible, the metallic coating should be avoided. An alternative solution consists in using the external box of the watch as a complementary reflective prism (see Fig. 4-6).

A further advantage of this configuration is that a high proportion of the rays are directed into the pipe branches by TIR, without any metallic reflection losses.

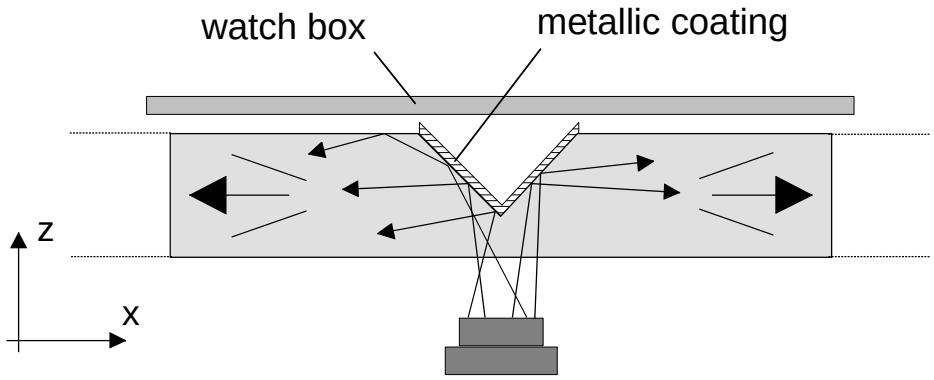

Fig. 4-5 Coupling into the pipe branches by a metallic reflection prism.

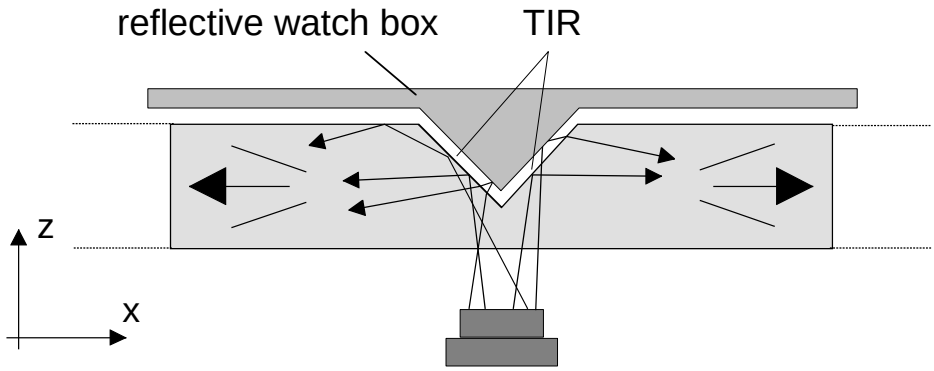

Fig. 4-6 Coupling into the pipe branches by a combination of TIR and metallic reflection.

As described, the only function of the LED-to-pipe coupler is to inject the light into the two branches of the pipe. However, in order to avoid any discontinuity of the lighting distribution, the coupler also has to direct part of the light towards the dial. This is achieved by distorting the shape of the watch box prism, as illustrated in Fig. 4-7. This way, part of the rays reflected by the watch box contribute locally to the illumination of the dial.

The LED-to-pipe coupler is sensitive to a misalignment of the diode with respect to the coupling prism. The simulations have shown that a misalignment of $100\,\mu m$ produces a variation of the contrast between the two branches of the pipe of less than 7%. This shows that the optical effects due to a mounting misalignment can be neglected.

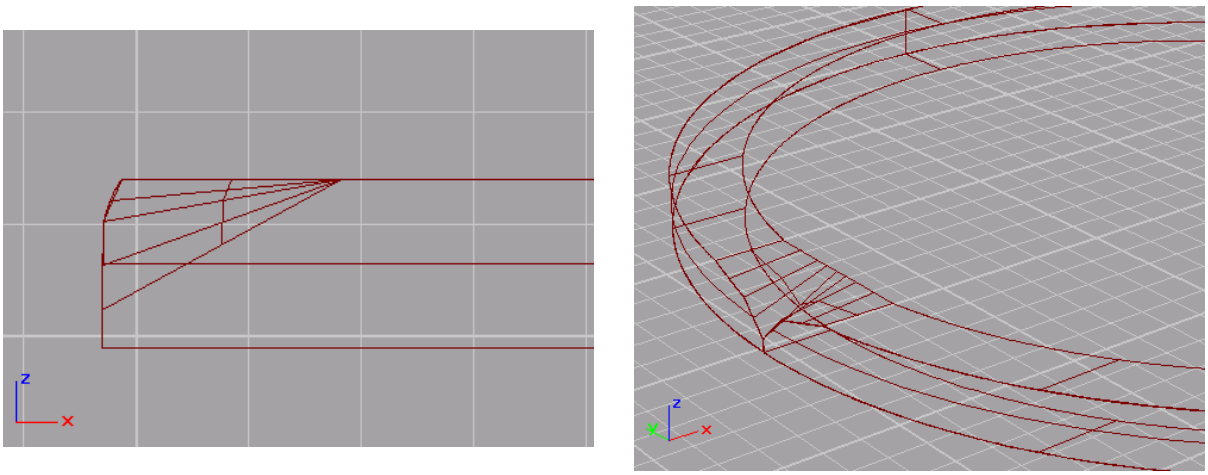

Fig. 4-7 3D views of the distorted prism of the watch box reflector.

Determination of the prism geometry

As shown in Fig. 4-2, the light coupled out from the pipe needs to be directed towards the watch dial in order to maximize the lighting efficiency and to minimize the dazzling rays. A top-down illumination of the dial is achieved if the outcoupling micro-prisms are placed on the top face of the pipe (see Fig. 4-8). The fact that the pipe manufacturing is easier if the prisms are placed on a flat surface is a further advantage of this configuration.

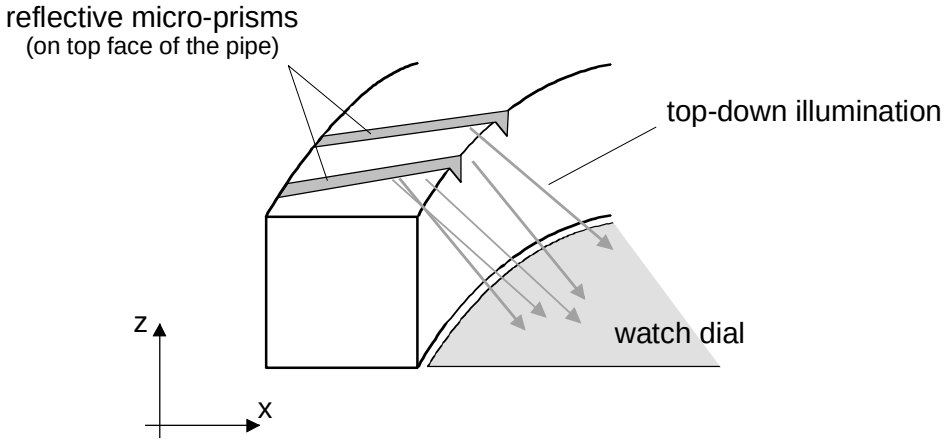

Fig. 4-8 Positioning of the prisms for the top-down illumination of the watch dial.

Figure 4-9 shows that the direction of the outcoupled rays (vector $\mathbf{s}'$) is determined by the direction of the guided rays inside the pipe (vector $\mathbf{s}$) and the orientation of the

prism working face (given by the vector $\mathbf{r}$). Every ray falling on a micro-prism is deviated following the vectorial law of reflection (see Appendix A)

$$\mathbf{s}' = \mathbf{s} - 2a \cdot \mathbf{r} \ , \tag{4-1}$$

where a is defined as

$$a = \frac{k\,K + l\,L + m\,M}{K^2 + L^2 + M^2} \ , \tag{4-2}$$

k,l,m and K,L,M being the directional cosines of the vectors $\mathbf{s}$ and $\mathbf{r}$.

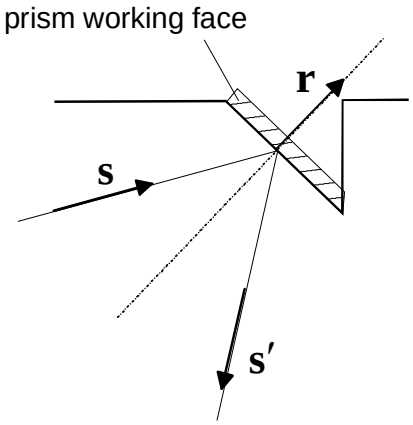

Fig. 4-9 Ray redirection by reflection on a micro-prism.

As discussed in section 3.2.3.1, the rays propagating inside the pipe form a cone defined by the half angle θ (Fig. 4-10). The outcoupled angular spectrum is illustrated by the projected angles θ'_{yz} and θ'_{xy}. The orientation of the micro-prism working face (vector $\mathbf{r}$) is calculated by Eq. (4-1) using the average propagation vectors $\mathbf{s}$ and $\mathbf{s}'$.

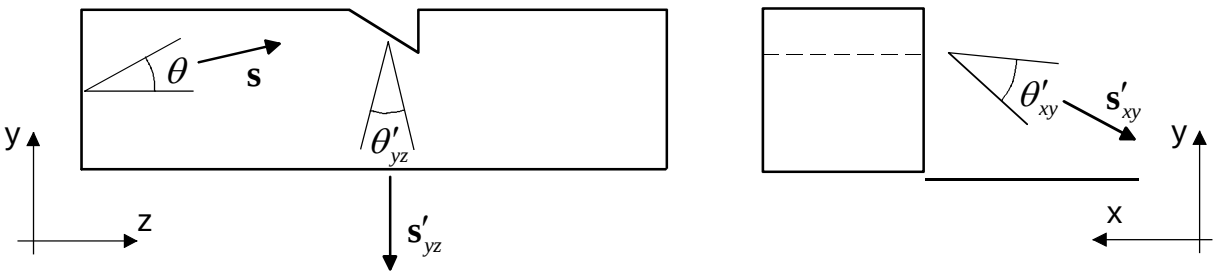

Fig. 4-10 Guided and outcoupled angular spectrums.

The typical orientation of the micro-prisms is illustrated in Fig. 4-11, in the case of a linear light pipe. The micro-prisms are rotated with respect to the orientation of the pipe. We speak about oblique micro-prisms and oblique micro-prism light pipes. The watch application requires micro-prisms having orientation angles of $\bar{\alpha} \cong 45°$ and $\bar{\gamma} \cong 20°$. This corresponds to sharp prisms angle of $\rho \cong 70°$, as defined in Chapter 3 (see Fig. 3-13).

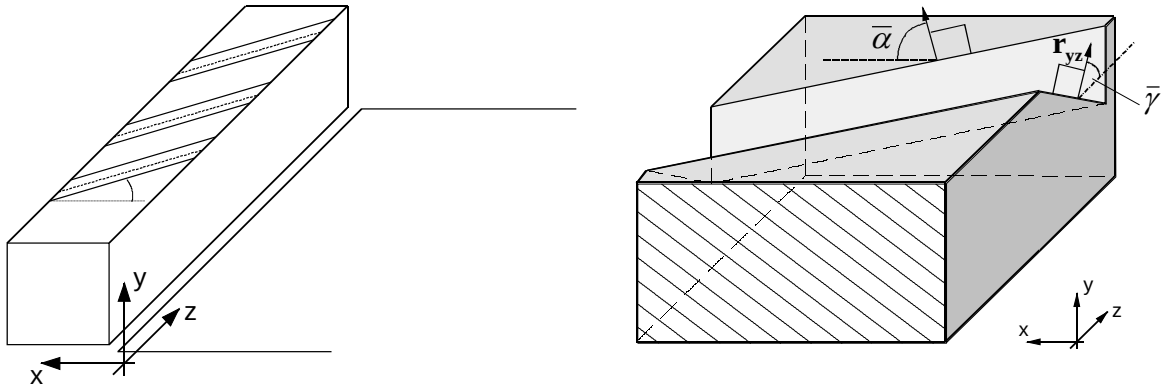

Fig. 4-11 Oblique micro-prisms light pipe, and a micro-prism zoomed view.

Oblique micro-prisms have an interesting side effect. Most of the light guided inside the pipe falls on the oblique micro-prisms fulfilling the TIR condition. Thus, oblique micro-prism light pipes can work without any metallic coating. They are therefore perfectly suited for low cost manufacturing, as required by the watch application.

Uniformization of the illumination

In order to get a uniform illumination of the dial, the outcoupled flux along the pipe has to be constant. The prism density on the pipe top surface is calculated by the OTB method as described in Chapter 3. Figure 4-12 shows the spatial distribution of the prisms on the pipe surface. We have chosen the fixed prism spatial frequency encoding scheme; the variation of the prism density along the pipe being achieved by a variation of the lateral prism size.

Due to the tangential nature of the illumination, the irradiance on the dial should decrease as we move away from the pipe. For circular light watches however, this effect

is compensated by the radial variation of the surface element dS (see Fig. 4-13). A constant illumination of the dial is therefore theoretically possible.

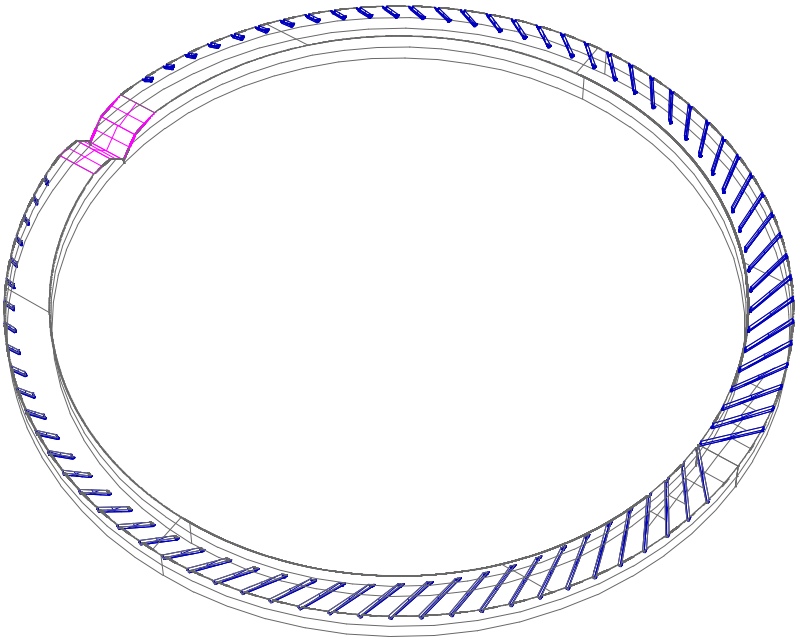

Fig. 4-12 Distribution of the micro-prisms along the circular light pipe.

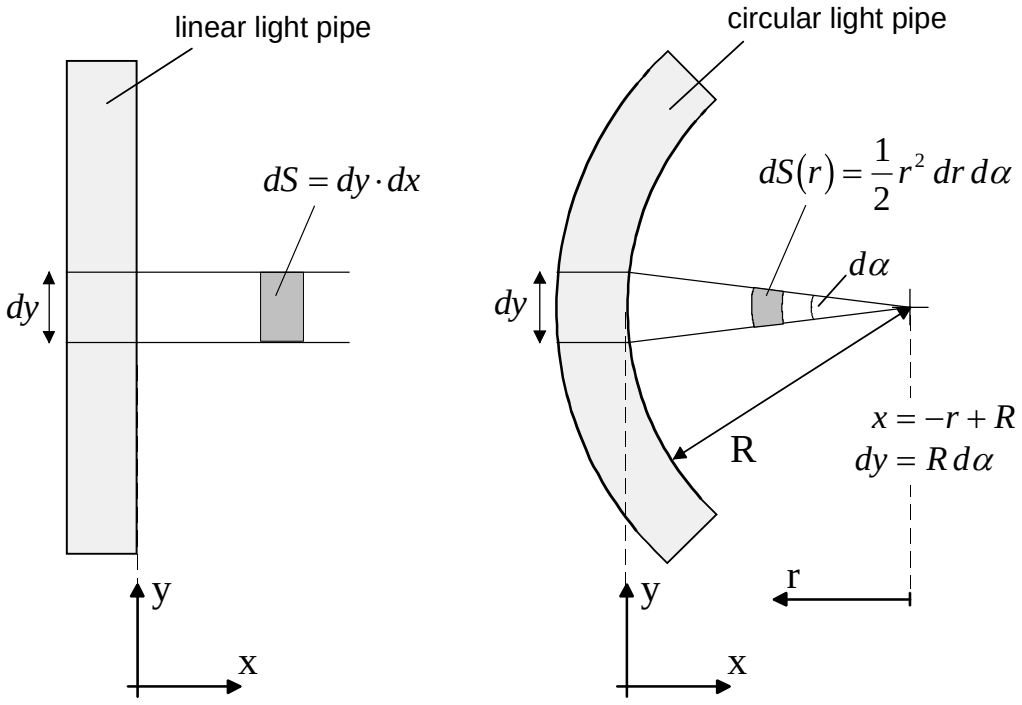

Fig. 4-13 Radial variation of the surface element dS for circular light pipes.

The ray-tracing analysis shows that roughly 60% of the energy emitted by the source reaches the dial. The rest of the energy is either absorbed (volume or metallic absorption), or misses the dial (dazzling rays).

The next figure shows the repartition of the irradiance on the dial. The distribution is not perfectly uniform. In particular, a peak of energy is observed, which corresponds to the position of the LED-to-pipe coupler. Moreover, the border of the dial receives an higher irradiance than the center. This default can easily be corrected by the fine tuning of the orientation of the prism working face. Nevertheless, despite the observed imperfections, this non optimized design represents already a big improvement compared to the current generation of watch lighting devices.

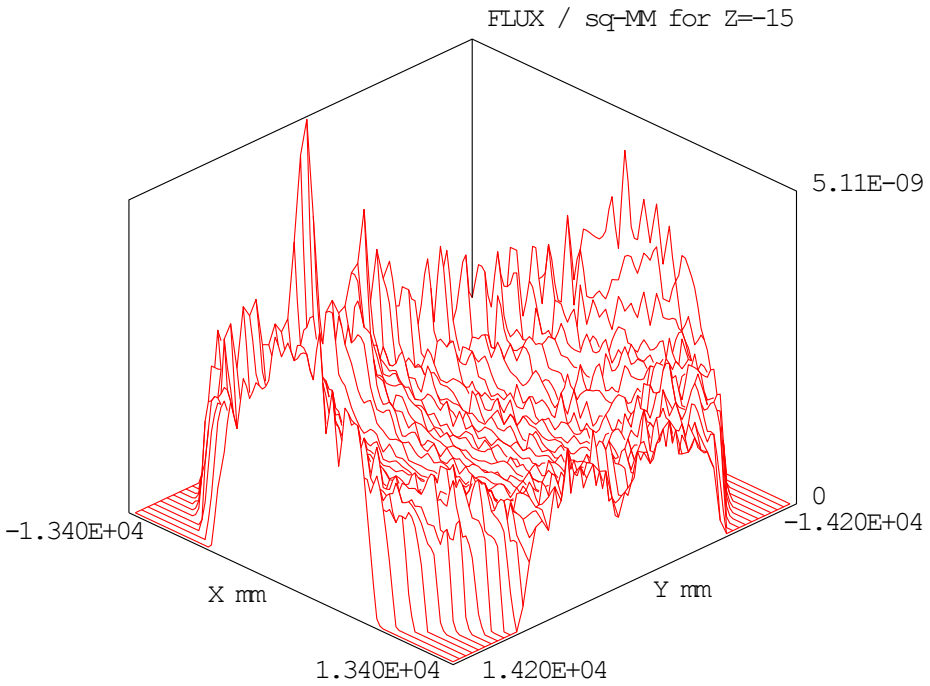

Fig. 4-14 3D view of the irradiance distribution on the dial.

Figure 4-15 shows the first experimental results measured with a CCD camera. The left figure shows the lighting distribution achieved with a traditional lighting device. The light is generated by a quasi-point source and the lighting distribution is far from uniform. The right figure shows the lighting distribution achieved with a non-optimized illumination light pipe prototype. The lighting distribution can still be improved as the center of the dial is poorly illuminated. However, when compared with the traditional

approach, the visibility of the dial has been greatly improved (the full circumference of the dial is yet visible).

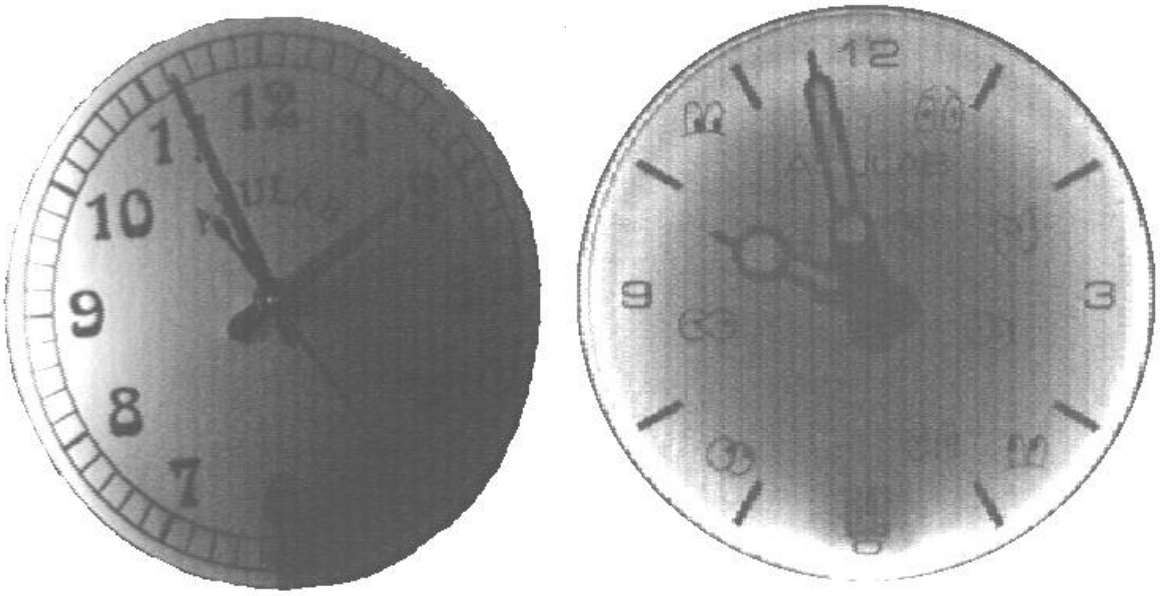

Fig. 4-15 Comparison of the lighting distribution on the watch dial achieved experimentally by a point source (left) and a circular light pipe (right).
(courtesy of Asulab S.A., CH-2074 Marin, Switzerland).

At the time of this writing, the design of the front-side watch lighting device is being fine tuned and the industrialization process is on the way. This concrete realization shows that illumination light pipes can push the limits of traditional light sources, particularly for compact devices. Moreover, we have showed how the manufacturing constraints can influence the design approach (the TIR micro-prism approach has been chosen because the deposition of metallic coatings was too expensive).

4.1 References

[4-1] J.-C. Poli, J. Grupp, J. M. Teijido, H. P. Herzig, *Dispositif d'illumination uniforme du cadran d'un appareil d'affichage*,
Europ. Patent EP860755A1 (1998)

[4-2] J. M. Teijido, J.-C. Poli, J. Grupp, H. P. Herzig, *Dispositif d'illumination orientée d'une surface par un guide à microprismes*,
Europ. Patent EP99109018.4 (1999)

[4-3] D. B. Roitman, et al., "Polymers fulfill promise for electroluminescence",
Optoelectronics World, 163-167, July 1998

Chapter 5

Summary and conclusions

The objective of the present thesis was to give the necessary background knowledge for the realization of illumination light pipes.

We have presented a critical review of the different algorithms, which can potentially be used for the analysis of illumination devices. The algorithms, based on ray-tracing and on the radiance equation, are evaluated on their precision and on their computer efficiency. These methods are not adapted for automatic optimization of illumination devices. We have proposed a design strategy to overcome this major drawback. The chosen hierarchical approach is based on the optical transfer block (OTB) method and allows to reduce the number of analysis-optimization cycles. In complement to standard design tools, the OTB method has proven to be efficient for the design of illumination light pipes.

A good understanding of the light pipe working principles is essential in order to select the right design options. The different types of light pipe outcouplers have been evaluated, based on their optical characteristics as well as on their fabrication techniques. Reflective micro-prism light pipes have been extensively analyzed. Reflective micro-prisms are well suited for the realization of directive illumination light pipes. Moreover, micro-prisms light pipes can be realized by injection molding and allow the realization of cheap illumination devices. However, we have shown that reflective micro-prisms produce shadowing effects which affects the optical performances of light pipes. We have introduced a design criteria which allows to minimize the effects of shadowing.

Light pipes are particularly interesting when the distribution of the illumination needs to be perfectly controlled. We have shown that the lighting distribution depends mainly on the spatial distribution of the outcouplers along the pipe. The OTB method has been used for the calculation of the outcoupler spatial density. We have introduced two encoding schemes for the exact positioning and dimensioning of the outcouplers.

Finally, the different design principles have been applied to the realization of a watch frontal-lighting device. This application is very demanding and illustrates perfectly the potential of illumination light pipes. We have shown how the optical, electrical and manufacturing requirements impact on the design choices. The selected approach based on TIR micro-prisms has allowed to realize a low cost and efficient lighting device.

We hope that this thesis will contribute to the design of illumination light pipes. However, the proposed design strategy does not allow a straightforward optimization process. In particular, precise performance criteria (uniformity of illumination, angular spectrum, manufacturing constraints) have to be proposed in view to formalize the definition of a merit function. Moreover, the opportunity to integrate the different design algorithms (ray-tracing, radiance equation, OTB) into a single tool in order to simplify the design process could be investigated. The application of the OTB method for the design of optical systems with scattering media could also be investigated.

In conclusion, there is no doubt that future advances in the field of illumination design tools are going to simplify the design of illumination light pipes. These improvements are going to further expand the performance and the field of application of illumination light pipes.

Appendix A

Vectorial form of ray-tracing equations

The rule of ray-tracing consists in calculating the position and the direction of the rays propagating through the optical system. When the rays reach an interface, they change their direction of propagation, either by refraction, reflection, diffraction, or surface scattering.

A.1 Refraction law

In the plane of incidence, the deviation of optical rays due to refraction is defined by Snell's law

$$n\sin\alpha = n'\sin\alpha' \,, \qquad \text{(A-1)}$$

where α is the angle of incidence, α' the new angle of propagation, n and n' are the indices of refraction of the respective materials.

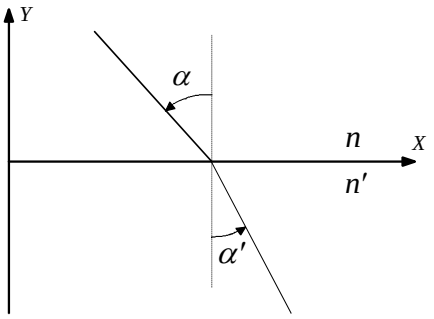

Fig. A-1 Representation of Snell's law in the plane of incidence.

In the 3D space, Snell's law can be derived with the help of Fig. A-2. The incident ray is represented by a vector $\mathbf{s}$ of magnitude n, and the refracted ray by a vector $\mathbf{s}'$ of magnitude n'. The Snell's law may be rewritten as

$$|\mathbf{s}|\sin\alpha = |\mathbf{s}'|\sin\alpha' \,. \tag{A-2}$$

The relation between the refracted vector $\mathbf{s}'$ and the incident vector $\mathbf{s}$ is given by

$$\mathbf{s}' = \mathbf{s} - \mathbf{a} \,. \tag{A-3}$$

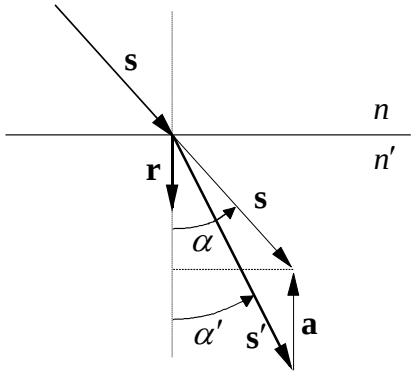

Fig. A-2 Derivation of the vectorial law of refraction.

The vector $\mathbf{a}$ is parallel to the unity vector $\mathbf{r}$ which is normal to the refractive surface. The magnitude of the vector $\mathbf{a}$ is given by

$$\begin{aligned} |\mathbf{a}| &= \Gamma \\ &= |\mathbf{s}'|\cos\alpha' - |\mathbf{s}|\cos\alpha \\ &= n'\cos\alpha' - n\cos\alpha \\ &= n'\left[\left(\frac{n}{n'}\cos\alpha\right)^2 - \left(\frac{n}{n'}\right) + 1\right]^{1/2} - n\cos\alpha \\ &= n'\left[\left(\frac{n}{n'}\cdot\frac{\mathbf{s}\cdot\mathbf{r}}{|\mathbf{s}|\cdot|\mathbf{r}|}\right)^2 - \left(\frac{n}{n'}\right) + 1\right]^{1/2} - n\cdot\frac{\mathbf{s}\cdot\mathbf{r}}{|\mathbf{s}|\cdot|\mathbf{r}|} \end{aligned} \,. \tag{A-4}$$

The vectorial law of refraction becomes

$$\mathbf{s}' = \mathbf{s} + \Gamma\mathbf{r} \,. \tag{A-5}$$

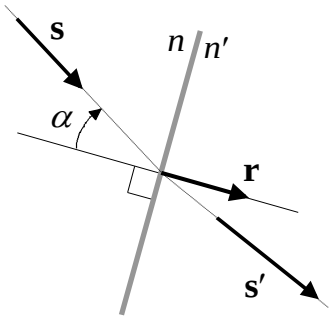

Fig. A-3 Parameters for the calculation of the vectorial law of refraction.

A.2 Reflection law

In the plane of incidence, the deviation of optical rays due to reflection is defined by

$$\sin\alpha = -\sin\alpha' \ , \tag{A-6}$$

where α is the angle of incidence of the ray, and α' the new angle of reflected ray.

From Eq. (A-6), we conclude that

$$\alpha = -\alpha' \ . \tag{A-7}$$

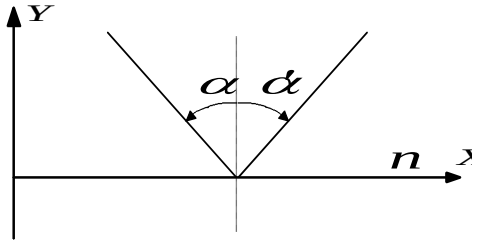

Fig. A-4 Representation of the reflection law in the plane of incidence.

In the 3D space, the reflection law is easily derived with the help of Fig. A-6. The incident ray is represented by a vector $\mathbf{s}$ and the reflected ray by a vector $\mathbf{s}'$. The unity vector $\mathbf{r}$ is normal to the reflective surface.

The reflection law may be rewritten as

$$\mathbf{s}' = \mathbf{s} - 2\mathbf{a} \ . \tag{A-8}$$

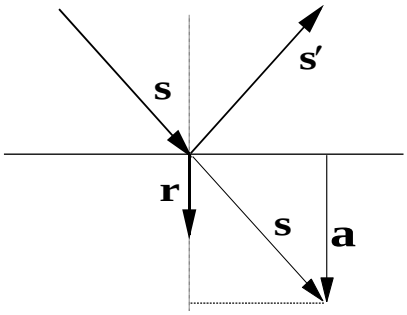

Fig. A-5 Derivation of the vectorial law of refraction.

The vector $\mathbf{a}$ is parallel to the vector $\mathbf{r}$. The magnitude of the vector $\mathbf{a}$ is given by the scalar product

$$|\mathbf{a}| = \mathbf{s} \cdot \mathbf{r} \ . \tag{A-9}$$

The vectorial form of the reflection law becomes

$$\mathbf{s}' = \mathbf{s} - 2(\mathbf{s} \cdot \mathbf{r})\mathbf{r} \ . \tag{A-10}$$

A.3 Diffraction formula

In the plane of incidence, the deviation produced by a thin diffraction grating is defined by the law of diffraction (also called grating equation)

$$n' \sin \alpha'_m - n \sin \alpha = \frac{m\lambda}{d} \ , \tag{A-11}$$

where α is the angle of incidence of the ray, α'_m the new angle of propagation for m^{th} order of diffraction, n and n' are the refraction indices of the respective materials, m the order of diffraction, λ the wavelength, and d the local grating period.

As illustrated in Fig. A-6, the grating law can be applied for gratings working in transmission (angles α'_{m_T}) and reflection (angles α'_{m_R}). For the reflection case, $n' = -n$ has to be substituted into Eq. (A-11).

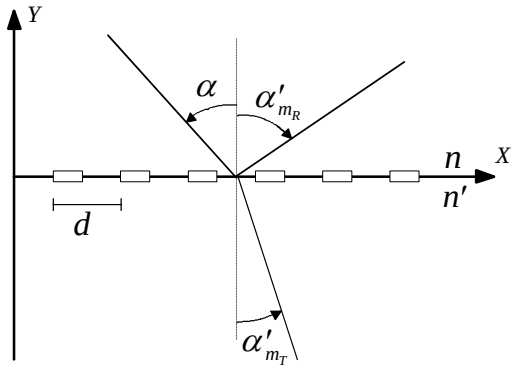

Fig. A-6 Representation of the grating law in the plane of incidence.

Figure A-7 shows the graphical representation of Eq. (A-11). The 0-orders correspond to the graphical reconstruction of the Snell's law and reflection law. The superior orders are constructed starting from the zero order and adding the term $m\lambda/d$ in order to find the sinus of the diffracted angles.

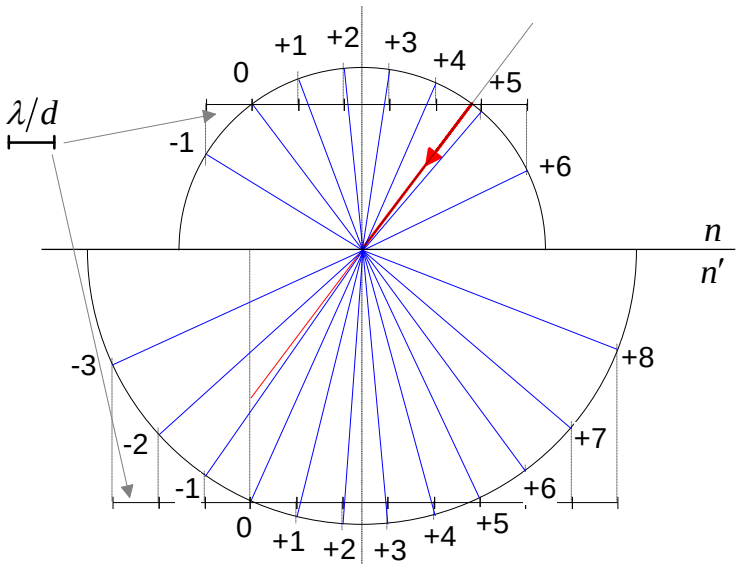

Fig. A-7 Graphical representation of the grating law.

The situation in the 3D space is illustrated in Fig A-8. The incident ray, represented by the vector $\mathbf{s}$ of magnitude n, intersects the surface at the point Q. The unit vector $\mathbf{r}$ represents the normal to the surface at the point Q. Locally, the grating has a period of d and the orientation of the fringes is normal to the unit vector $\mathbf{p}$. For each diffraction order m, the rays are represented by the vectors $\mathbf{s}'_{m_T}$ of magnitude n' for the transmitted rays, and by the vectors $\mathbf{s}'_{m_R}$ of magnitude n for the reflected rays.

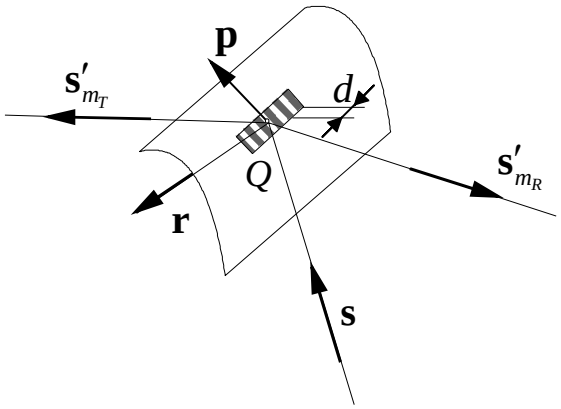

Fig. A-8 Parameters of the vectorial grating law.

As discussed in [A-1], the vectors $\mathbf{s}'_m - \mathbf{s}$ and $\mathbf{r}$ form a (diffraction) plane normal to the fringes of the grating; that is to say, normal to $\mathbf{p}$ at the point Q. The vectorial form of grating law can be written as

$$\mathbf{r} \times \left(\mathbf{s}'_m - \mathbf{s}\right) = a \cdot \mathbf{p} \ , \tag{A-12}$$

where a is a scalar defined as

$$a = \frac{m\lambda}{d} \ . \tag{A-13}$$

Equation (A-12) can be rewritten as

$$\mathbf{r} \times \mathbf{s}'_m = \mathbf{r} \times \mathbf{s} + \frac{m\lambda}{d}\mathbf{p} \ . \tag{A-14}$$

The resolution of Eq. (A-14) requires a change of coordinates. If the z-axis is orientated along the local normal, Eq. (A-14) separates into two components

$$\begin{aligned} L'_m &= L + \frac{m\lambda}{d}U \\ M'_m &= M + \frac{m\lambda}{d}V \end{aligned} \ , \tag{A-15}$$

where L, M, N represent the director cosines of the vector $\mathbf{s}$, L'_m, M'_m, N'_m the director cosines of the vectors $\mathbf{s}'_m$, and U, V, W the director cosines of the vector $\mathbf{p}$.

The third component of the unit "diffracted" vectors $\mathbf{s}'_m$ is defined as

$$N'_m = \sqrt{1 - L'^2_m - M'^2_m} \quad . \tag{A-16}$$

A.4 References

[A-1] W. T. Welford, "A vector raytracing equation for hologram lenses of arbitrary shape", Optics Comm. **14**, 322-323, (1975)

Appendix B

Representation of bidirectional scattering distribution functions

Bidirectional scattering distribution function (BSDF) is the generic term used to describe the distribution of light generated by a ray reaching a scattering surface. Two other terms are commonly used : *Bidirectional Reflectance Distribution Function* (BRDF), when only the reflected response is considered, and *Bidirectional Transmittance Distribution Function* (BTDF), when only the transmitted response is considered.

BSDFs are used by analysis programs to simulate the interaction of light with scattering surfaces, or thin volume scattering layers. For instance, the BSDF is used for the calculation of the direction of propagation of the rays in Monte Carlo ray-tracing programs. As shown in Chapter 2, the BSDF is also used for the calculation of the exchange of radiant energy between surface elements in the global illumination model (see Eqs. (2-5) and (2-6)).

For a small illuminated area dA (Fig. B-1), the BSDF is defined as the radiance in a given scatter direction divided by the irradiance reaching the surface from a given direction. If θ_s and ϕ_s denote the polar and azimuthal angles of the scatter direction and θ_r and ϕ_r are the polar and azimuthal angles for the specular direction, the BSDF is a function of four variables and is written as

$$BSDF = \rho\left(\theta_i, \phi_i; \theta_s, \phi_s\right) = \frac{L\left(\theta_s, \phi_s\right)}{E\left(\theta_i, \phi_i\right)} \ , \qquad \text{(B-1)}$$

where E_i is the incident irradiance $\left(W \cdot m^{-2}\right)$ and L_s is the resulting scattered radiance $\left(W \cdot m^{-2} \cdot sr^{-1}\right)$.

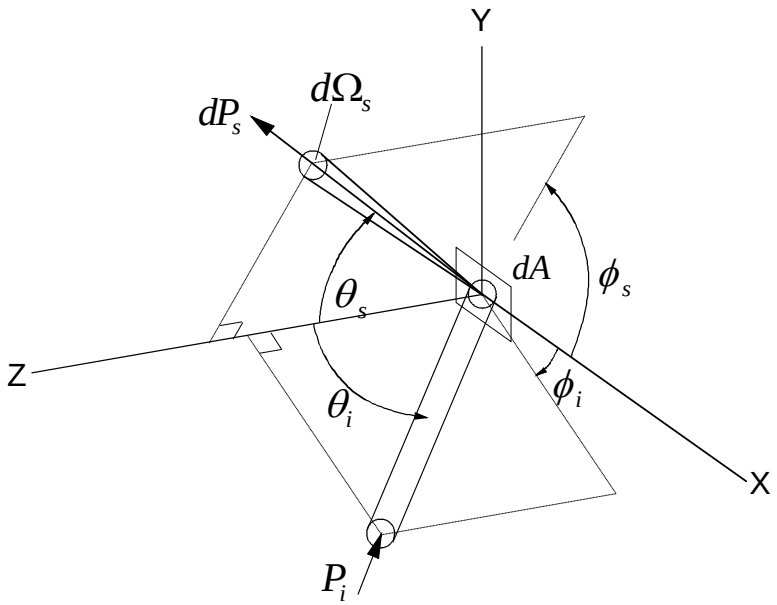

Fig. B-1 Opto-geometrical parameters for the BSDF definition.

In general, the BSDF is determined experimentally with some type of goniometric instrument. For each incident angle, a detector scans the 3D space to measure the optical response of the surface. Then the illumination angle is changed and the measurement process is repeated. Each measured value is recorded into a database. The ASTM 1392 database format is being recognized as standard by most leading software manufacturers [B-1]. The database can be directly imported into the analysis programs.

Actually, for small perturbations of the surface, the BSDF also depends on the wavelength and on the state of polarization of the incident light. However, the light sources used for illumination purposes are generally incoherent and unpolarized. It is important that the light reaching the probe during the experimental characterization of the BSDF is also incoherent and unpolarized. If a laser is used, the light has to be made incoherent (e.g. with a rotating diffuser placed in the light path) in order to avoid any speckle interferences.

Instead of representing the BSDF with a large amount of values stored in a database, it may be interesting to represent the BSDF with an analytical function. The analytical

approach has the advantage that only a few coefficients are necessary to describe the complete BSDF. Several (more or less accurate models) have been proposed by the computer graphics industry [B-2]. Recently, a modal approach based on the Zernike polynomials has been proposed [B-3]. This model allows to reproduce the BSDFs produced by most natural and synthetic materials, including anisotropic BSDFs. The flexibility of the modal approach allows to separated the different contributions of the BSFD, such as the Lambertian lobe, the backscattered lobe, and the specular lobe. Moreover, the shape and the relative size of each lobe can be chosen independently. We let the interested reader look at [B-3] for the details of the mathematical derivations. However, due to the relative complexity of the calculations, the use of the modal approach is not optimal, when millions of ray-to-surface interactions have to be simulated.

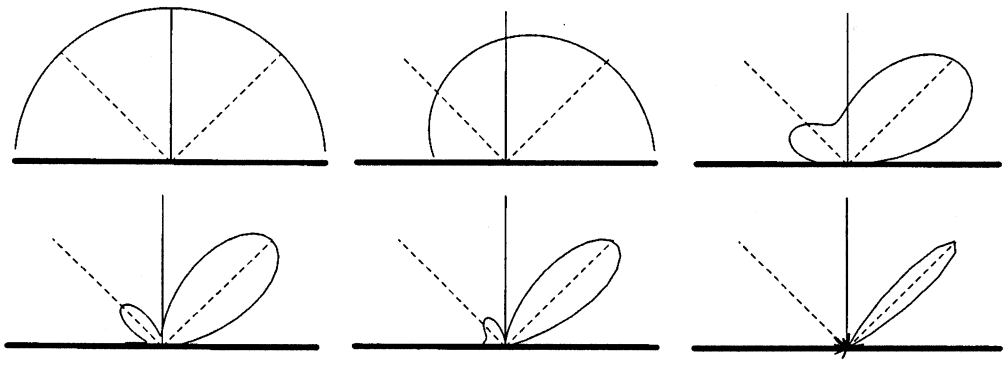

Fig. B-1 Examples of BRDFs calculated with the modal approach.

Shift-invariance property of polished surfaces

Harvey has shown [B-4, B-5], that the BSDF of most optically polished surfaces is independent of the direction of incidence, when expressed as a function of the direction cosines instead of the angles. This property is called shift-invariance, as in linear system theory, and can be related to the shift theorem of the Fourier transform. Surface scattering is a diffraction process whose aperture exhibits random phase variations. And diffraction (as the Fourier transform) is shift invariant in the Fresnel approximation region. As shown hereafter, the shift-invariance property allows to represent the full BSDF (actually the BRDF for reflective surfaces) with a reduced set of parameters.

Figure B-2 shows the graphical conventions used for the definition of the shift-invariant property. The direction of incidence is represented by the unit vector $\mathbf{r}_i$, which determines the specular direction described by the unit vector $\mathbf{r}_0$. The scattering direction of interest is determined by the unit vector $\mathbf{r}$. β_0 and β are the projection onto the surface of the vectors $\mathbf{r}_0$ and $\mathbf{r}$ respectively. The shift-invariance property says that the BSDF is function of the magnitude of the difference $|\beta - \beta_0|$. Note that in the plane of incidence : $\beta_0 = \sin\theta_0$ and $\beta = \sin\theta$.

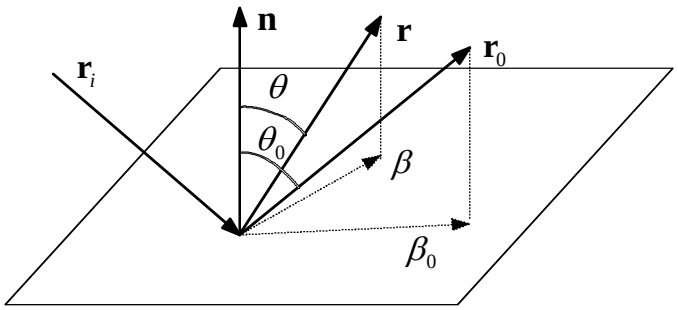

Fig. B2 Definitions used for the representation of the shift-invariant BSDF.

The shift-invariance property of the BSDF is illustrated by the two curves of Fig. B-3. Figure B-3a shows the relative scattered intensity produced by a scattering surface for different angles of incidence. We observe that the shape of the scattered intensity changes with the angle of incidence. However, as shown in Fig. B-3b, if these measurements are divided by the cosines of the scattering angle and then reploted as function of $\beta - \beta_0$, all the curves are superposed. The shift-invariant property is demonstrated.

Figure B-4 shows that, if the BSDF is plotted in log-log format, all the curves lie on a straight line. Actually, for small values of $|\beta - \beta_0|$, the shift-invariant representation has a flat region (see Fig. B-5). Several analytical functions have been proposed to represent the shift-invariant curve. The measured BSDF can be represented by the fitted coefficients of the analytical function. This compact representation is particularly interesting for the calculation of scattering surfaces in Monte Carlo ray-tracing programs.

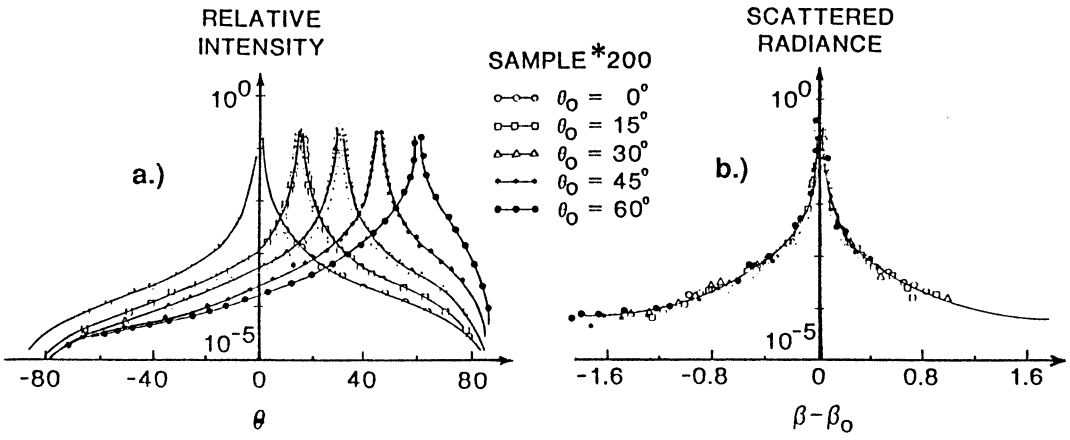

Fig. B-3 a) Scattered intensity versus scattering angle;
b) scattered radiance in direction cosines space.
(Picture published in [B-5], courtesy of J. E. Harvey).

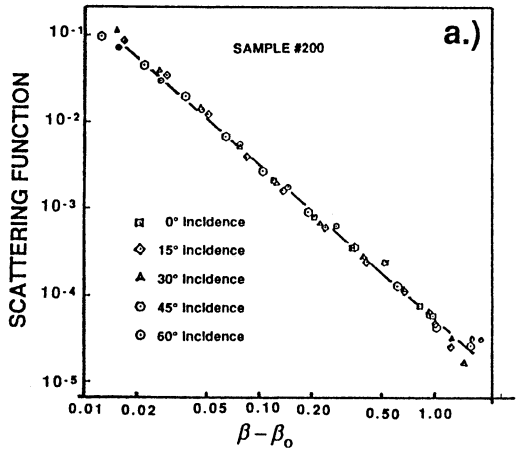

Fig. B-4 Measured BSDF plotted in the log-log format.
(Picture published in [B-5], courtesy of J. E. Harvey).

Freniere in [B-6] has proposed to represent the shift-invariant curve with the ABg model, defined as

$$BSDF\left(\bar{\beta}-\bar{\beta}\right)=\frac{A}{B+\left|\bar{\beta}-\bar{\beta}_0\right|^g}\ , \tag{B-2}$$

where A, B, and g are the coefficients to fit the measured data. Figure B-5 shows the curve generated by the ABg model for the values $A=0.0025$, $B=0.001$, and $g=1.8$.

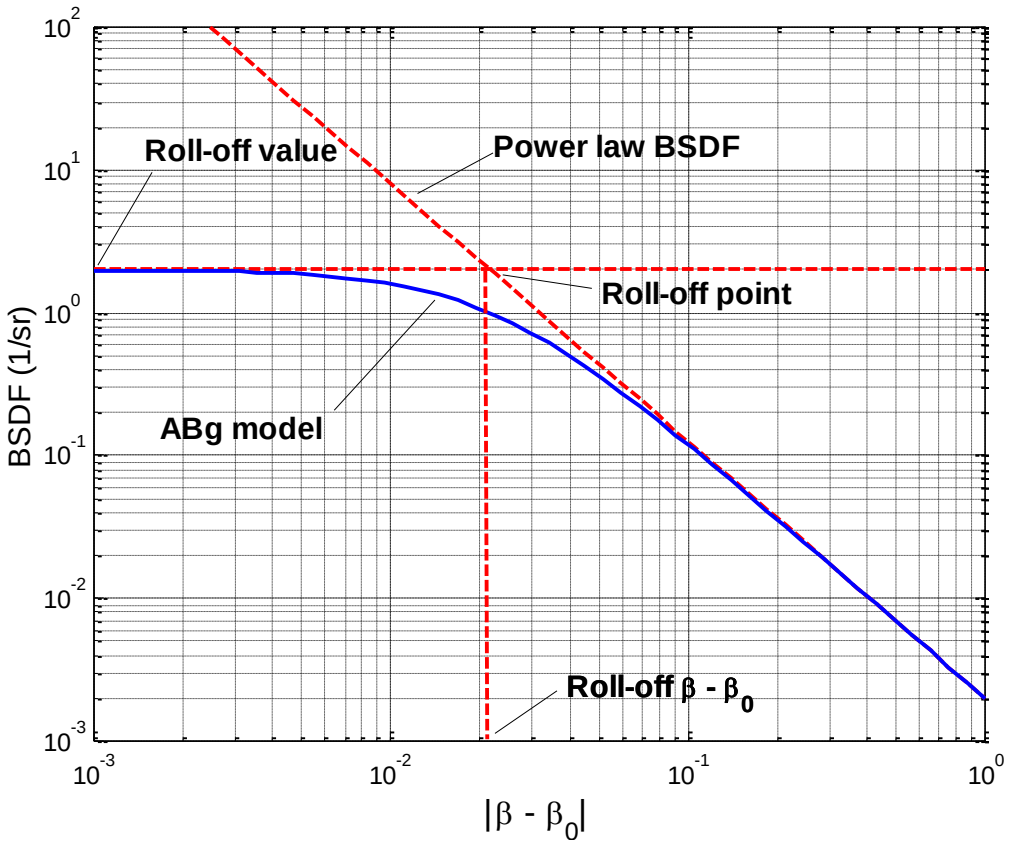

Fig. B-5 Shift-invariant representation as defined in [B-6]. Note the flat region for small values of $|\beta - \beta_0|$.

The curve of Fig. B-5 is characterized by the slope of the BSDF for large values of $|\beta - \beta_0|$ (designated by the *power law BSDF*) and the position of the *roll-off point* (transition region). The slope of the power law BSDF is determined by the coefficient g. The typical values of g are between 1 and 3 depending on the material, the polishing method, and the degree of polishing. The vertical position of the roll-off point is determined by the roll-off value

$$BSDF(0) = \frac{A}{B} \ . \qquad \text{(B-3)}$$

The horizontal position of the transition region is determined by the parameter B, which is related to the roll-off $|\beta - \beta_0|$ by

$$B = (\beta)^g \ . \qquad \text{(B-4)}$$

Values of B are typically 0.001 or smaller, and values of A vary widely.

Freniere has shown that the ABg BSDF can be scaled from one wavelength λ_1 to another wavelength λ_2. The wavelength scaling allows to determine the BSDF of a surface for different wavelengths, based on the experimental measurements made at a single wavelength. The new A and B coefficients have to be calculated, g remaining unchanged,

$$A_2 = A_1 \left(\frac{\lambda_2}{\lambda_1} \right)^{g-4}, \tag{B-5}$$

and

$$B_2 = B_1 \left(\frac{\lambda_2}{\lambda_1} \right)^{g} . \tag{B-6}$$

In summary, the shift-invariance property allows to represent the BSDF by a simple analytical function (e.g. the Freniere's ABg model). This model describes the behavior of most polished surfaces for which the roughness profile is much smaller than the optical wavelength (in other words, surfaces which respect the Rayleigh smooth surface criterion as defined in [B-7]). However, the shift-invariance property does not apply to diffusers (volume scattering), or to surfaces generating anisotropic scattering. In these cases, the BSDF is either interpolated from measured data, or calculated by more complicated analytical functions (as Koenderink's modal approach).

B.1 References

[B-1] S. Bäumer, et al., "SLIOS – a contribution to standard procedures in stray light measurements", proc. SPIE **3739**, 414-421 (1999)

[B-2] C. Schlick, "A Survey of Shading and Reflectance Models", Computer Graphics Forum, **13**, 121-131 (1994)

[B-3] J. J. Koenderink, A J. van Doorn, "Phenomenological description of bidirectional surface reflection", J. Opt. Soc. Am. A, **15**, 2903-2912 (1998)

[B-4] J. E. Harvey, *Light-Scattering Properties of Optical Surfaces*, PhD Dissertation, University of Arizona, 1976

[B-5] J. E. Harvey, A. Kotha, "Scattering Effects from Residual Optical Fabrication Errors", proc. SPIE **2576**, (1995)

[B-6] E. R. Freniere, G.G. Gregory, and R.C. Chase, "Interactive Software for Optomechanical Modeling", proc. SPIE **3130**, 128-133 (1997)

[B-7] J. C. Stover, *Optical Scattering: Measurement and Analysis*, SPIE Optical Engineering Press, 1995

Appendix C

Fresnel reflection & refraction

Fresnel reflection / refraction plays an important role in the design of illumination devices and in stray-light analysis. Total internal reflection (TIR) and metallic absorption can be explained by the Fresnel equations [C-1]. Moreover the polarization sensitivity of Fresnel reflection can be used for the optimization of the back-lighting of LCD displays (see [C-2] and [C-3]).

We present hereafter the formula of the reflection coefficients and the calculated reflectivity curves of some typical materials. Moreover, we show the reflection curve of the pipe-air-metal interface. This curve is particularly interesting for the design of light pipes surrounded by a reflector.

Reflection coefficients

The amplitude reflection coefficients for the *s* (perpendicular to the plane of incidence) and *p* (parallel to the plane of incidence) polarizations are defined as

$$r_p = \frac{n_1 \cos\alpha_2 - n_2 \cos\alpha_1}{n_1 \cos\alpha_2 + n_2 \cos\alpha_1} \ , \qquad \text{(C-1a)}$$

$$r_s = \frac{n_1 \cos\alpha_1 - n_2 \cos\alpha_2}{n_1 \cos\alpha_1 + n_2 \cos\alpha_2} \ , \qquad \text{(C-1b)}$$

where n_1 and n_2 are the indices of refraction of materials, α_1 the angle of the incident ray, and α_2 the angle of the refracted ray (defined by Snell's law).

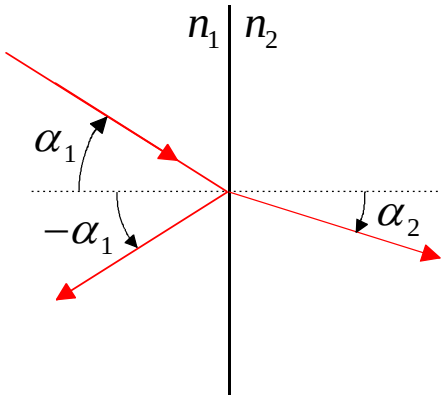

Fig. C-1 Opto-geometrical parameters of the Fresnel reflection / refraction.

The reflection and transmission coefficients for polarized light are given by

$$R_p = r_p^2 \,, \tag{C-2a}$$

$$R_s = r_s^2 \,, \tag{C-2b}$$

$$T_p = 1 - R_p \,, \tag{C-2c}$$

$$T_s = 1 - R_s \,. \tag{C-2d}$$

If the light is unpolarized, the reflection coefficient R and the transmission coefficient T are defined as the average of the coefficients of the polarized case

$$R = \frac{R_p + R_s}{2} \,, \tag{C-3a}$$

$$T = \frac{T_p + T_s}{2} \,. \tag{C-3b}$$

Typical reflectivity of dielectric media

We present hereafter some typical reflection curves for polarized and unpolarized rays for typical materials. The influence of Fresnel reflection/refraction on the device efficiency may be critical in case of multiple reflections (see Chapter 3). In the case of illumination light pipes, we try to take profit of the total internal reflection (TIR) for the guiding of light.

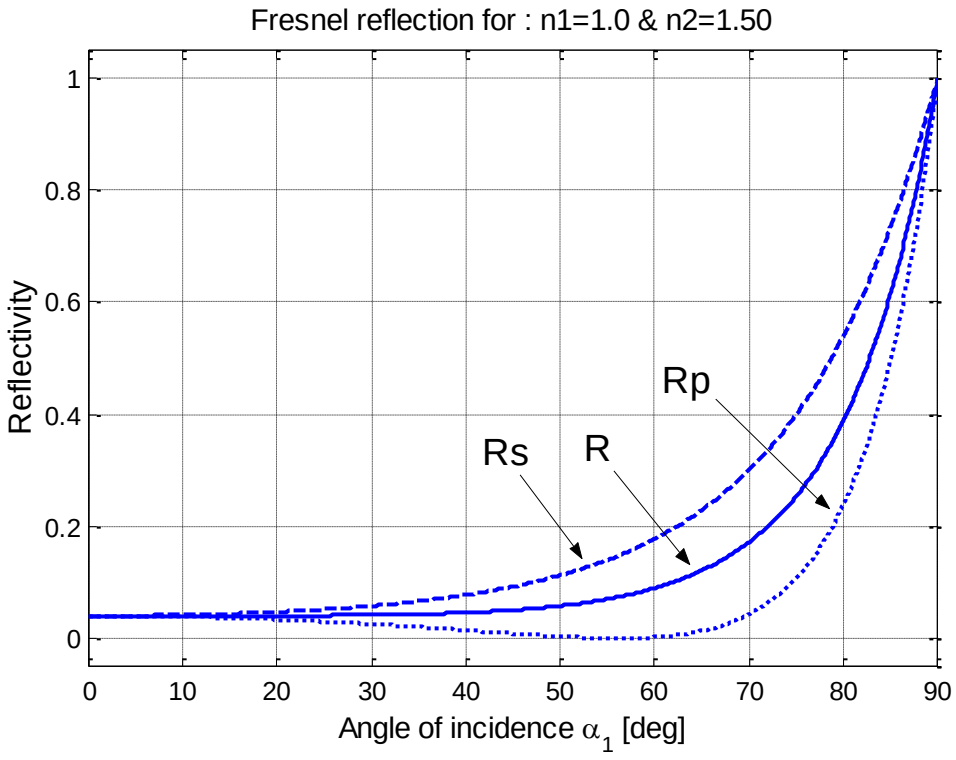

Fig. C-2 Reflectivity for $n_1 = 1.0$, *and* $n_2 = 1.5$.

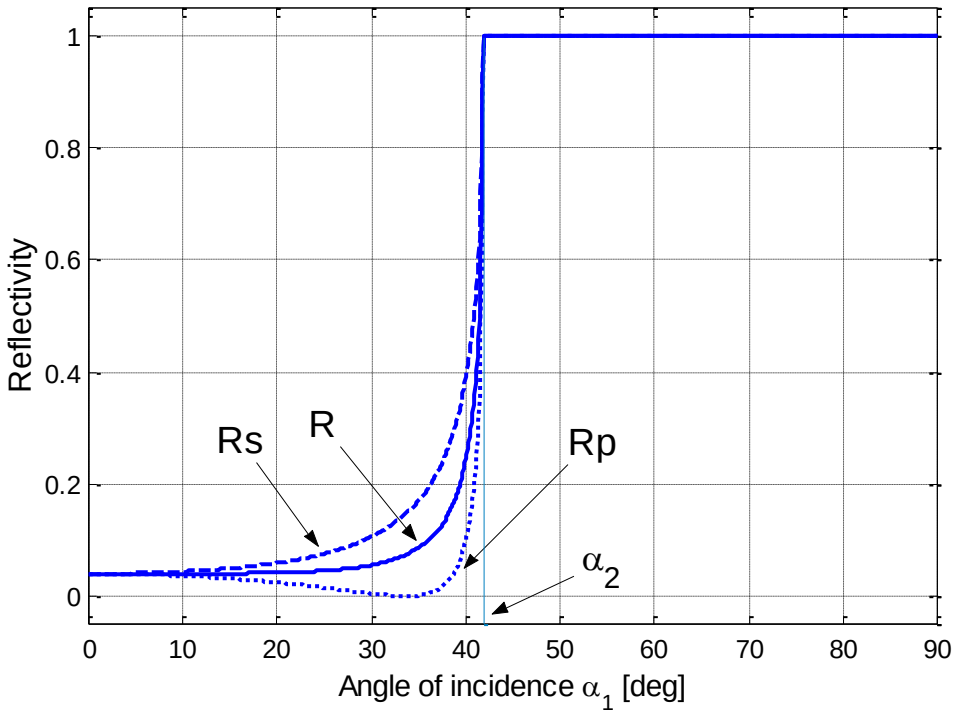

Fig. C-3 Reflectivity for $n_1 = 1.5$, *and* $n_2 = 1.0$.

As illustrated in Fig. C-3, if $n_1 > n_2$, there is a critical angle of incidence α_c, above which the light is loss less reflected by total internal reflection ($R = 1$). The critical angle is defined as

$$\alpha_c = \sin^{-1}\left(n_2/n_1\right) . \qquad \text{(C-4)}$$

The parameters for the presented example were $n_1 = 1.5$ and $n_2 = 1.0$, $\alpha_c = 41.8°$.

Typical metallic reflectivity

When a ray is reflected by a metallic substrate, a few percents of the flux is lost by absorption inside the material. These losses can be critical for coated light pipes, for which the light is guided by multiple metallic reflections.

The next figures (C-4 and C-5) present the reflectivity of gold (Au), aluminum (Al), and silver (Ag) for unpolarized light at a wavelength of $\lambda = 652nm$. At this wavelength, the complex refractive indices of theses materials are $n_{Au} = 0.166 + 3.15i$, $n_{Al} = 1.39 + 7.65i$, and $n_{Ag} = 0.140 + 4.15i$.

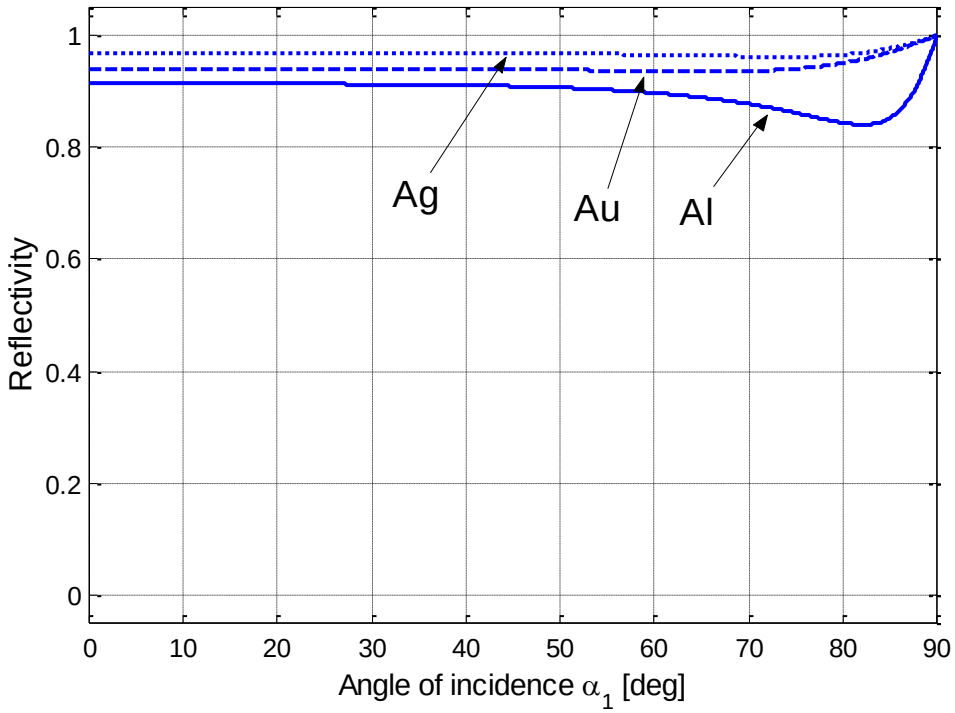

Fig. C-4 Reflectivity of gold, silver, and aluminum for $n_1 = 1.0$.

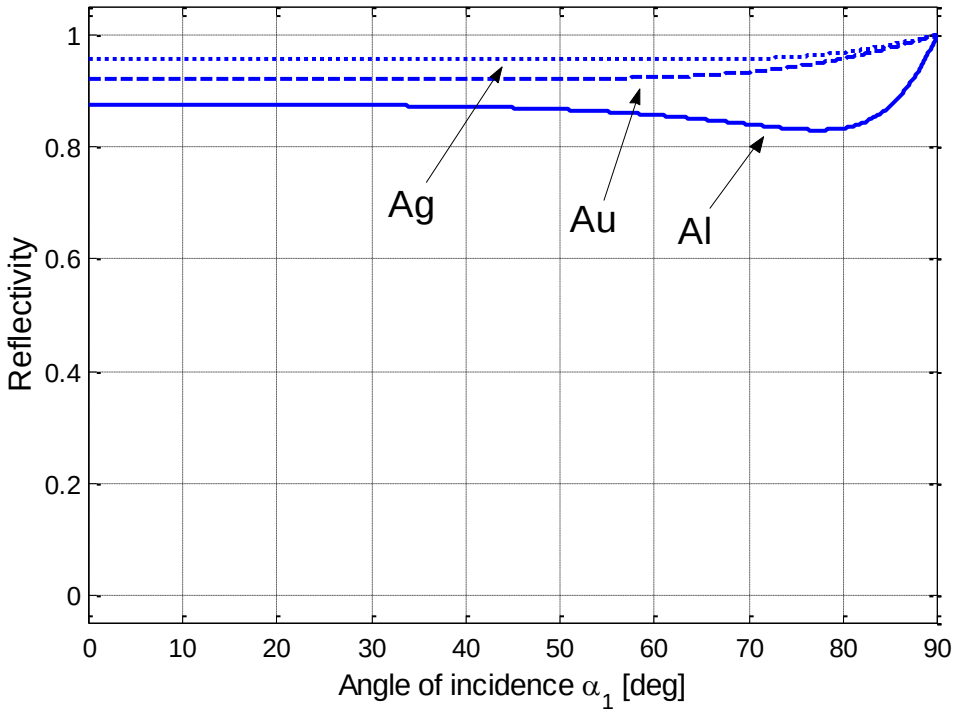

Fig. C-5 Reflectivity of gold, silver, and aluminum for $n_1 = 1.5$.

We observe in Fig. C-5, that for Al-coated light pipes the absorption due to a single metallic reflection can reach 17% of the incident flux. The interest of TIR light pipes becomes evident.

Reflectivity of the pipe-air-metal interface

Illumination light pipe are often surrounded by a reflector, whose function consists in redirecting "lost" rays towards the desired direction. This configuration is also used by the prism LED-to-pipe coupler presented in Chapter 4.

The configuration is illustrated in Fig. C-6. The pipe has an index of refraction $n_1 = 1.5$, and the Al reflector an index of refraction $n_3 = 1.39 + 7.65i$ (at $\lambda = 652nm$). The calculation parameters are : the angle of incidence α_1, the interreflection angle α_2 (determined by Snell's law), and the different reflection and transmission coefficients. We want to know the relative energy which is back reflected into the pipe in function of the angle of incidence α_1.

The next equation shows the contribution of each interreflection R_i, the total reflected

energy being defined by $\sum R_i$.

$$\begin{aligned}
&0: \quad R_0 = R_{12}(\alpha_1) \\
&1: \quad R_1 = T_{12}(\alpha_1)\cdot R_{23}(\alpha_2)\cdot T_{21}(\alpha_2) \\
&2: \quad R_2 = T_{12}(\alpha_1)\cdot R_{23}(\alpha_2)\cdot R_{21}(\alpha_2)\cdot R_{23}(\alpha_2)\cdot T_{21}(\alpha_2) \\
&3: \quad R_3 = T_{12}(\alpha_1)\cdot R_{23}(\alpha_2)\cdot R_{21}(\alpha_2)^2\cdot R_{23}(\alpha_2)^2\cdot T_{21}(\alpha_2)
\end{aligned} \tag{C-5}$$

The total reflected energy is now defined as

$$\begin{aligned}
R &= \sum_i R_i \\
&= R_{12}(\alpha_1) + T_{12}(\alpha_1)\cdot R_{23}(\alpha_2)\cdot T_{21}(\alpha_2)\cdot\left[1 + R_{21}(\alpha_2)\cdot R_{23}(\alpha_2) + R_{21}(\alpha_2)^2\cdot R_{23}(\alpha_2)^2 + \ldots\right]. \\
&= R_{12}(\alpha_1) + \frac{T_{12}(\alpha_1)\cdot R_{23}(\alpha_2)\cdot T_{21}(\alpha_2)}{1 - R_{21}(\alpha_2)\cdot R_{23}(\alpha_2)}
\end{aligned} \tag{C-6}$$

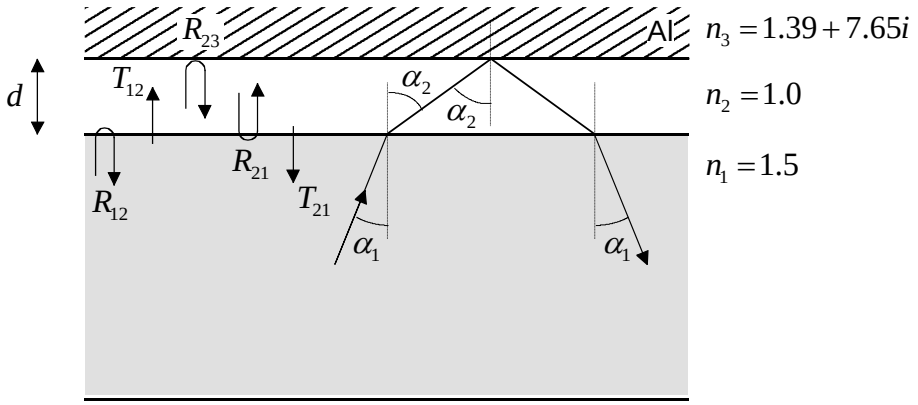

Fig. C-6 Parameters of the pipe-reflector configuration.

Note that the size of the air gap d does not influence the absorbed energy or the angle of propagation of the rays reaching the reflector. Nevertheless, the air gap d should be larger than the penetration depth δ of the evanescent light in order to avoid any losses by tunneling effect. The penetration depth is defined as

$$\delta = \frac{\lambda}{2\pi\sqrt{n_1^2 \sin^2\alpha_1 - n_2^2}} \ . \tag{C-7}$$

This implies that the air gap should be $d > 1.0\mu m$ for the visible.

The reflectivity of the pipe reflector configuration is plotted in Fig. C7, for the average, s, and p polarizations. As expected, if $\alpha_1 > \alpha_c$, the light is totally reflected. The light reaching the Al reflector is redirected into the pipe with a reduced flux due to the metallic absorption.

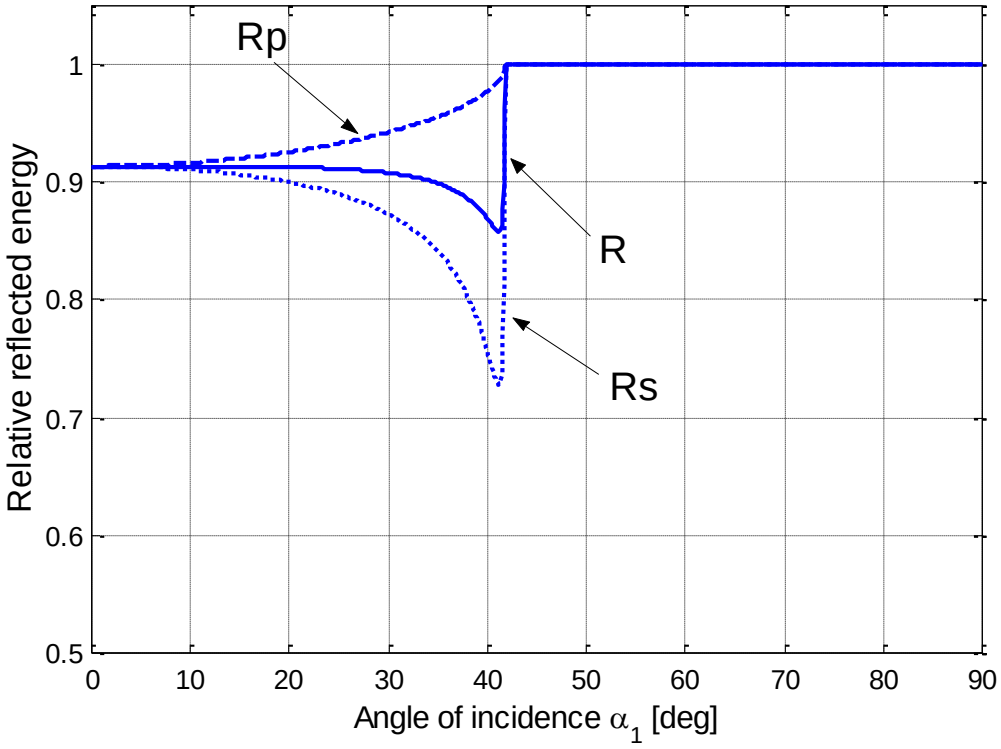

Fig. C-7 Reflectivity of when the pipe is surrounded by a Al reflector.

C.1 References

[C-1] E. Hecht, *Optics, second edition*, Addison-Wesley, 1987

[C-2] M. Suzuki, J. Mamiya, et al., "Improvement of Backlighting Method by Means of Light Pipe Polarizer", Proceedings of the 16th International Display Research Conference, 229-232 (1996)

[C-3] M. Suzuki, Y. Oki, "A Backlighting Unit with Polarization Recycle by Stacked Transparent Plates", SID AsiaDisplay Digest, (1998)

Appendix D

Radiometry and photometry quantities

The transfer of optical energy between bodies is described by the radiative transfer. The radiative transfer is characterized in terms of power and geometrical parameters. We describe the definition of the different terms to consider, as defined in [D-1].

Solid angle

As shown in Fig. D-1, a solid angle ω corresponds to the projection A_p of an area A onto a sphere divided by the square of the sphere radius R. An alternative definition takes the projected area $A\cos\theta$ (θ is the angle between the surface normal and the line of sight) divided by the square of the line-of-sight distance ρ. The solid angle unit is the steradian sr (a sphere subtends 4π steradians).

$$\omega = A_p / R^2 = A\cos\theta / \rho^2 \ . \qquad \text{(D-1)}$$

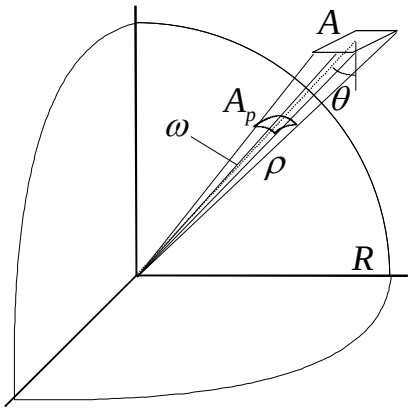

Fig. D-1 Definition of the solid angle.

Radiometric quantities

Power is the time rate of change of energy Q. Usually the power is described by the symbol P. However, in the context of radiometry, the term *radiant flux*, designated by the symbol ϕ, is used instead of power. The flux unit is the watt designated by W.

$$\phi = dQ/dt \ . \tag{D-2}$$

The power emitted per unit area is called the *radiant exitance* (also called emittance). The radiant exitance $M \ \left(W\,m^{-2}\right)$ is defined as

$$M = \frac{\partial \phi}{\partial A} \ . \tag{D-3}$$

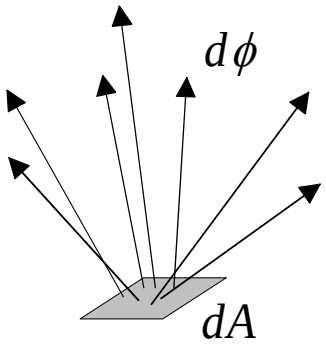

Fig. D-2 Definition of the radiant exitance.

The power received per unit area is called the *radiant incidance* (also called irradiance). The radiant incidance $E \ \left(W\,m^{-2}\right)$ is defined as

$$E = \frac{\partial \phi}{\partial A} \ . \tag{D-4}$$

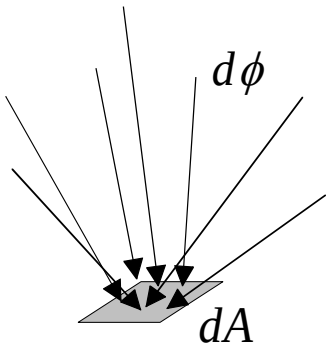

Fig. D-3 Definition of the radiant incidance.

The flux emitted by solid angle is called the *radiant intensity*. The intensity is typically used to describe the emission of point source. But it can also be used to describe, in the far-field, the average flux per unit solid angle emitted by an entire area. The radiant intensity I $\left(W\,sr^{-1}\right)$ is defined as

$$I = \frac{\partial \phi}{\partial \omega} \ . \tag{D-5}$$

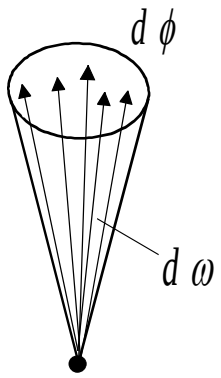

Fig. D-4 Definition of the radiant intensity.

The flux per unit projected area and per solid angle is called the *radiance* (sometimes called radiant sterance). The radiance L $\left(Wm^{-2}sr^{-1}\right)$ is defined as

$$L = \frac{\partial I}{\partial A\cos\theta} = \frac{\partial^2 \phi}{\partial\left(A\cos\theta\right)\partial\omega} \ . \tag{D-6}$$

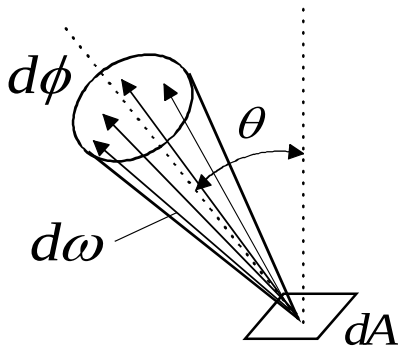

Fig. D-5 Definition of the radiance.

Photonic quantities

Photonic quantities are based on the *photon flux* $\phi_q \left(s^{-1}\right)$, which is defined as the average time rate of the number of photons N

$$\phi_q = \frac{\partial N}{\partial t} \ . \tag{D-7}$$

The other symbols M_q, E_q, L_q, and I_q are found by replacing $\phi(W)$ by $\phi_q\left(s^{-1}\right)$ in Eqs. (D-3) to (D-6). For a given wavelength, the radiometric quantities can be found from the photonic quantities by multiplying by the energy of the photon at that wavelength.

Spectral radiometric quantities

The spectral radiometric quantities are distributions with respect to the wavelength λ. For example, the spectral radiance is defined as the amount of radiance per unit wavelength

$$L_\lambda = \frac{\partial L}{\partial \lambda} \ , \tag{D-8}$$

where $\partial\lambda$ is the considered spectral range.

Photometric (luminous) quantities

A special set of quantities is used to describe the flux transfer for visible light. All the photometric quantities M_v, E_v, L_v, and I_v are based on the *luminous flux* (sometimes called lumen). The luminous flux $\phi_v \ (lm)$ is defined as

$$\phi_v = \int V(\lambda)\phi(\lambda)d\lambda \tag{D-9}$$

where $V(\lambda)$ is the spectral response of the human eye.

RADIOMETRY				PHOTOMETRY			
Term	Symbol	Definition	Units	Term	Symbol	Units	Equivalent
Radiant flux	ϕ	$\frac{dQ}{dt}$	$[W]$	Luminous flux	ϕ_v	$[lm]$ lumens	
Radiant irradiance	E	$\frac{d\phi}{dA}$	$[W\ m^{-2}]$	Luminous Incidence	E_v	$[lx]$ lux	$[lm\ m^{-2}]$
Radiant exitance	M	$\frac{d\phi}{dA}$	$[W\ m^{-2}]$	Luminous Exitance	M_v	$[lm\ m^{-2}]$	
Radiant intensity	I	$\frac{d\phi}{d\omega}$	$[W\ sr^{-1}]$	Luminous Intensity	I_v	$[cd]$ candela	$[lm\ sr^{-1}]$
Radiance (radiant sterance)	L	$\frac{d^2\phi}{d\omega dA\cos\theta}$	$[W\ sr^{-1}\ m^{-2}]$	Luminance (luminous sterance)	L_v	$[cd\ m^{-2}]$	$[lm\ sr^{-1}\ m^{-2}]$

Table D-1 Definitions of the radiometric and photometric quantities.

D.1 References

[D-1] W. L . Wolfe, *Introduction to Radiometry*, SPIE Press, 1998

Acknowledgments

Many thanks to all of you who made this work possible, and specially to

- *Prof. René Dändliker*, director of the thesis, who gave me the opportunity to work in his group and to put in practice his teaching. I fully appreciated his pertinent advices and encouragements.
- *Prof. Hans Peter Herzig*, for his help and guidance throughout these past years. His competence and his permanent good mood made this work easier.
- the members of the jury, *Prof. Joseph Braat* and *Prof. Pierre-Jean Erard*, for critically reviewing my thesis and for spending part of their precious time in Neuchâtel to discuss it.
- *Dr. Harthmuth Buczek*, who received me at CSEM for my diploma work and gave me my first job in the field of Optics.
- *Prof. Neal Gallagher*, who welcomed me for one year at Purdue University. Neal introduced me to the electromagnetic theory of gratings. He also tried to convince me that American Football is a clever game …
- the *University of Neuchâtel*, the *Commission pour la Technologie et l'Innovation (CTI)*, and our industrial partners *Asulab S.A.* (Marin, Switzerland) and *Hella KG* (Lippstadt, Germany) for supporting financially my research.
- *Joachim Grupp*, *Gian-Carlo Poli* and *René Viennet*, from the firm Asulab S.A, with who it was a pleasure to collaborate. Thank to their tenacity, they have proved that illumination light pipes were suitable for the demanding watch application.

- *Detlef Decker* and *Torsten Ruths*, from the firm Hella KG. Their interest in finding new fields of application for the light pipe concept gave a great impulse to my research.

- my colleagues at IMT, for their help, competence, and the excellent atmosphere they have brought to the group. My gratitude goes to all of you :

  Christophe Bagnoud, Christoph Berger, Peter Blattner, Manuel Bouvier, Stéphanie Clément, Neil Collings, Alain Courteville, Markus Duelli, Peter Ehbets, Mary-Claude Gauteaub, Frédéric Gonté, Marcel Groccia, Karim Haroud, Kurt Hug, Peter Kipfer, Markku Kuittinen, Omar Manzardo, Jacques Morel, Antonello Nesci, Christian Ossmann, Yves-Alain Peter, Irène Philipoussis, Ali Pourzand, Jean-Christophe Roulet, Yves Salvadé, Olivier Ripoll, Etienne Rochat, Carsten Rocksthul, Toralf Scharf, Andreas Schilling, Urban Schnell, Wolfgang Singer, Silke Traut, Urs Vokinger, Reinhard Völkel, Ken Weible, Alain Woodtli, Wei Xue, Eric Zimmermann.

  Special thanks to my officemate and friend *Philippe Nussbaum* who has supported my changing mood for more than six years. He is the living proof that nothing is impossible.

- my former colleagues at CSEM, *Thomas Sidler, Aldo Ravedoni, Fabien Droz, Jean-Michel Mayor, Yvar Kjelberg, Frank Ess* and *Pierre Genequand*, who helped me to have a good start in my professional life.

- the members of the optical community I met during these past years at conferences and seminars for their precious advices. Special thanks to *Horst Greiner*, from Philips Research Labs, who shared some of his bright ideas about non-sequential ray-tracing.

- my parents who have always believed in me. I hope to be strong enough to follow the path they teach me. Thanks to my sister *Patricia* and to all my family and friends for being there whenever help was needed.